Quest Trial Q348

Evaluation of WaMoS II Data

Tyson Hilmer
Rutter Inc.

Prepared by:
Rutter Inc.
63 Thorburn Road
St. John's, NL A1B 3M2 Canada

PWGSC Contract Number: W7707-135635/001/HAL

Contract Scientific Authority: Eric Thornhill, Defence Scientist, 902-426-3100 x347

Defence Research and Development Canada

Contract Report
DRDC-RDDC-2014-C49

Report Documentation Page

Form Approved
OMB No. 0704-0188

1. REPORT DATE	2. REPORT TYPE	3. DATES COVERED
APR 2013		**00-00-2013 to 00-00-2013**

4. TITLE AND SUBTITLE	5a. CONTRACT NUMBER
Quest Trial Q348: Evaluation of WaMoS II Data	5b. GRANT NUMBER
	5c. PROGRAM ELEMENT NUMBER
6. AUTHOR(S)	5d. PROJECT NUMBER
	5e. TASK NUMBER
	5f. WORK UNIT NUMBER
7. PERFORMING ORGANIZATION NAME(S) AND ADDRESS(ES) **Rutter Inc,63 Thorburn Road,St. John's, NL A1B 3M2 Canada,**	8. PERFORMING ORGANIZATION REPORT NUMBER
9. SPONSORING/MONITORING AGENCY NAME(S) AND ADDRESS(ES)	10. SPONSOR/MONITOR'S ACRONYM(S)
	11. SPONSOR/MONITOR'S REPORT NUMBER(S)

12. DISTRIBUTION/AVAILABILITY STATEMENT
Approved for public release; distribution unlimited

13. SUPPLEMENTARY NOTES

14. ABSTRACT

15. SUBJECT TERMS

16. SECURITY CLASSIFICATION OF:			17. LIMITATION OF ABSTRACT	18. NUMBER OF PAGES	19a. NAME OF RESPONSIBLE PERSON
a. REPORT	b. ABSTRACT	c. THIS PAGE			
unclassified	**unclassified**	**unclassified**	**Same as Report (SAR)**	**95**	

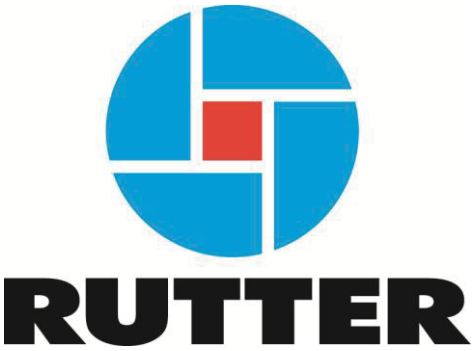

Quest Trial Q348

Evaluation of WaMoS II Data

April, 2013

Contents

1 INTRODUCTION

OceanWaveS participated in the DRDC trial "Q348" in November of 2012 to install and operate the wave radar "WaMoS II" aboard the CFAV vessel "Quest". This report details the experimental setup, methods, and analysis results from trial Q348. References to the prior OceanWaveS report "Quest Trial Q341: Evaluation of WaMoS II data", dated May 2012, will hereafter be referred to as OWS-Q341.

OWS duties during the Q348 trial included optimal configuration and full-time operation of WaMoS II, as well as real-time analysis and networked data distribution in support of the DRDC Sea keeping Operator Guidance project. The necessary requirement for the DRDC Wave Data Fusion (WDF) algorithm is direct measurements of the ocean surface. It was concluded in OWS-Q341 that the primary difficulty in validating this requirement was accurately co-locating the wave buoy and WaMoS II measurements.

Thus setup of both instruments was improved for this trial. The buoy was equipped with an additional GPS module to provide frequent position fixes. Setup of WaMoS II focused on maximizing data resolution, range, and overlap with the buoy position. To further address the goal of validation through direct comparison, the analysis in this report is dedicated to quantifying, explaining, and removing error sources prior to comparison. The resulting data product is the WaMoS II-derived sea surface elevations maps, which have been optimized to directly correspond to the buoy vertical displacements.

Included in this report is a background explanation of the issues faced and the approach taken (Section 2). Following is a complete description of the experimental trial and methods (Section 3), including some of the logistical issues encountered during the trial. Co-location analysis results are detailed in Section 4. WaMoS and buoy comparison results are given in Section 5. Conclusions and recommendations for further work are in Section 6.

1.1 MOTIVATION

The following is excerpted from the original Q341 trial plan to summarize motivation for this research.

"Wave data fusion algorithms (WDF) for shipboard measurement of the wave environment have been developed under the DRDC Sea keeping Operator Guidance (11gw) project to improve wave height measurements from wave radar. These systems have been found to generally provide good wave frequency and direction information but often poor wave height measurement on a moving ship. Within the 11gw project, and in the follow-on DRDC Sea state Awareness and Operational Guidance project (11gi), the WDF algorithms are being incorporated into ship operator guidance systems for sea keeping operations, helicopter operations, and slam warning."

"In July of 2011, as part of the 11gi project, DRDC acquired and installed a new WaMoS® II wave radar[1] on QUEST with the capability to provide sea surface elevation "snapshots". As part of the 11gi project it is planned to evaluate the use of consecutive snapshots of the sea surface to reconstruct the wave field, then forecast the arrival of waves at the ship and finally forecast the resultant ship motion. ONR is currently conducting an Environmental and Ship Motion Forecasting (ESMF project) which seeks to provide sea-based forces with environmental and ship motion forecasting as input to the Common Operation Tactical Picture (COTP), in order to forecast windows of opportunity for inter/intraship material and personnel movement. ONR is providing support for the DRDC 11gi project activities which fit well with the ESMF project objectives. One of the deliverables to ONR will be the Q341 trial data and subsequent analysis. DRDC will also provide access to QUEST for other ONR researchers and ESMF team members to conduct related studies during the Q341 sea trial."

"The main objectives of the [Q341] sea trial are:

a) The testing of an Integrated Seakeeping Operator Guidance system, comprised of the Flight Deck Motion System (FDMS), Tactical Operator Guidance, and the Wave Data Fusion (WDF) system that uses ship motion measurements and ship motion predictions to improve wave heights measured with the new QUEST WaMoS II Wave Radar Processor.
b) Test and evaluate the sea-surface elevation mapping capabilities of the new WaMoS II system.
c) Conduct time-domain wave height measurements in the vicinity of the ship with four moored wave buoys for post-trial evaluation of the RTWI algorithms and ship motion forecasting for both the DRDC and ONR projects. Also collect frequency domain directional wave spectra and wave statistics from the wave buoys for validation of the WDF system measurements.
d) Post-trial analysis of the WaMoS II data to provide improved calibration parameters for the WaMoS II wave radar systems."

2 BACKGROUND

2.1 STATISTICAL VS DIRECT MEASUREMENTS

The WDF system is a deterministic system in that it uses information of the ocean state at specific locations in space and time, combined with physical laws, to predict the future ocean state. This requirement for explicit, or direct measurements, contrasts to the traditional statistical parameters delivered by the WaMoS II. To clarify, the common role of oceanographic measurements is as a reporting and advisory tool; to reduce the large amount of information and observed states into a few highly descriptive parameters. A statistical approach is the most accurate; leveraging large sample sizes to reduce error in the parameter estimates.

[1] WaMoS® II is a registered trademark.
In the following manual, the notation of WaMoS® II takes place without the trademark label.

To understand the exponential difficulty in obtaining accuracy in direct measurements versus statistical, a simple analogy to averaging is invoked. For a measurement composed of signal and zero-mean noise, averaging of repeat measurements will improve the estimate accuracy. In contrast, a single measurement will contain the full proportion of noise. In physical oceanography, a single statistical parameter is often the product of thousands to millions of samples. In accordance with the goal of the WDF system, this report includes, but has not focused on, an analysis of the common statistical parameters (Section 4.3).

2.2 BASES

When measuring physical phenomena, the experimenter ensures the instrumentation has sufficient accuracy and resolution to resolve the process of interest. The characteristic time scale is a useful concept in this context, as it describes the scale over which the signal varies significantly. Similarly, this can be extended to the space dimension. For ocean waves, a minimum scale of *O*(m) and *O*(s) is sufficient to capture the majority of energy. An empirical estimate of the characteristic time scale is given in Section 5.3.1.

When comparing data from two instruments measuring the same signal, an often overlooked issue is the concept of basis. Basis may alternatively be termed “frame of reference”, dimension, or coordinate system. In short, basis provides an alignment for the recorded data. With each instrument comes the possibility for a unique basis. For example, the basis for most oceanographic pressure sensors is an internal quartz oscillator which is translated into time. No two quartz crystals oscillate at exactly the same frequency. Consequently, two sensors deployed as the same location for several months duration will exhibit gradual drift, or misalignment, in their signals.

This same argument can be extended to the comparison between any two instruments, regardless of their accuracy and precision. If the analyses involves a *point-to-point* comparison of the signal, the bases most be aligned and verified. Without additional information, this becomes a circular problem; “How does one reference a reference?” The simplest method is to transpose the roles of dependent and independent variables. A more desirable method is to share basis information between instruments during data acquisition (e.g. see the discussion of GPS in Section 2.3).

As discussed in the next section, errors and uncertainties in the bases for both the WaMoS II and reference sensors can easily exceed the characteristic time and space scales for ocean waves. Without calibration and correction for these errors, further direct comparative analyses become erroneous or impossible. Consequently, the first part of this report focuses on the accuracy and verification of bases data as recommended in OWS-Q341.

2.3 ERROR SOURCES

The principle of operation of WaMoS II is remote sensing combined with the application of physical laws to extract an accurate measure of the ocean surface. The effectiveness of this method requires

repeat measurements of the same location, i.e. an earth-fixed reference frame. The primary error source for registration of the WaMoS II radar images to an earth-fixed reference frame is ship motion, which includes both spatial position (latitude, longitude) and orientation (compass heading).

Following the discussion in Section 2.2, bases which are offset by a constant are relatively easy to correct. A far more difficult situation are bases with variable errors. Conceptually, this can be understood as blurring of the radar image. A common source of such variation are instrumental errors which are inherent to the instrument. A good example of such variation is GPS positioning errors. Standard commercial-grade L1 C/A GPS modules generally have *O*(m) error variation, usually quoted as +/- 5-8 m. To be specific, these errors are due to atmospheric propagation delays and satellite positioning, not the receiver module.

In addition to position, time and compass errors introduce comparable errors to the WaMoS II processing. Additional physical forcing, e.g. wind stress on the antenna rotation rate, or wave-induced roll and attitude of the vessel, can further degrade the results. For example, the typical WaMoS II analysis region is placed at a range of approximately 500 m and extends to approximately 1 km. Given 1 degree of error in compass heading, the resulting spatial errors are 8.7 and 17.4 m, respectively. For direct, or spatially registered, measurements of ocean waves, this exceeds the necessary spatial accuracy.

An additional requirement, imposed by the electromagnetic scattering process, is the geometrical relationship between the radar and earth-fixed measurement region must remain relatively constant. In short, the signal varies with the EM to wave vector relative geometry. If not constrained, this instrumental variation is difficult to separate from the ocean signal of interest. In summary, the two requirements for accurate WaMoS II results are:

- Sufficiently accurate bases to establish an earth-fixed reference frame the input data
- Relatively constant geometrical relationship between the radar and the measurement region

Both of these effects are compensated in the WaMoS II processing method. A primary goal of this analysis is to minimize these effects, *prior to processing*, in order to produce the most accurate output possible. When these conditions cannot be sufficiently met, the corresponding radar data is excluded from the final output. This ensures maximum data quality for subsequent analysis.

3 METHODS

3.1 LOCATION

WaMoS II data collection for Q348 occurred from 2012/11/19 to 2012/11/27. Data collection for the actual trial was from 11/21 to 11/27, prior measurements from the period when Quest was in harbor were used for calibration of the radar range and angle offsets (3.3.3).

The trial area of operations is a relatively flat area at the southwest end of the Emerald Basin about 8 nm square (Figure 1), located at 43 deg 29.11 N 63 deg 17.26 W, with an average water depth of approximately 200 m. This depth is sufficient to assume no influence on the wave field.

The buoys were distributed with a North-South separation of approximately 2 km. During the trial, Quest navigated regular patterns encompassing and bisecting the buoy grid (Figure 2). For this analysis, the geographic center of the experiment was taken as 43.48 deg N, 63.34 deg W. This position was the approximate center between two of the buoys, and used as the center for spherical to planar map transformation of the GPS coordinates. The drift radius of all buoys was approximately 150 m (Figure 4).

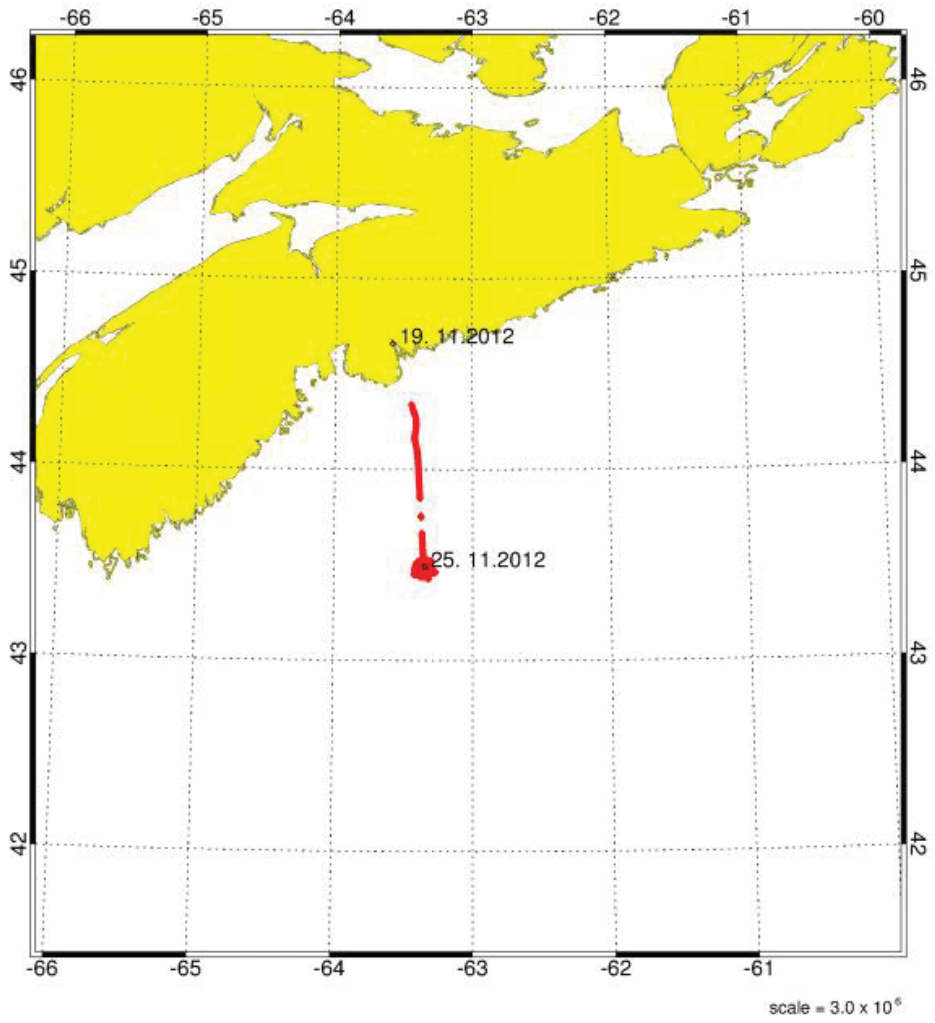

Figure 1: Geographic location for Q348. The vertical component is the transit track, and the circular region is the measurement grid.

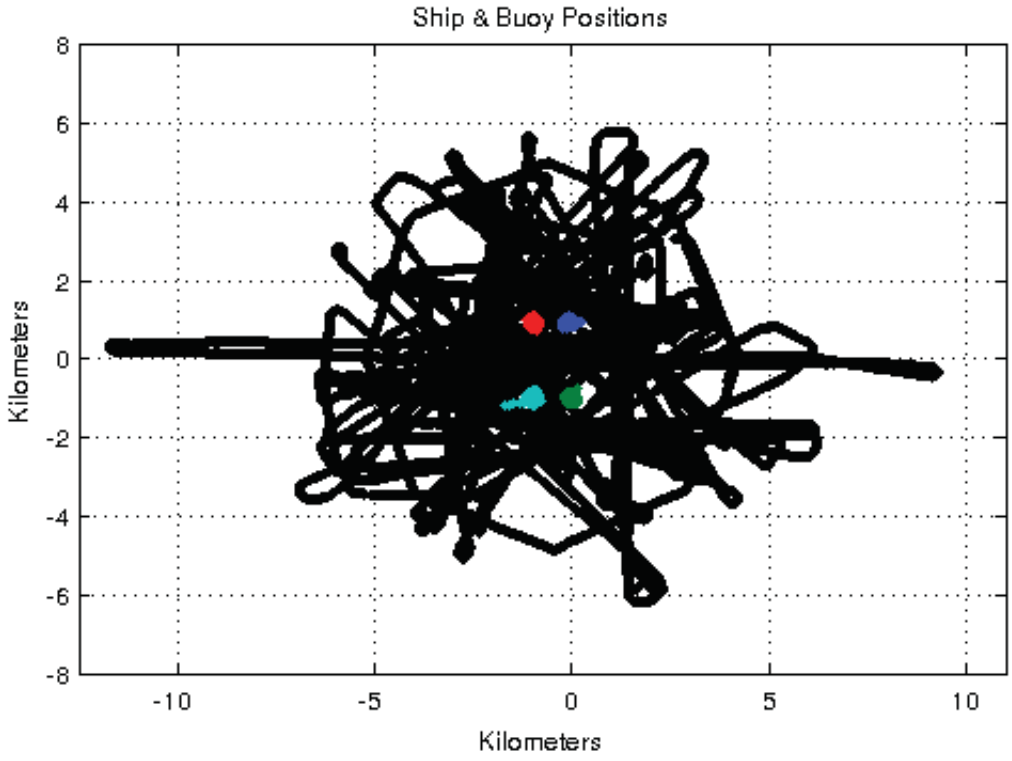

Figure 2: Overview of the geographical layout. Quest [black] repeated regular patterns circumnavigating and bisecting the buoy positions [colored]. Units are kilometers from the central position of -63.34 E, 43.48 N.

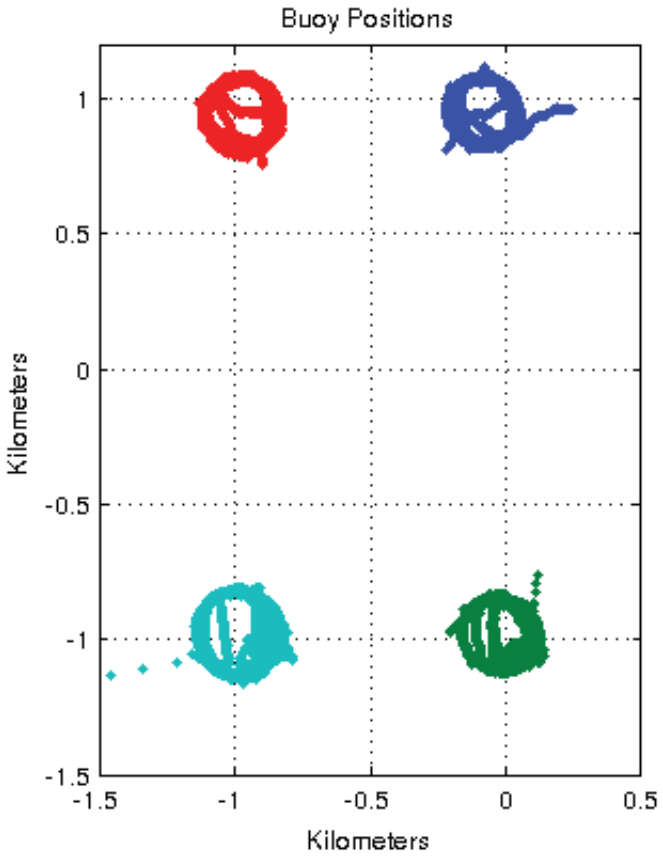

Figure 3. Buoy positions during the trial. All four buoys drift within approximately the same radius of their individual moorings. The geographic center of -63.34 E, 43.48 N (x,y = 0) for this analysis was taken as halfway between the two eastern buoys.

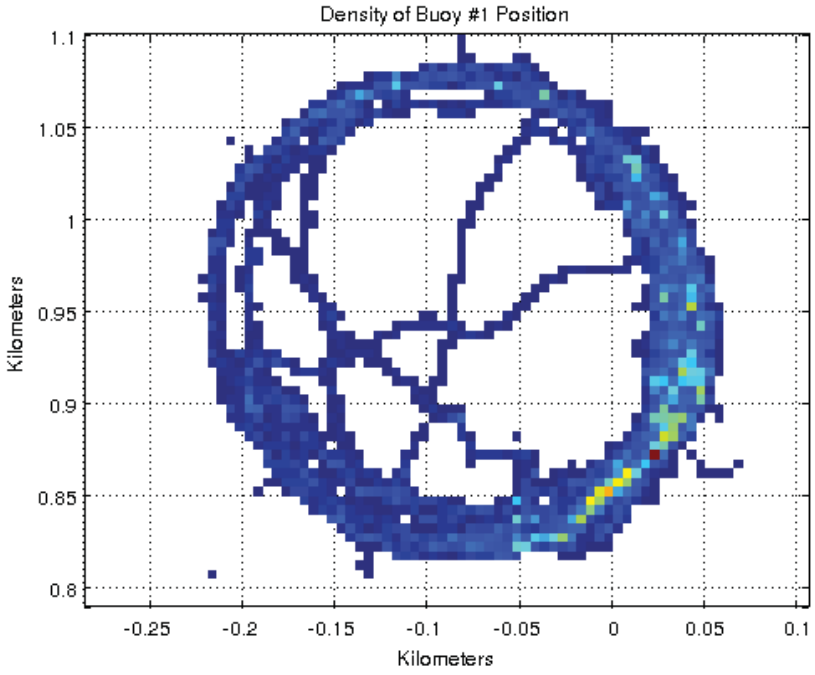

Figure 4: Drift Radius of Buoy #1. The drift radius was ~ 300 m. Positions are plotted as probability density. Similar drift radii were observed for all four buoys.

3.2 RADAR SETUP

As concluded during OWS-Q341, the older existing Furuno radar was of insufficient quality for wave measurements, primarily due to the small antenna size. The existing Decca radar was borderline acceptable, providing usable data only a fraction of the time. Thus a new Furuno model 2117 radar was installed for Q348.

A contractor performed the initial setup of the new Furuno 2117 radar, which was calibrated for range and angle to a known landmark. The reference used was a large tower on the bridge crossing the channel, with GPS and GIS data from the on-board plotter. The Furuno 2117 was connected to the WaMoS II via slave jumper #617 within the remote-processing-unit (RPU). This jumper is independent, i.e. prior, to nearly all configuration changes that occur on the MU-190 display unit. Thus the WaMoS II sampling occurs without user-introduced variation. It was noted that the range and angle offsets set on the MU-190 display unit did affect the WaMoS II data orientation, i.e. its spatial alignment.

3.3 WAMOS II SETUP

The installation of the WaMoS II system occurred on 2012/11/16 and 2012/11/19. The work mainly consisted of adapting the existing hardware and software aboard Quest. For this trial, the single image recording software was installed. This version of the WinWamoS software differs from the standard version, in that it creates a continuous series of complete radar images at a uniform rate. The standard version operates in a burst mode; sampling, pausing for analysis (1-2 min), then repeating. For scientific applications, the single image version is preferable due to its lack of data gaps.

The following software versions were used:

- WaMoS server 1.0.0.4a (stores the radar raw data)
- WaMoS client 1.0.0.22 (prepares analysis and displays the results)
- Calcwave 3.4.3 (calculates and analyses wave spectra)

Note that the same software versions were used for Q341, to aid in data comparison. Additional software for deriving sea surface elevations was used in post processing after the trial.

With the goal of maximizing co-location of WaMoS II data with the buoys, the operational settings were modified for maximum range and resolution. Increasing the range of WaMoS II increases the probability the buoy will exist within the WaMoS II measurement field for a given geometry. Increasing the resolution increases statistical confidence and the probability of resolving physical signals.

3.3.1 Operational Constants

The operational constants are independent properties of the data set, i.e. cannot be modified after data creation. WaMoS II allows for varying the sampling resolution in multiple dimensions. Compared to Q341, the dimensional resolution was increased as following:

Trial	Q348	Q341
Maximum Range (m)	3072	2160
Minimum Range (m)	0	240
Range Resolution (m)	3.0	7.5
Angular Resolution (m)	0.025	0.050
Image Interval (s)	2.5	2.2
Sampling Rate (MHz)	50	20
Range Samples	1024	256/512
Angle Divisor	1	2
Data Rate (GB/day)	420	58

Note the increases to dimensional size and resolution result in a significant increase in data rate.

Operational constants inherent to the radar:

- The radar antenna rotation interval determines the image interval.
- The radar Pulse Repetition Frequency (PRF) and antenna rotation interval determine the maximum angular resolution.

Operational constants inherent to the WaMoS II:

- The Sampling Rate determines the Range Resolution*.
- The Sampling Rate combined with Range Samples determines the Maximum Range.
- The Minimum Range is an adjustable setting.
- The Angle Divisor (optionally) decimates the Range Resolution by a factor

*The WaMoS II Sampling Rate determines the range resolution to the point where it is no longer the limiting factor. The Minimum Range Resolution is not determined by the WaMoS II, rather by the pulse length of the radar. Most radars have a 70 ns pulse length, corresponding to a range resolution of 10.5 m and a sampling rate 28.6 MHz.

3.3.2 Analysis Variables & Setup Logistics

The analytic variables are not dependent on the data set, and may be adjusted for optimal results.

Trial	Q348	Q341
Image Count	32	32
Spatial Count	512x512	128x128
Spatial Size (km^2)	2.4	0.9
Analysis Regions	5	5
Frequency Resolution (Hz)	0.012	0.012
Maximum Frequency (Hz)	0.35	0.35

The size of the cartesian analysis areas doubles, and the resolution increases from 128^2 to 512^2. During the initial day of the trial, a significant improvement in spectral agreement between WaMoS II and the real-time buoy spectra was observed when switching to higher WaMoS II analysis resolution. At a resolution of 128^2, ocean spectra exhibited 6 modes, 3 mirrored pairs, which were clearly non-physical. Upon enabling 512^2 resolution, the ocean spectra reduced to a single well-defined mode in close agreement with the Triaxys buoy. The higher resolution was enabled for the remainder of the trial.

The WinWaMoS software periodically adjusts the PC clock using time obtained from NMEA. On the initial day of the trial, NTP software was running, which also synchronizes the PC clock using the network time protocol. Running both processes simultaneously introduced large, 1-2 sec, variations in PC clock time. After this was identified, the NTP software was removed.

During the trial, inspection of the recorded data rate showed that the expected sample period of 2.5 seconds was occasionally exceeded, and/or the analysis was being interrupted. This same situation

had been noted in OWS-Q341. The cause was frequent network access to the data drive combined with constant i/o activity from the WaMoS II software. The solution was to isolate the data drive from the network, and provide the necessary real-time data via a copy operation to a network share. Furthermore, all non-WinWaMoS critical processes which access data were routed to a second hard drive. This issue was found and fixed early in the trial.

During the peak of the swell event, the WinWaMoS software occasionally did not process data products. Data recording was not interrupted. The cause was traced to extreme roll events, which seemed to induce an "EPFS" error on the Furuno display unit MU-190, and corresponded to a skipped processing step on WinWaMoS, and a rotation rate error display. The radar image data recorded during these events seems unaffected.

3.3.3 WaMoS II Range and Angle Calibration

This section refers to the range and angle calibration of the WaMoS II data. Two sets of these calibration parameters exist, which mutually combine to create a single effective calibration. The first is within the radar, the second within the WaMoS II software. Since these parameters are simple offsets, setting one (or the final), is sufficient. For this trial, the radar-internal values were set by the DRDC-contracted technician responsible for the initial setup of the radar. The method used was a comparison to the vessel's GPS plotter, in both range and angle, to a prominent structure on a nearby bridge. The WaMoS II-internal range and angle calibration values were both set to zero for the duration of the experiment.

The calibration data files were recorded on 2012/11/19 and 2012/11/20. At this time, Quest was in harbor and the radar data shows structures of the port and channel (Figure 6). This is an ideal situation for calibration, as the vessel is not moving, and relational geometry can be checked from an external source. To improved GPS positional accuracy, averaging was used. To add confidence two independent estimation methods were used; WinWaMoS and Matlab. Both of these software allow interactive measurements of features within the image. The references used were four structures visible in both the radar image and Google Earth. The accuracy of coordinates taken from Google Earth is unknown.

While Quest was moored at harbor, 8289 GPS position fixes were available for calibration. The mean coordinates were 44.65937721 N, -63.58296600 E. Average offsets were 95.33 m in range and 0 deg in angle. There was good agreement between the range offsets measured in WinWaMoS and Matlab (Figure 9). Matlab consistently estimated ~15 m more than WinWaMoS, suggesting a difference in the range calculation method. The angle offsets showed similar agreement between methods (Figure 8). Their amplitude / variance ratio, i.e. standard deviation, was insufficient to warrant a non-zero calibration value.

Reference Point	Google Earth	WinWaMoS	Matlab
Bridge	570.5	498	486
Ref 1	973.5	877	867
Ref 2	399.1	314	300
Ref 3	2047.2	1950	1926

Reference Point	Google Earth	WinWaMoS	Matlab
Bridge	352.9	350	353.2
Ref 1	342.3	340	343.3
Ref 2	399.1	314	317.9
Ref 3	330.0	329	331.8

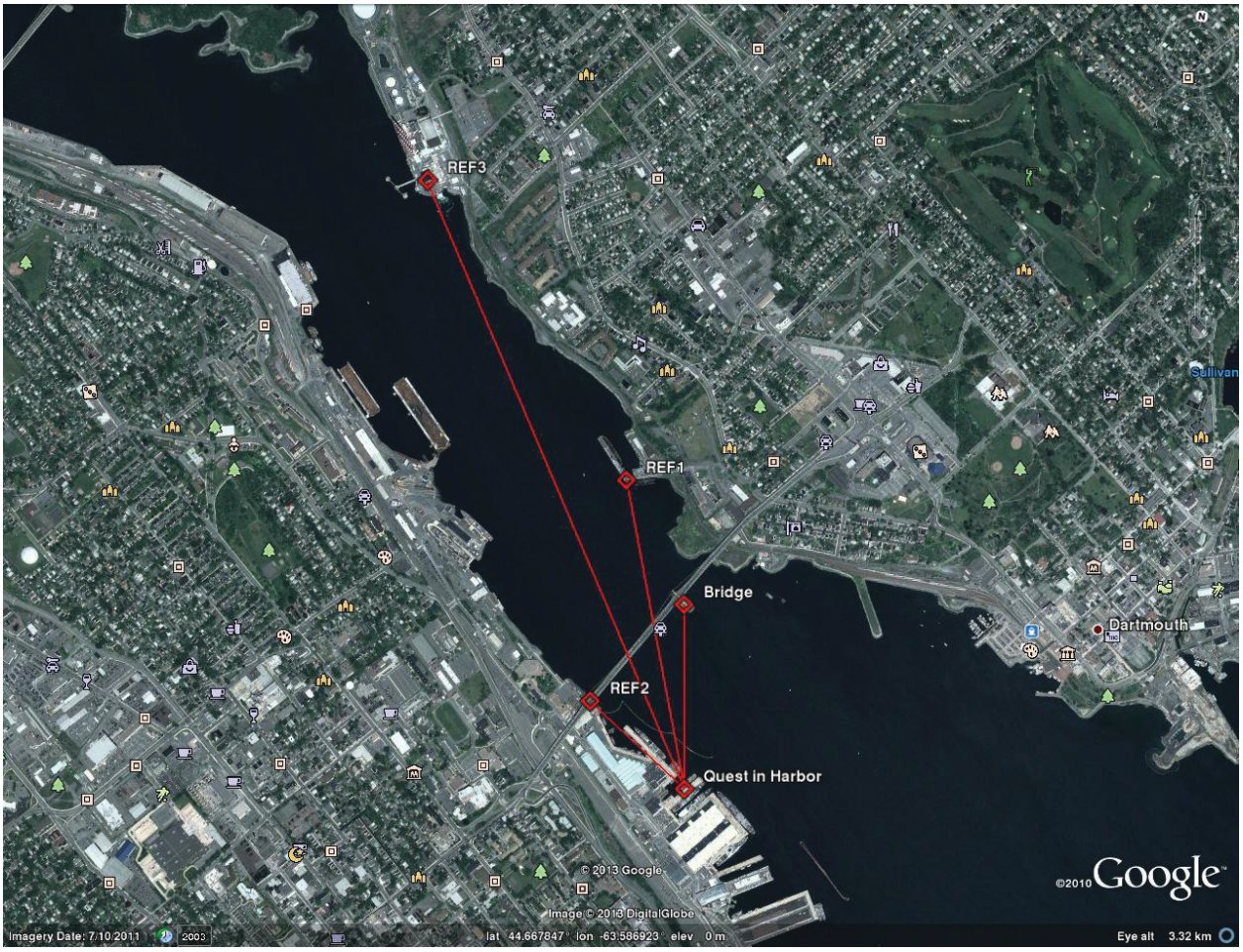

Figure 5: Google Earth data used for calibrating range and angle offsets. Indicated are the four reference locations used for calibration and corresponding vectors.

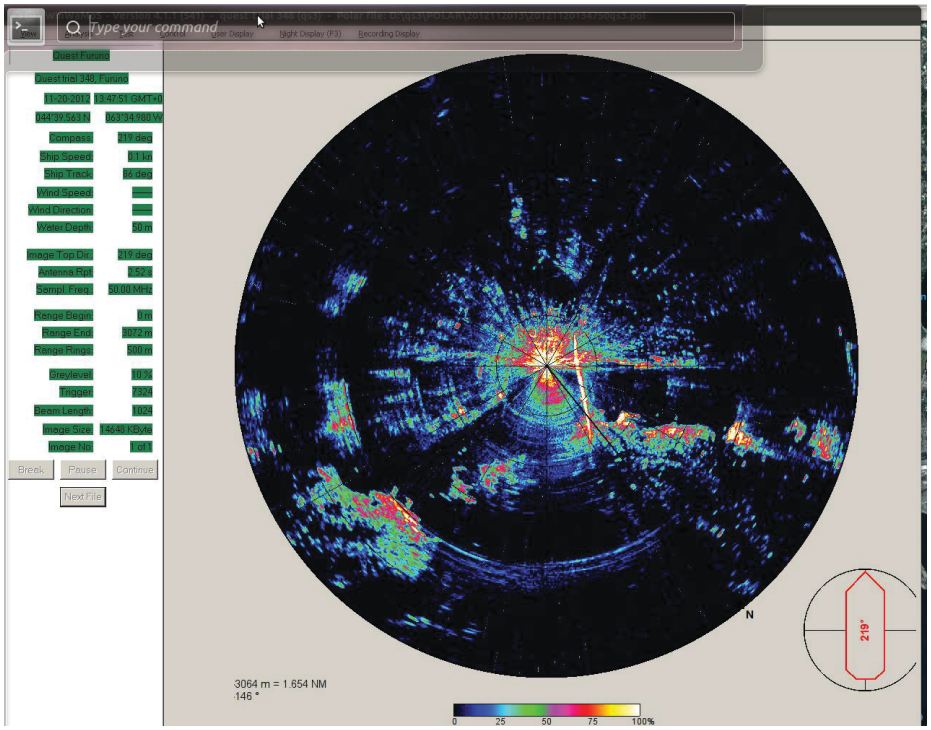

Figure 6: WinWaMoS and radar image used for calibration. The interactive display reports range and angle to targets visible in the image.

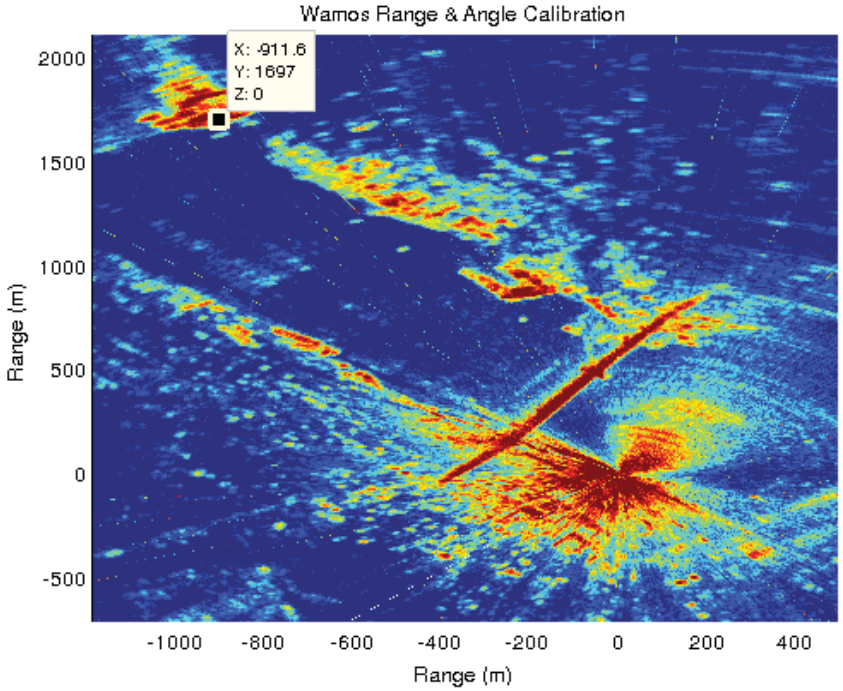

Figure 7: Matlab GUI and radar image used for calibration. The interactive display reports North and East distances, which are converted to range and angle.

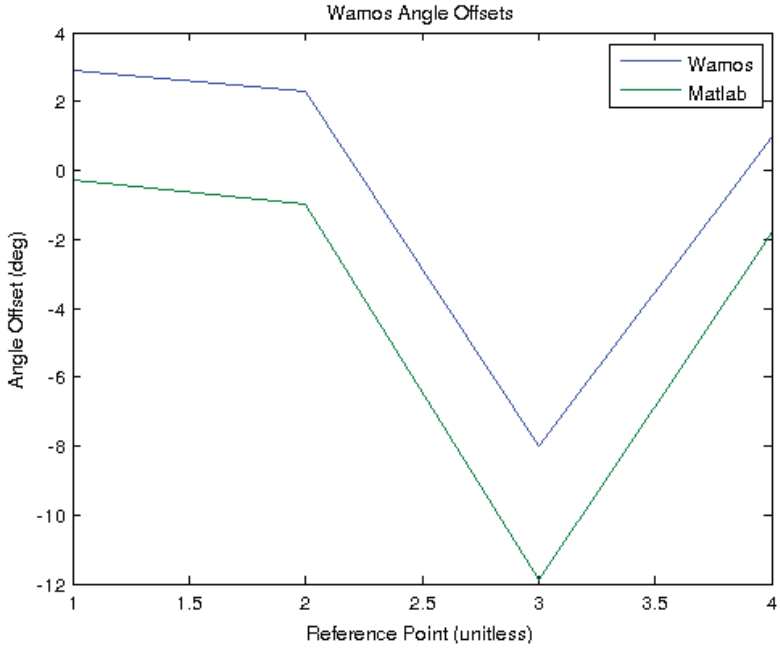

Figure 8: Angle Calibration Results, difference from Google Earth. The empirical results measured in WinWaMoS and Matlab show strong agreement.

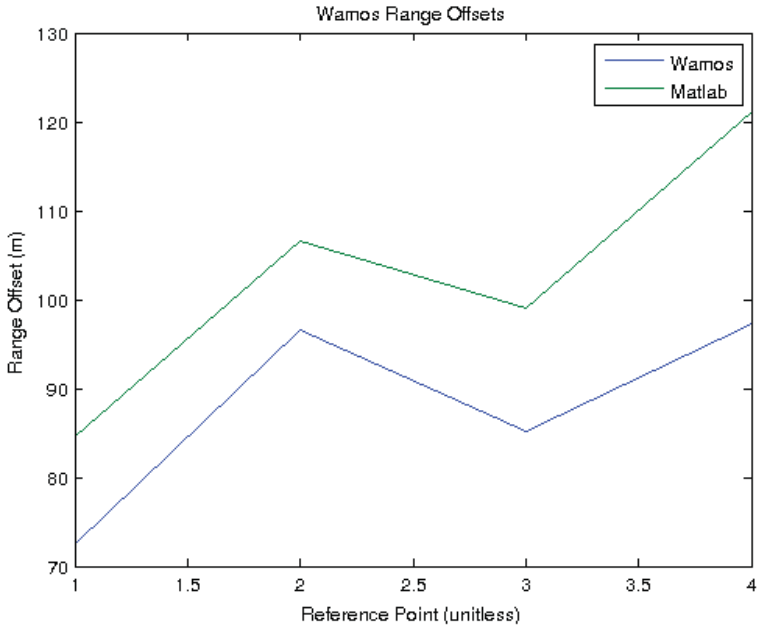

Figure 9: Range Calibration Results, difference from Google Earth. The empirical results measured in WinWaMoS and Matlab show strong agreement.

3.3.4 WaMoS II Calibration, Full-Field

Determination of radar offsets in range and angle based on a few ground control points can lead to false estimates for simple statistical reasons – a false location of one point can have a severe impact on the overall result due to the low number of samples. Therefore, the estimated offsets were rechecked using “ground control structures”. For this purpose, port basin edges were digitized from google maps aerial imagery and overlaid with the geo-referenced radar images (Figure 9).

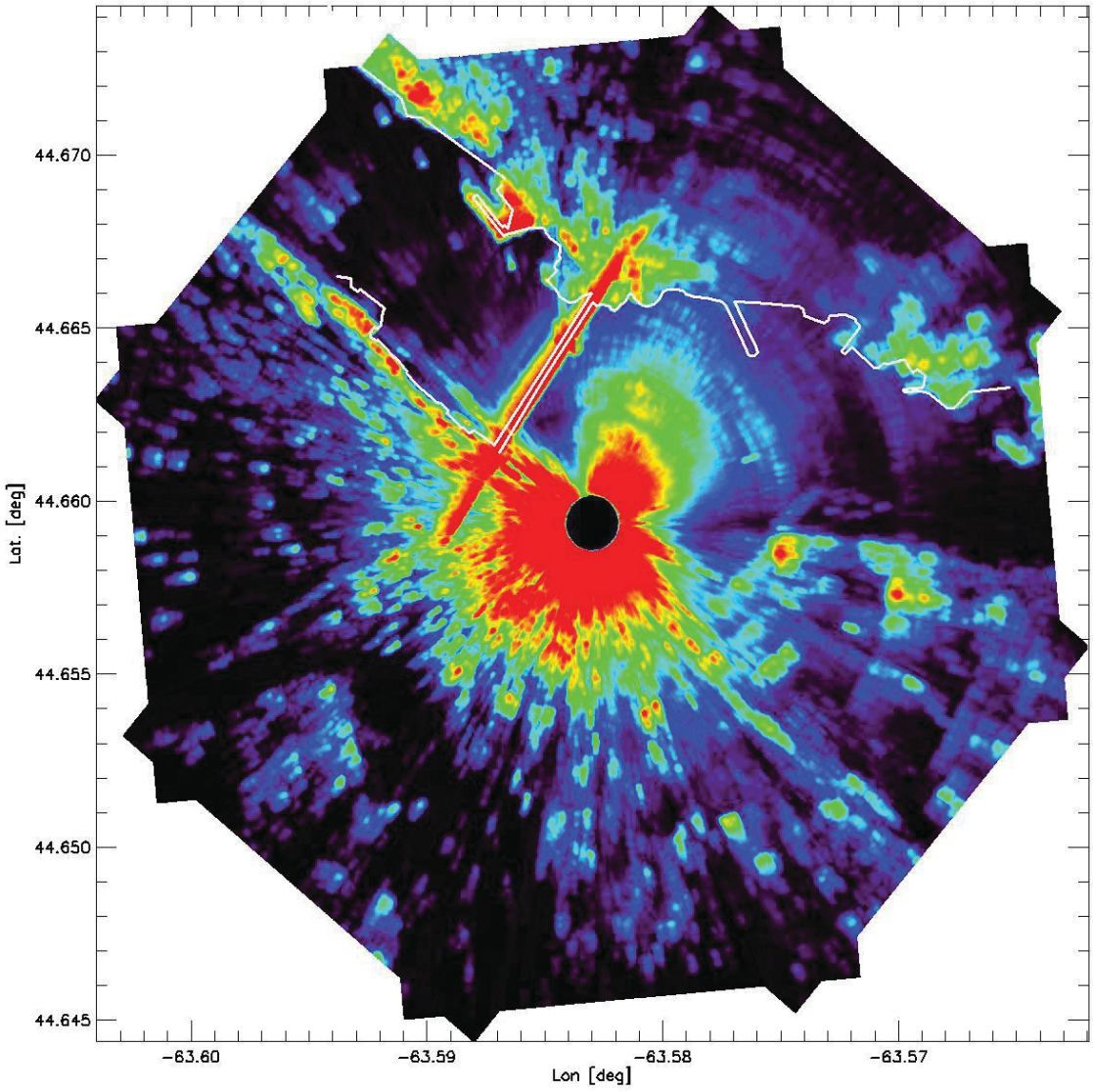

Figure 10 Composite of 9 Cartesian files with overlaid port structures (white). The radar data was collected on 2012 11 20 13:42:18 UTC. The radar backscatter is averaged over 128 images to reduce the noise.

For this calibration, the radar backscatter and geographical positions of nine WaMoS analysis areas were used. These radar cut outs and the assignment of geographical locations are derived with the same software module used for the wave elevation analysis. Thus, the comparison described here helps to estimate the accuracy of locations to be expected for the sea surface elevation maps.

The chosen areas are equally distributed over all look directions, for each pixel in the area the geographical positions were stored, applying the offsets described in Section 3.3.3. To reduce the noise floor in the data, an average over 128 images was used. The white line overlaid to the radar data indicates the edges of a bridge and part of the port basins.

When comparing port structures visible in the radar to the overlaid port edges, a good visual match of the structures is observed. In some areas, the look direction of the radar are obviously blocked. Here, no radar signatures of the port structures are visible. Overall, this full-field calibration is in good agreement with the calibration offsets given in 3.3.3.

3.3.5 Sea Surface Elevation

The WaMoS II inversion module was used to create sea surface elevation maps as a product of this analysis. Details of the used methods for this investigation and criteria for data selection are described in Section5.1.

3.4 Reference Sensors

3.4.1 NMEA

For this trial, DRDC setup multiple (N ~ 5) laptops connected to sensors for broadcasting the NMEA sentences over Ethernet, encapsulated in UDP packets. Additionally, the NMEA: UDP software pre-pended timestamps to all NMEA sentences. This added a time basis to all sensors that did not have a clock source, e.g.

2012-11-20T15:43:31.796,$GPZDA,154330,20,11,2012,04,00*4F

Where “$GPZDA,154330,20,11,2012,04,00*4F” is the NMEA sentence and “2012-11-20T15:43:31.796” is the pre-pended timestamp, corresponding to the clock of the laptop, hereafter referred to as the PC timestamp. This particular sentence type, $GPZDA, has an internal timestamp “154330” which translates to 15:43:30. The PC timestamps have millisecond precision. All of the NMEA timestamps have second precision. All sentences were transmitted at a rate of 0.5 Hz, except for the compass, which was 10 Hz.

For this analysis, the NMEA sentences of interest refer to the GPS time and position, and compass bearing. The WinWaMoS software acquires NMEA data which it uses to apply bases to the recorded

radar images. Additionally, it logs the NMEA sentences to a separate file with pre-pended WaMoS II PC time, similar to above. DRDC also logged NMEA data, which were made available for this analysis.

3.4.2 Oceanographic Buoys

DRDC deployed four Triaxys wave buoys for this trial. All were equipped with radio for transmission of real-time data to Quest. Following the recommendation from OWS-Q341, the buoys were equipped with additional external GPS sensors operating at 1 Hz. The GPS *position* data from the buoy internal sensor was not used for this trial due to its low data rate. The buoys provided both raw 3-dimensional displacement timeseries at 6.7 Hz, and summaries of processed oceanographic parameters; including significant wave height, peak wave period, and peak wave direction. The buoys operated in burst sampling mode, 19.4 min on (N=7761 samples) followed by 10.2 min off. A primary goal of this analysis was to create WaMoS II-derived sea surface elevation maps which will directly correspond to the unprocessed buoy vertical displacements. This is a comparison of direct measurements. It is prohibitively difficult to determine the accuracy of the buoy time basis, lacking a known *in-situ* reference, and thus no modification was made. Since the buoys have an internal GPS sensor, it is reasonable to assume their time basis is the same as the other GPS reference sensor used in this trial aboard QUEST.

4 Bases Results and Sea State Parameters

4.1 Data Availability

Gaps or losses in the data availability may be caused by a variety of factors. Examples include user control, hard drive limitation in free space and bandwidth, or other computer resource limitations preventing the WaMoS II software from executing at the desired rate. Incorrect configuration or the radar or WaMoS II may prevent data acquisition. The setup for this trial was exceptional in the choice of high-resolution settings. A total of four 1 TB external USB 3.0 hard drives were used, with a final data size of 2.6 TB. The total number of radar images recorded was 209152. Total availability and continuity of radar data was quite good, with only one significant gap of approximately 6 hours on 2012.11.23. WinWaMoS performs the function of merging NMEA data streams with the recorded radar images. Inspection of the radar images showed near-complete availability for the essential NMEA data.

Time	99.99952%
Compass	99.99761%
Latitude, Longitude	99.54244%

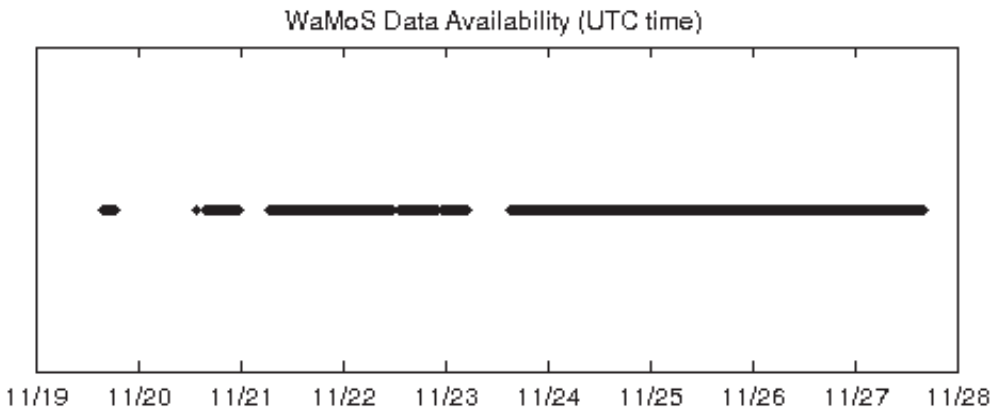

Figure 11: WaMoS II data availability. One significant gap occurred on 2013.11.23 for approximately 6 hours. Prior gaps are during instrument setup in harbor, before the trial.

For analyses, the radar images are processed in sets of 64 images, 2.5 s * 64 = 160 s. This is a fundamental property of the WaMoS II processing method, which uses Fourier transforms in space and time. Since the Fourier transform requires monotonic and continuous series, gaps within the available data preclude the possibility of analysis. Actual sampling intervals will vary, depending on radar and software performance. Assuming perfect software performance, the sampling interval is equal to the antenna rotation time, i.e. complete images are recorded and time-stamped synchronous with the antenna rotation. For this trial, observed sampling intervals matched the expected 2.5 s, with variation (Figure 12). The period from 11.25 to 11.26 is identified as having extreme variation in antenna rotation time. During this period, the WinWaMoS software consistently reported and warned of this variation. Similarly, the Furuno radar display reported errors on an unknown code. An inspection of the WaMoS II hardware and software operation revealed no cause. Also, this period coincided with the most extreme waves encountered during the trial (Figure 41). It is hypothesized that extreme waves induced ship motion, and the resulting accelerations affected the antenna rotation rate. A two-dimensional histogram, i.e. density scatter plot, suggests the possibility of a relationship between Hs and rotation rate (Figure 14). Above an Hs of ~ 3 m, the rotation rate is observed to vary.

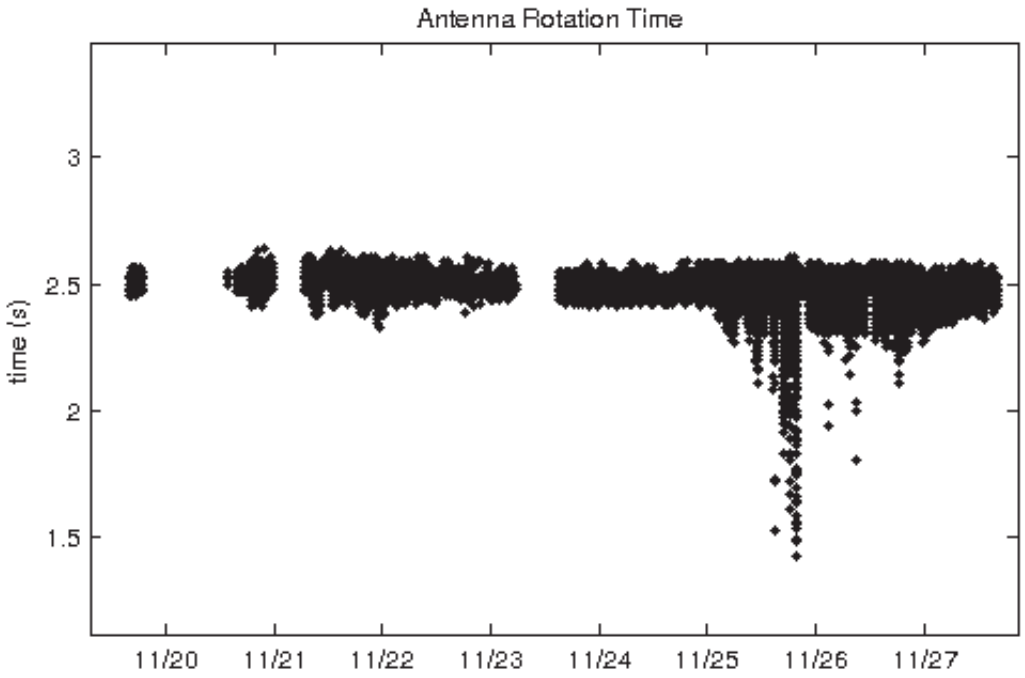

Figure 12: Antenna Rotation Time, or equivalently, WaMoS II Sample Rate. The expected 2.5 s interval was observed for the duration of the trial, with occasional large differences. These differences corresponded to the period of greatest Hs.

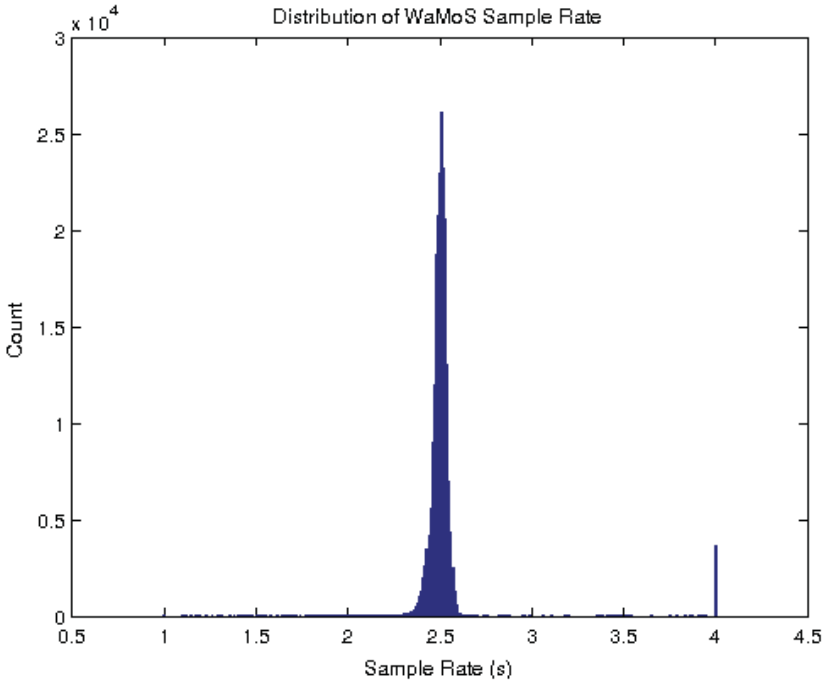

Figure 13: Distribution of WaMoS II Sampling Rates. The expected interval was 2.5 seconds per image. Actual intervals will vary depending on radar and software performance.

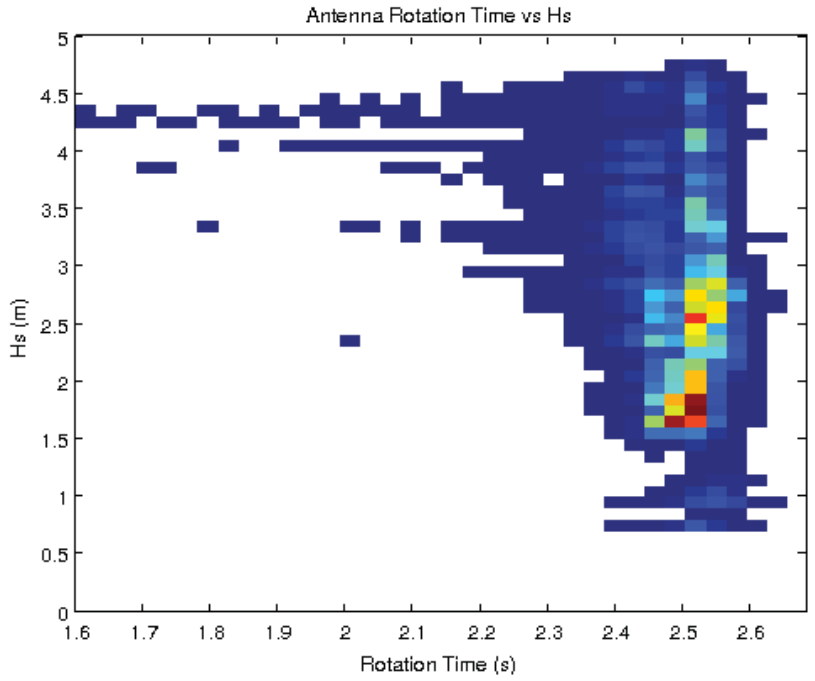

Figure 14: 2-Dimensional Histogram of Rotation Time and Hs. No clear relationship exists between rotation time and Hs. Above an Hs of ~ 3 m, the rotation rate is observed to vary.

As mentioned in Section 3.3.1, the combination of range samples (FIFO) and sampling rate determines the maximum range. The FIFO was reduced for a period of approximately two days, decreasing the range from 3.2 to 2.4 km. This was done to preserve limited available hard drive space, and chosen to coincide with a period of lesser Hs.

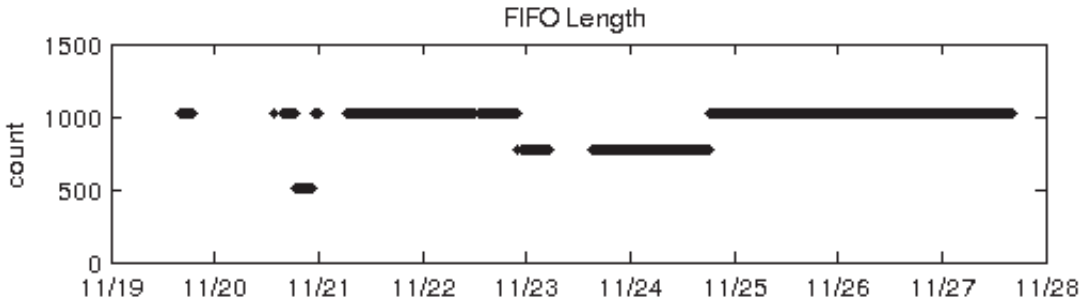

Figure 15: Distribution of WaMoS II Sampling Rates. The expected interval was 2.5 seconds per image. Actual intervals will vary depending on radar and software performance.

4.2 BASES

WaMoS II requires external sensors, i.e. NMEA sources, to provide time and space bases. These can be supplied via serial interface or Ethernet protocol. The required inputs are time, latitude, longitude, and compass bearing. WinWaMoS records radar images as mixed text (ASCII) and binary formatted files. The metadata section, referred to as the "header", is text formatted with the operational constants and other necessary parameters. The goal of the following analyses is to establish shared bases between the WaMoS II data, the external inputs (GPS time, position, and compass), and the reference buoys.

4.2.1 NMEA Time

The most accurate time basis for this trial was GPS. Of the NMEA sentence types, five contained an internal time basis. Using the full duration of the trial and taking all unique timestamps to be a set, set membership for 4 of the sentences is greater than 91 %, with type GPBWR comparably sparse. Excluding GPBWR, this indicates the associated sensors were sampling at nearly the same moment, for the same duration. Consequently, linear interpolation to a shared time basis in not likely to cause spurious effects. Note that set membership means numerically identical. GPZDA and GPRMC are known to be sentences broadcast from GPS time receivers. GPGGA and GPGLL have an unknown source. GPBWR will be ignored.

GPZDA	92.89 %
GPRMC	91.59 %
GPBWR	16.90 %
GPGGA	92.05 %
GPGLL	93.45 %

Given NMEA sentences with internal and PC pre-pended timestamps, a comparison of time differences was made, i.e. latency. Probable causes of latency include time offsets between clocks, or software delay. The term latency does not imply a constant difference.

The following inspection of latencies exists to illustrate a single argument; for NMEA sentences without an internal (and accurate) timestamp there may be variation in the appended time base. The importance of this statement, and relevance to this trial, is in regards to the compass heading NMEA sentence (Section 4.2.6).

The GPZDA latency exhibited 2-30 seconds differences throughout the trial (Figure 16). There were two regimes; one period from 11/21 to 11/25 where the latency was ~2 s, and another from 11/26 to 11/28 where the latency increased to ~30 s. Another interesting feature of the GPZDA latency is the semi-regular pattern (Figure 17). PC clocks do not drift at such extreme rates. The latencies for each of the 5 NMEA time sources differed (Figure 18). Furthermore, the relative latencies varied in time, indicating independent error sources. Since most of the variation is shared, a carefully chosen average removes most of the variation, to within < 2 s, and nominally to < 0.5 s (Figure 19). This indicates two sources of error; one that is shared between the NMEA types and of greater magnitude, and another that is unique to each NMEA type and of lesser magnitude. It is hypothesized that the shared latency source is related to the NMEA distribution system prior to the laptops, and the unique latency source is related to UDP broadcast software on the laptops.

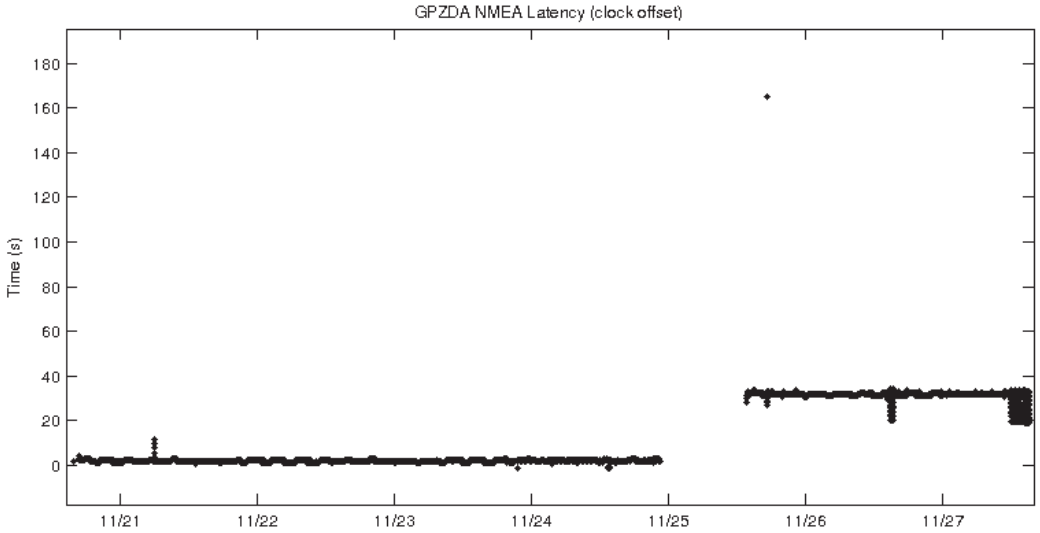

Figure 16: GPZDA latency timeseries. Two regimes were observed; one period from 11/21 to 11/25, and another from 11/26 to 11/28. Mean latencies were approximately 2 and 30 seconds, respectively.

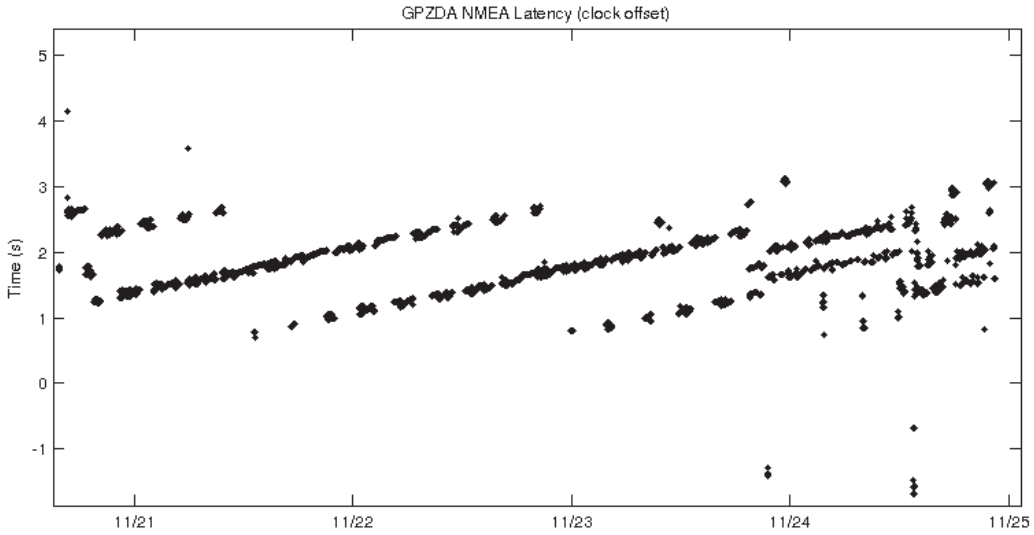

Figure 17: GPZDA latency timeseries subset from 11/21 to 11/25. A semi-regular pattern of variation is observed from 1 to 3 s.

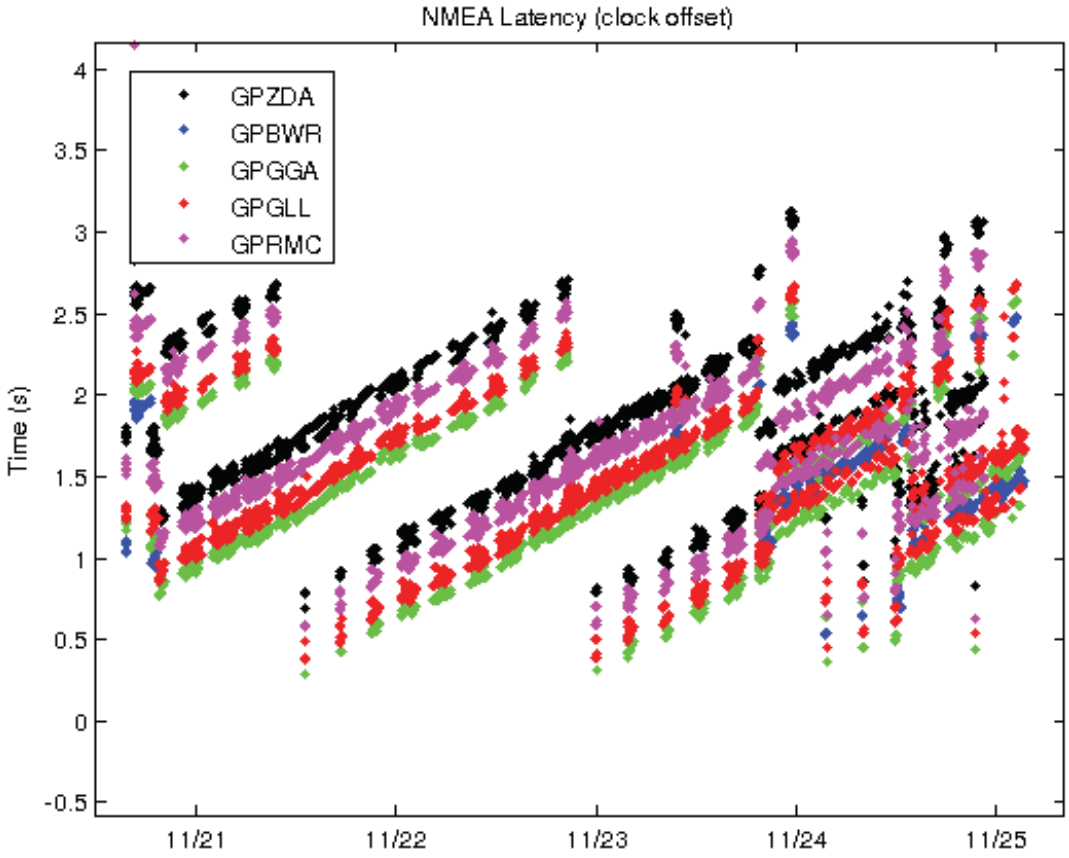

Figure 18: NMEA latencies for all time bases. Each NMEA type exhibited a different latency function. Shown is a subset of the trial from 11/21 to 11/25.

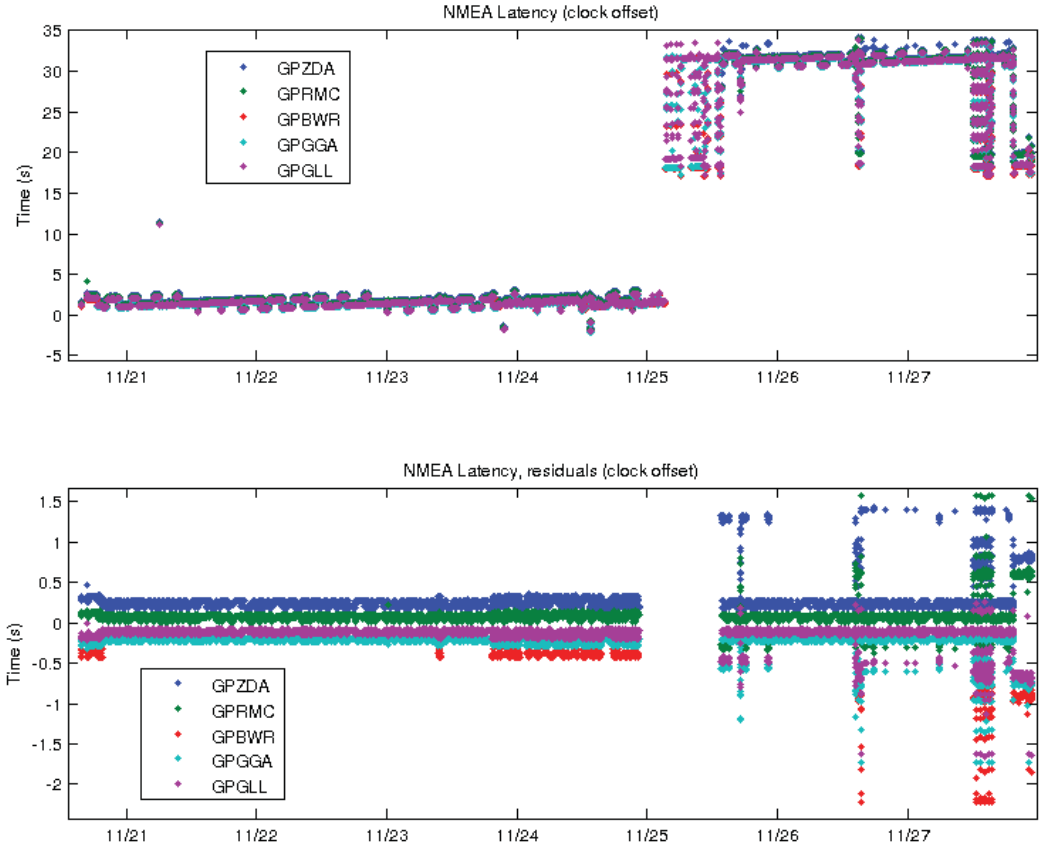

Figure 19: NMEA latencies. [Top] Latency timeseries for each NMEA type. The majority of variation is shared between the types. [Bottom] After removal of shared variation, latency differences remain between the NMEA types.

Taking the hypothesis that NMEA:UDP broadcasting software causes latencies in the PC timestamp, the use of multiple independent PCs will create unique latencies for each source. Thus, for a comparison between any two sensors, the basis variation will be double. Ideally, a single PC should be used. From this analysis it is concluded that PC timestamp latency is an error source for NMEA sentences which do not have an internal timestamp. For such sentences, the unknown latency function may be estimated from a comparable NMEA source with internal timestamps, although the efficacy of such a method is unknown. For this trial and at best, application of this method will result in residual latencies of nominally +/- 0.5 s (Figure 19).

4.2.2 NMEA Position

With the time basis quantified, it is then possible to construct a position basis, i.e. latitude and longitude, as a function of the time basis. The 3 NMEA position sentences (GPRMC, GPGGA, GPGLL) all have internal timestamps, which is to be expected for GPS NMEA sources. Since GPS provides both time and position measurements, it was chosen as the reference system for subsequent analyses.

The position basis analysis method is similar to the time basis, using complex numbers to represent the 2-dimensional position vector. Creating a set of the unique positions from all sentences, and finding percent membership of this set yielded approximately equal coverage. We can conclude that these sentences contain the same information, i.e. > 90% set union. Furthermore, the equality extended to position as a function of time; $\boldsymbol{x} = f(t)$, where t is the time basis from the preceding section. Thus it was trivial to combine the 3 types into a single position basis (Figure 20).

GPRMC	91.67 %
GPGGA	92.14 %
GPGLL	93.53 %

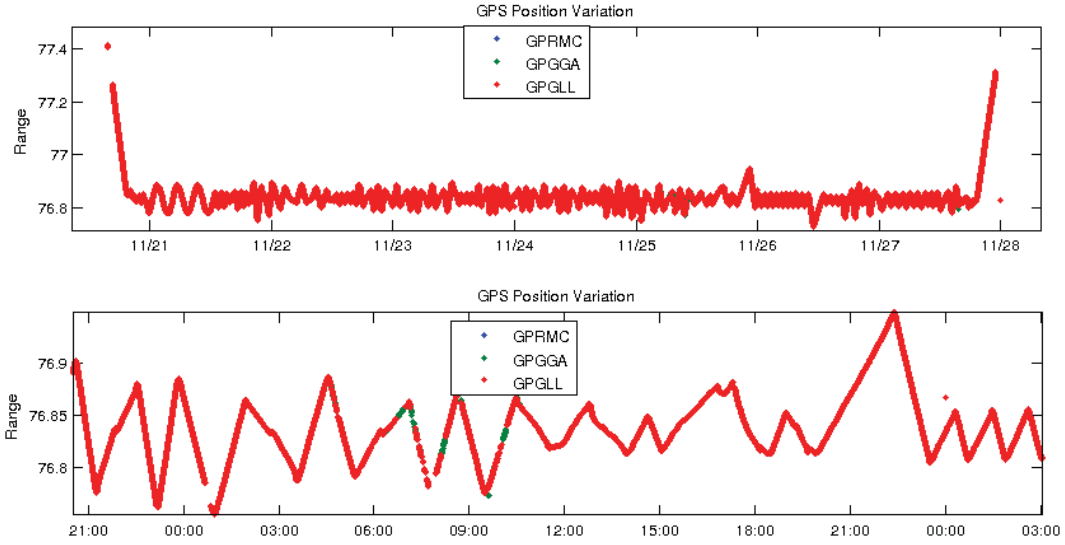

Figure 20: GPS position timeseries. [Top] GPS range for the duration of the trial. [Bottom] A subset of the trial duration of approximately 1 day. The 3 position types have identical values, with slight differences in availability.

Accuracy of the GPS positions was investigated using position values recorded during an interval of known constant position, i.e. when the vessel was in harbor. Consequently, any variation in position can be attributed to instrumental errors. Using the same data subset from Section 3.3.3, 8289 GPS position fixes were inspected. The maximum radial error was observed to be 30 m, with a nominal (> 90%) radial error of < 10 m (Figure 21). The positional errors were not randomly distributed in time.

Rather, they exhibited coherent “drift” over a time scale of approximately 15 min (Figure 22). This temporal coherence of error prevents simple averaging from reducing the error.

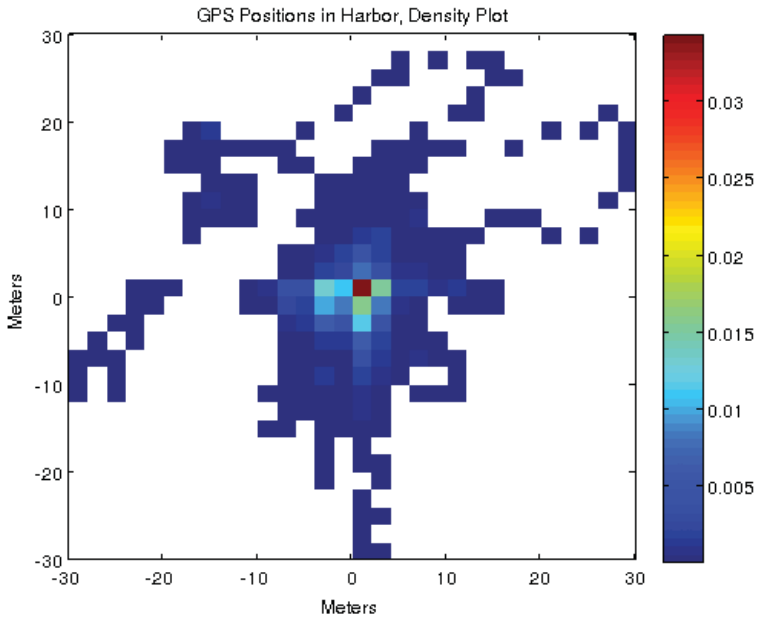

Figure 21. Spatial density of GPS position errors. Errors are taken as difference to an arbitrary (mean) location, known to be constant. Radial error occasionally reaches 30 m, with a nominal error of < 10 m.

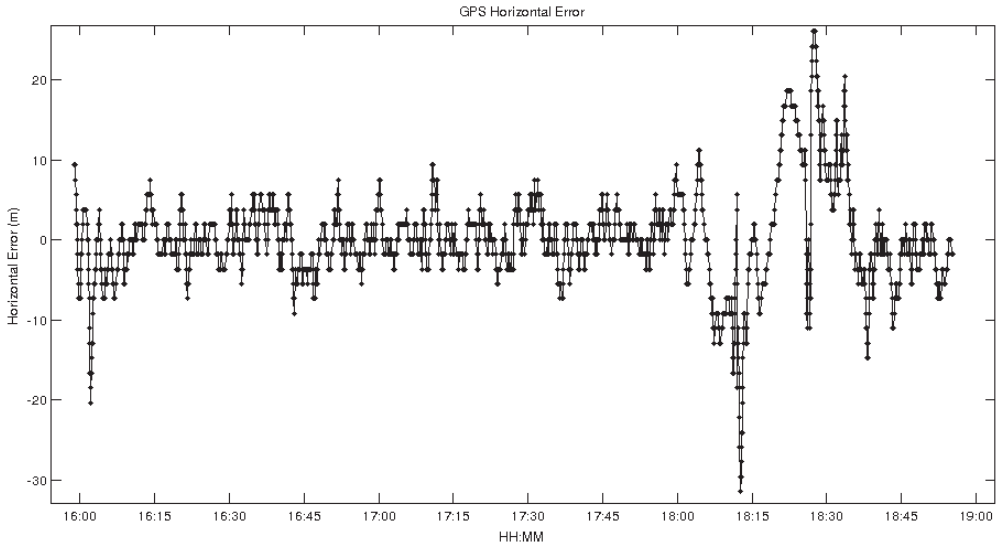

Figure 22. Horizontal (east) component of GPS position error as a function of time. The timeseries exhibits coherence at several time scales.

4.2.3 NMEA Compass

A note on directional statistics. The fact that 0 degrees and 360 degrees are identical angles precludes the use of standard (non-periodic) statistical methods on angular data (periodic). This analysis applies the method of complex numbers to calculate statistical properties of compass data.

The secondary necessary spatial basis is compass heading. For spatial colocation at a range of 500 m, a minimum of 1 degree of error is desired. Since NMEA type GPRMC was identified in the two preceding sections as the reference system, it is used as the reference for comparing to the other two compass sentences GPVTG and HEHDT. Both GPRMC and GPVTG are GPS-derived compass headings, as opposed to a true magnetic measurement.

Comparing the GPRMC and GPVTG timeseries shows strong agreement over hour timescales, but significant variation over minute timescales (Figure 23). GPVTG appeared to be lagging GPRMC, which could be explained by the latency discussion in Section 4.2.1. To show that latency is a variable function of time, two independent measures of latency were made. The first had already been performed in the analysis of Section 4.2.1, as the mean shared latency over the five available NMEA types. This is appropriate for GPVTG, which has no internal timestamp. The second measure of latency was a comparison to GPRMC which is referenced to GPS time. The two methods showed good agreement.

	Mean Latency (s)	GPVTG – GPRMC Latency (s)
2012/11/21 04:44:26	1.3 (0.4 std)	1.5
2012/11/25 18:58:53	31.2 (0.5 std)	31.6

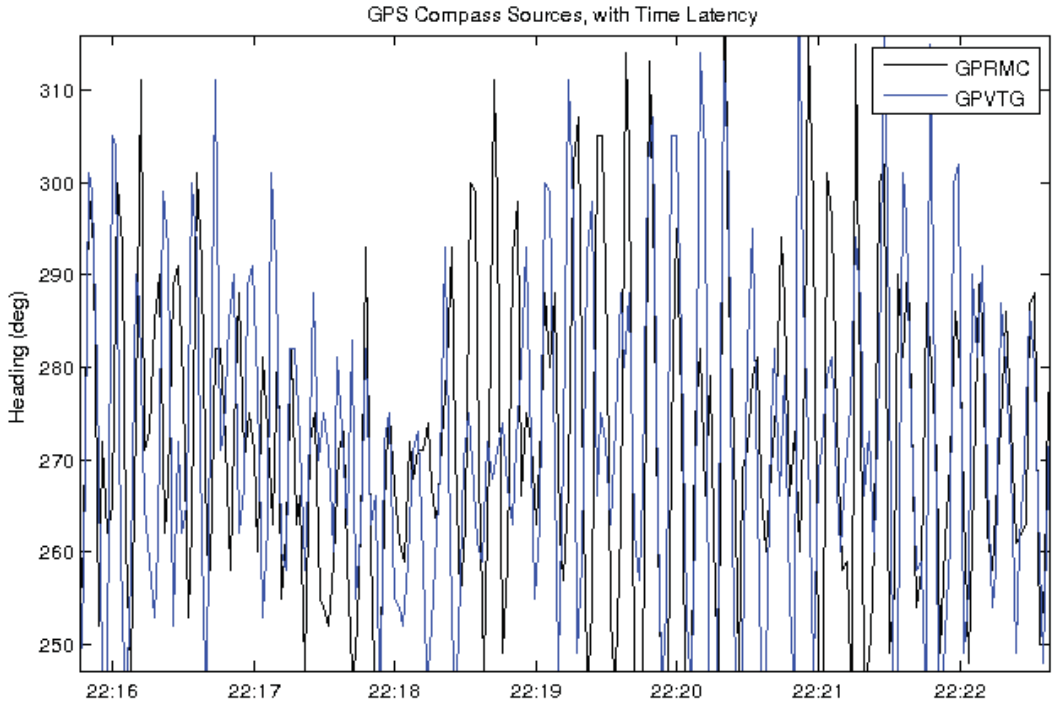

Figure 23: GPS-derived compass headings. GPRMC and GPVTG showed strong agreement over hour timescales, and significant difference over minute timescales.

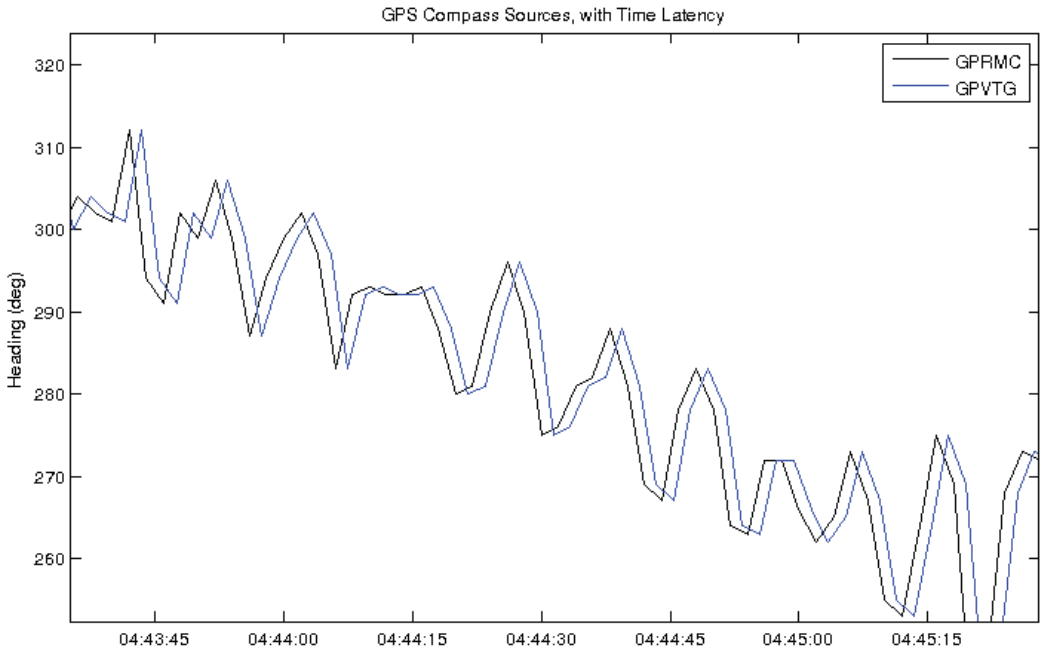

Figure 24: GPVTG to GPRMC Latency on 2012.11.21 04:44:26. Mean PC latency was 1.3 s. Empirical latency was 1.5 s.

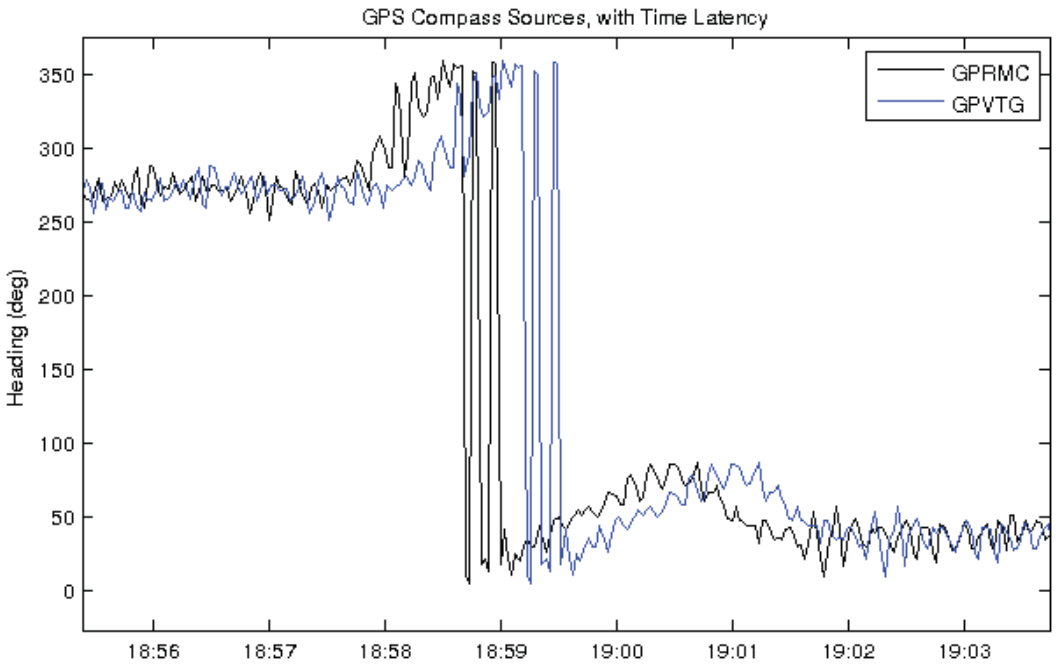

Figure 25: GPVTG to GPRMC Latency on 2012.11.25 18:58:53. Mean PC latency was 31.2 s. Empirical latency was 31.6 s.

For these two GPS compass sources, correcting for latency using the mean latency function increased the rotational complex correlation coefficient from 0.974730 to 0.999751 for the duration of the experiment. Since the mean latency function is only an estimate, complex correlations were calculated for the remaining latency functions, resulting in a maximum of 0.999888 for the GPRMC latency function. Indeed, the data became numerically identical, only differing in data gaps. This indicates the PCs were receiving the same information, but broadcasting it at different times, up to 30 s!

The HEHDT NMEA sentence is from a magnetic compass, at a higher update rate, offering potentially greater accuracy and resolution. Unfortunately the HEHDT sentence does not contain an internal timestamp. Thus an attempt was made to estimate the HEHDT time basis by correlating to the GPRMC signal, and applying the available latency estimates from Section 4.2.1. Maximum correlation was found for no latency correction.

Latency Function	Complex Correlation
No correction	0.973546
GPGGA	0.967247
GPGLL	0.967204
Mean	0.967142
GPRMC	0.967116
GPZDA	0.966967

This may indicate any combination of the following possibilities;

- the HEHDT time basis is closely equivalent to GPS time
- none of the available latency estimates approximate the HEHDT latency function
- the HEHDT and GPRMC compass signals are insufficiently similar to allow for such a comparison

A visual comparison of the two timeseries, at the same dates as the previous example, indicates no relative latency between GPRMC and HEHDT. Thus we conclude that GPRMC and HEHDT are on an equivalent time basis, to the extent of evidence. These two sentences provide the required time and space bases for WaMoS II operation.

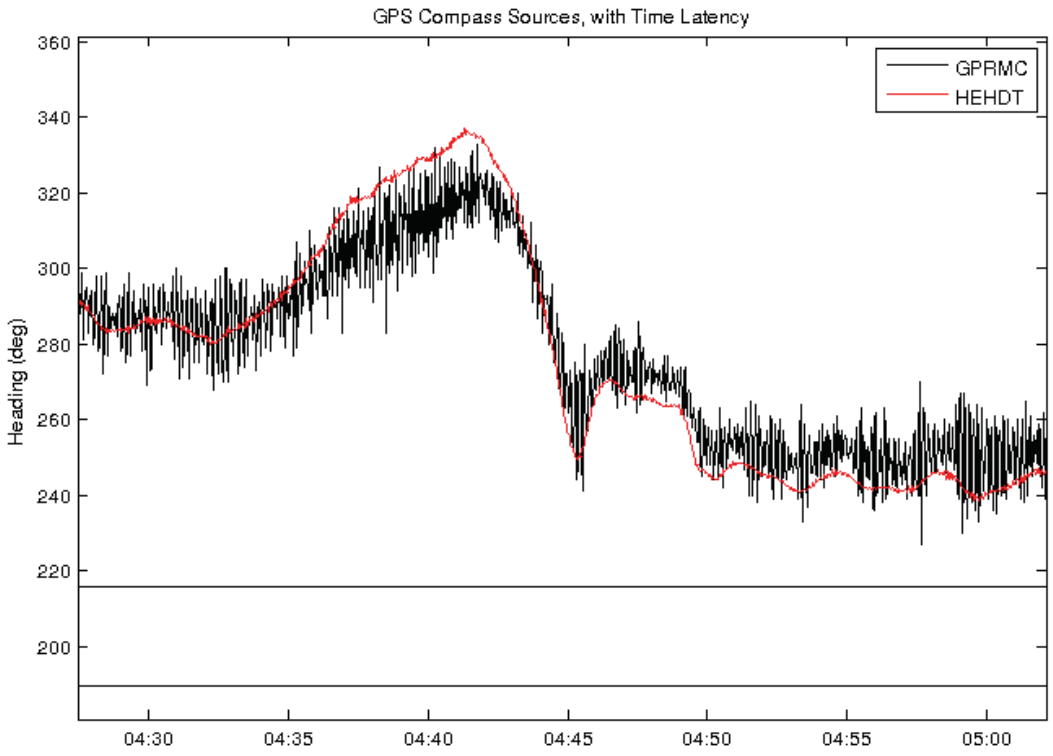

Figure 26: GPS and Magnetic Compass Sources on 2012.11.21 04:44:26. GPRMC and HEHDT are GPS-derived and magnetic compass sources, respectively. Visually, no appreciable lag is seen. GPRMC exhibits high frequency variations of up to 20 degrees.

Regarding signal accuracy, the GPS-derived compass source exhibited continuous high frequency variations of up to 20 degrees. It was assumed these are errors due to the method of estimating heading from a sequence of positions. It is also possible these variations are true signal, as their approximate period of 12 s is close to the dominant wave period (Figure 41).

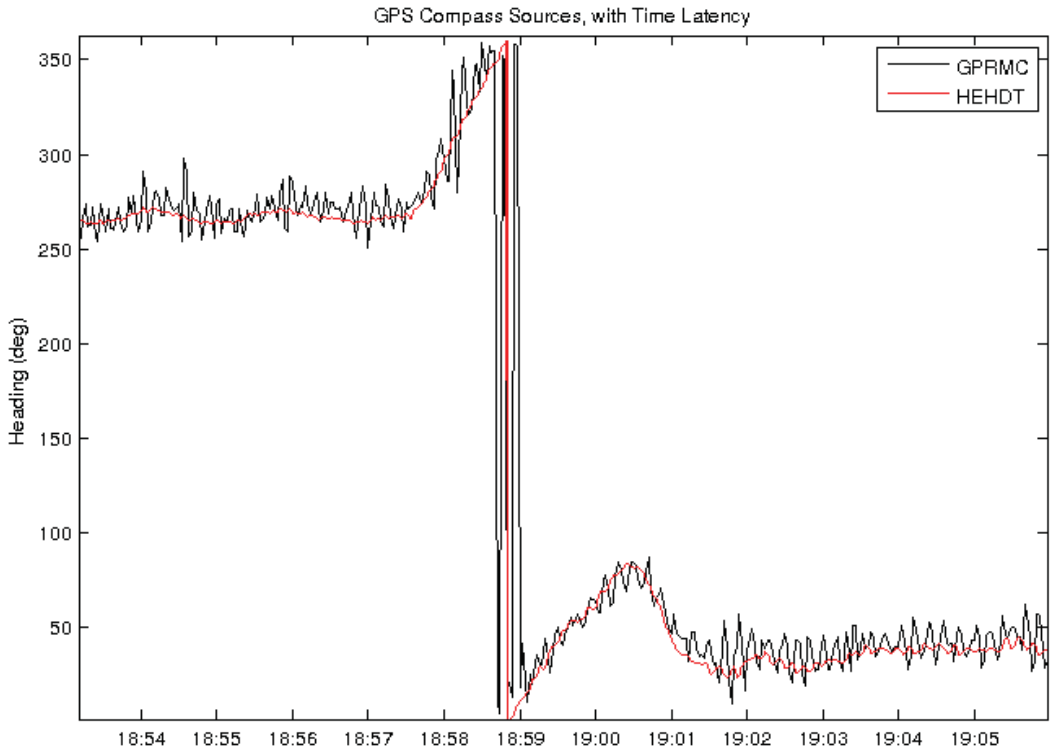

Figure 27: GPS and Magnetic Compass Sources on 2012.11.25 18:58:53. GPRMC and HEHDT are GPS-derived and magnetic compass sources, respectively. Visually, no appreciable lag is seen.

4.2.4 WaMoS II Time

There exist three possible sources for the WaMoS II time basis, often referred to as the "timestamp"; the filename, the header, and the frame-data. The filename timestamp is simply the name of the file, while the other two timestamps are internal to the radar image, within the metadata header. Both the filename and header timestamp have integer second precision. The frame-data timestamp has millisecond precision. An inspection of these time bases was performed. The filename timestamp was observed to vary by up to one minute from the header timestamp (Figure 28). Typically, the header time lagged the filename time, but not always; e.g. 2013.11.22 ~12:00. The distribution of these differences was uniform (Figure 25).

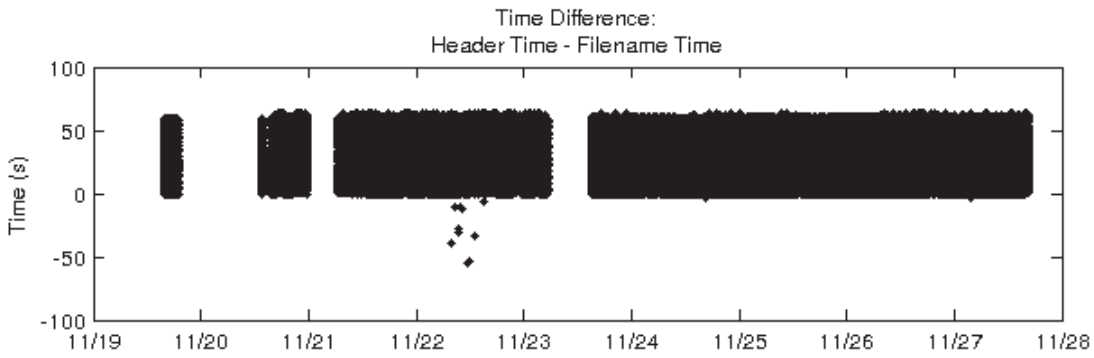

Figure 28: Timeseries of time difference between Header and Filename timestamps. Up to one minute of difference is observed throughout the trial.

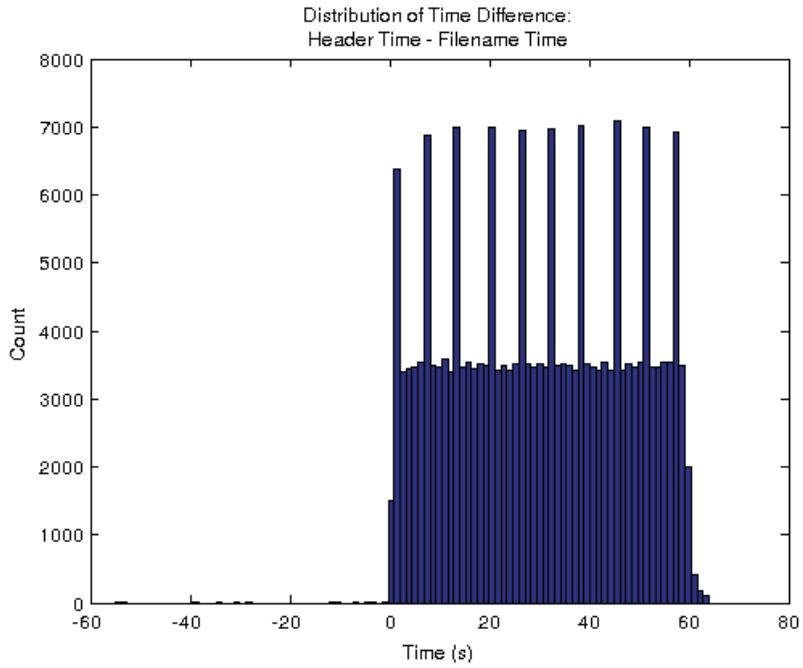

Figure 29: Distribution of time differences between Header and Filename timestamps. The distribution is uniform, with "preferred" values probably related to numerical rounding.

Similarly, there was an observed difference between the header and frame-data timestamps (Figure 30). This difference was not due to numerical precision, as it often exceeded the precision difference of one second. The distribution was semi-normal (Figure 27).

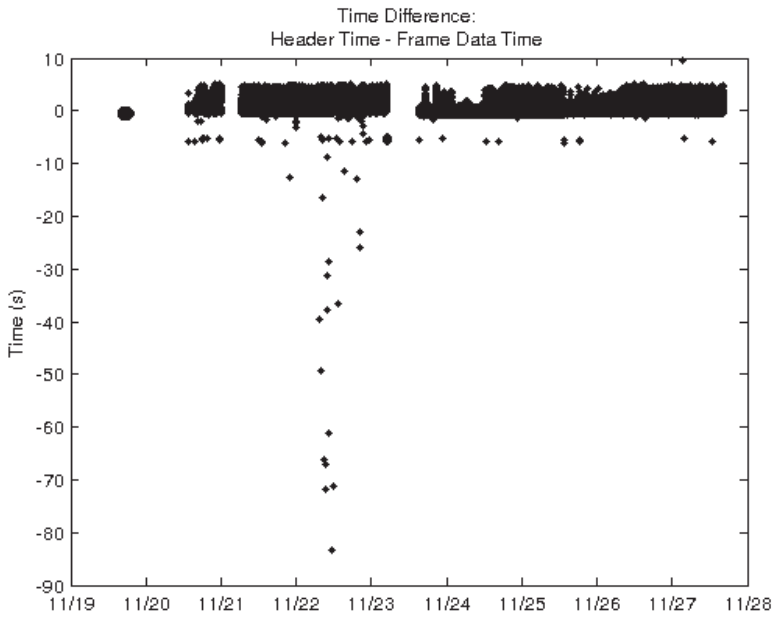

Figure 30: Timeseries of time difference between Header and Frame-Data timestamps. Up to 85 s of difference was observed throughout the trial. The nominal difference was 8 s.

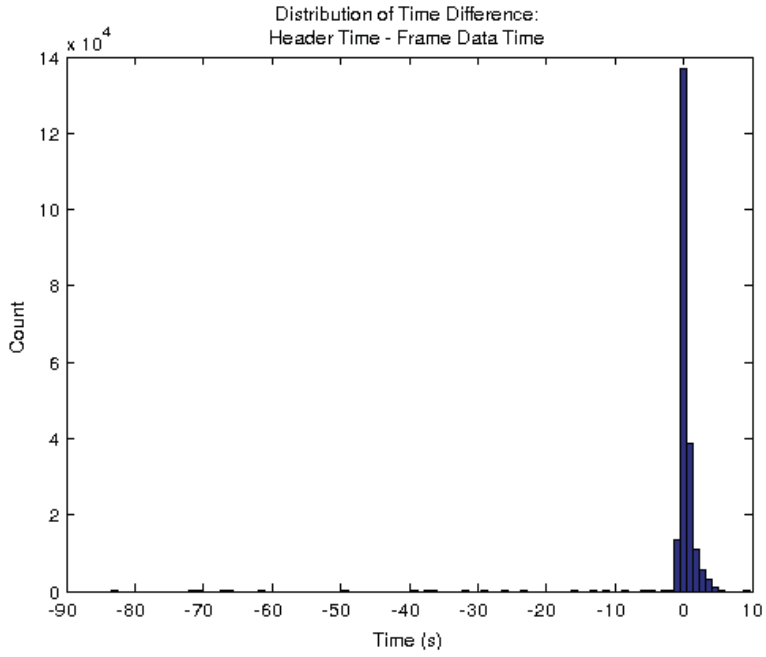

Figure 31: Distribution of time differences between Header and Frame-Data timestamps. The distribution is semi-normal.

The conclusion is to use the frame-data timestamp, entirely because of its higher precision. No statement of accuracy can be made from these results, without an evaluation to a reference signal with a known time base. Such an evaluation is made in the proceeding sections.

4.2.5 WaMoS II Position

A comparison of the WaMoS II GPS positions to the NMEA GPRMC basis shows occasional differences of varying magnitude (Figure 32). The distribution of differences is Rayleigh-like with a maximum likelihood of approx. 1 m difference (Figure 33). A Rayleigh distribution is to be expected for the magnitude of a squared vector components.

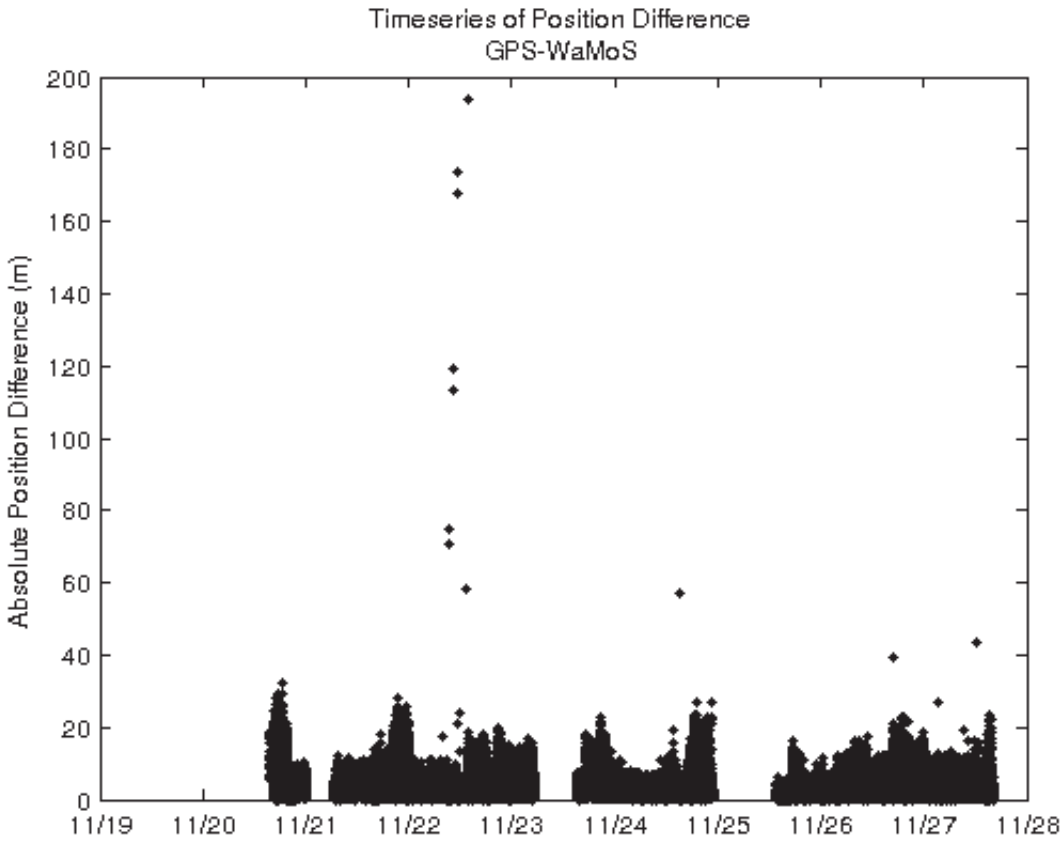

Figure 32: Timeseries of GPS – WaMoS II position differences. The magnitude and frequency of differences is not uniform in time.

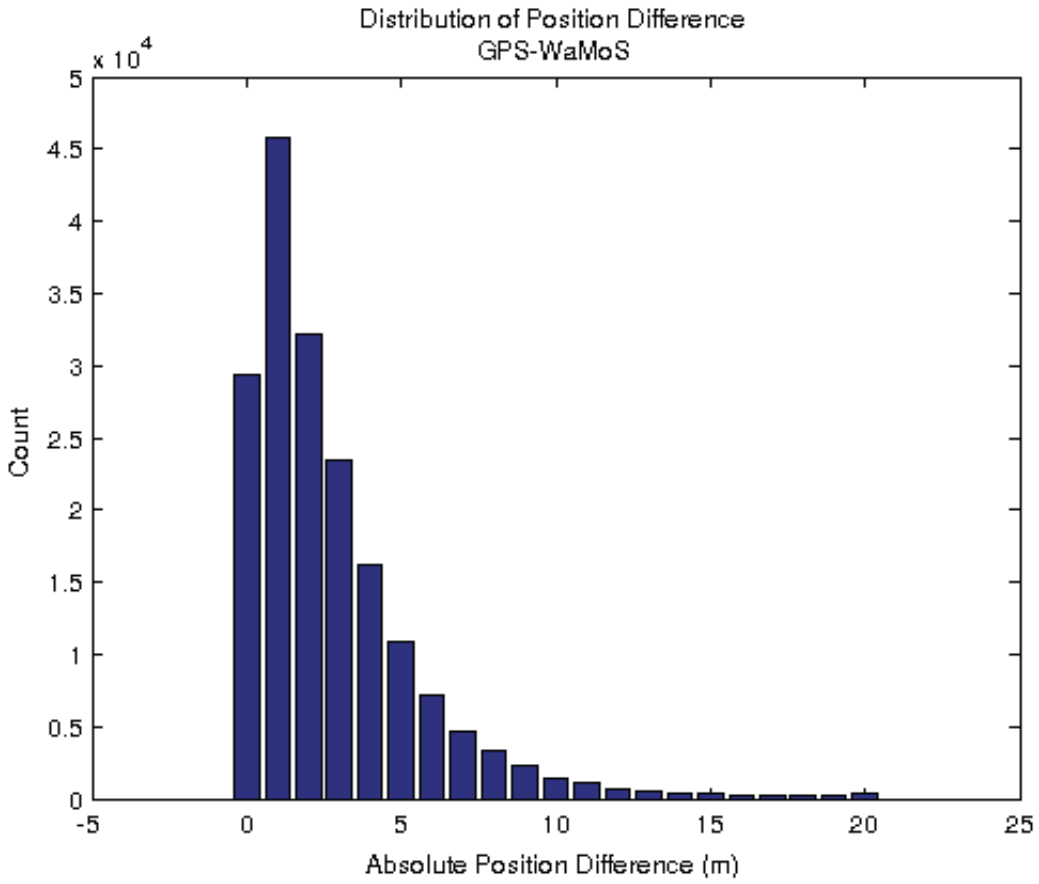

Figure 33: Distribution of GPS Position Difference; GPS-WaMoS II. The distribution is Rayleigh-like with a maximum likelihood of approx. 1 m difference. Time basis is from the frame-data.

Ideally, the WaMoS II position is a direct copy of the NMEA sentence. Two likely possibilities exist for the observed differences. The WaMoS II position data has a precision of milli-minutes of latitude and longitude. This is approximately 1.8 m. The GPRMC sentence has micro-degrees of latitude and longitude, corresponding to 0.1 m of precision. The order of magnitude difference in precision could account for the observed differences. In accordance with this hypothesis, one would expect to see uniform frequency of differences in time, whereas this is not observed (Figure 32). Thus the alternative hypothesis is taken; that these are due to latencies within the WinWaMoS II software, i.e. recording an "old" GPS position at a later time. The WaMoS II data files were inspected during intervals of large positioning difference, and were found to contain a varying signal, i.e. the same values were not repeated.

The previous figures were generated using the frame-data timestamp, which was chosen for its precision and unknown accuracy. Applying the same analysis using the header timestamp resulted in increased differences. The maximum likelihood is shifted to zero difference, with a second mode centered at 3 m difference (Figure 34). A comparative analysis of the WaMoS II latency to GPS positional difference was unable to explain this relationship. Methods applied were correlation,

scatter plots, and visual inspection. For the remainder of the analyses, the frame-data timestamp was retained as the WaMoS II time basis.

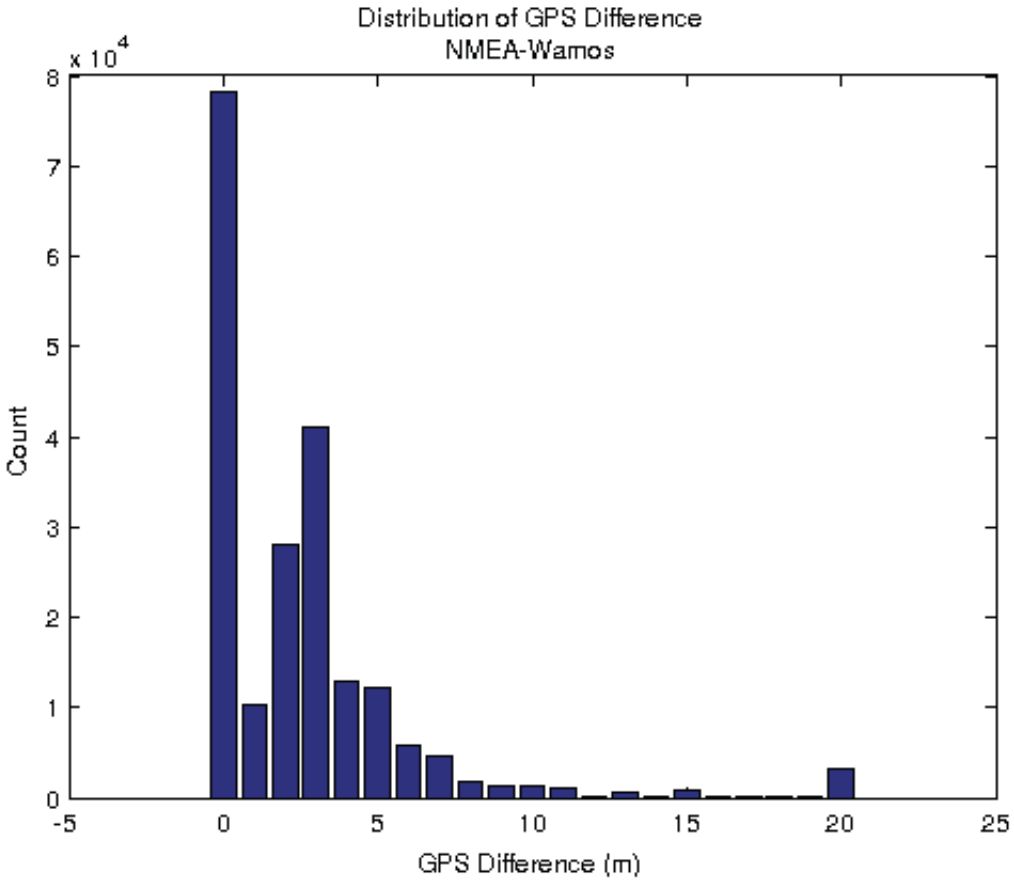

Figure 34: GPS Position Difference; GPS-WaMoS II. The distribution is bi-modal with a maximum likelihood of 0 m difference, and a second peak at 3 m difference. Time basis is from the header.

4.2.6 WaMoS II Compass

The WaMoS II compass exhibited consistent difference, i.e. error, from the HEHDT NMEA source. The HEHDT sentence has milli-degree precision, whereas WaMoS II has deca-degree precision. Observed compass differences exceeded 5 degrees throughout the trial (Figure 35). The distribution of compass differences was normal (Figure 32). The empirical cumulative distribution function yielded a 90,95% probability the absolute compass error was less than 5.4307, 6.6120 degrees, respectively (Figure 37).

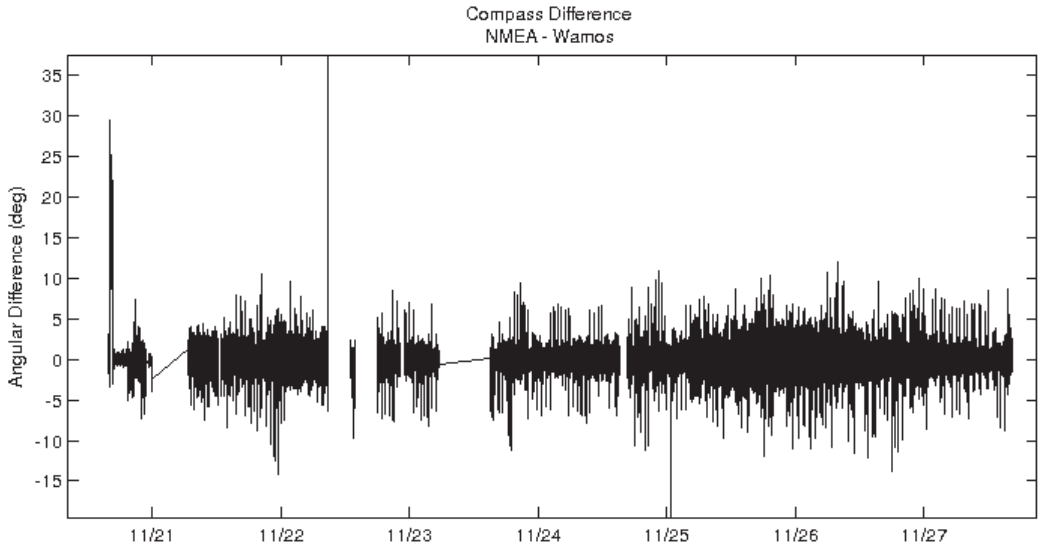

Figure 35: Difference in Compass, NMEA – WaMoS II. Observed differences exceeded 5 degrees throughout the trial.

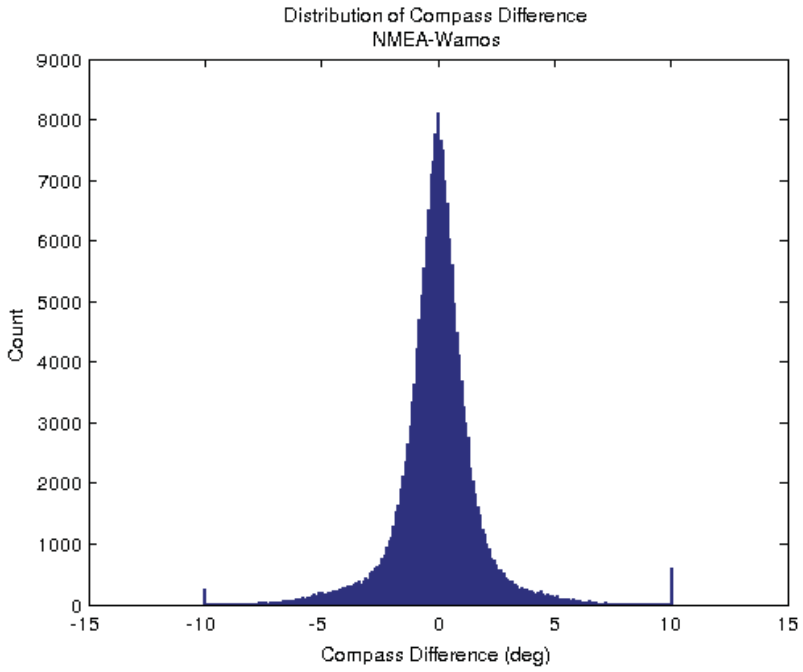

Figure 36: Distribution of Compass Differences. The distribution is normal with zero mean.

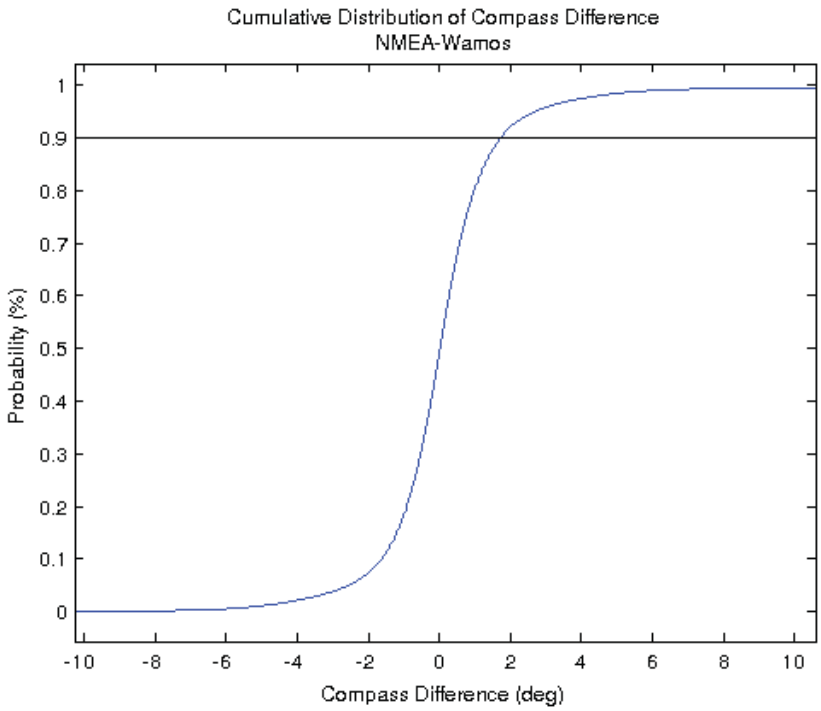

Figure 37: Empirical CDF of compass error. The 90, 95% probabilities are 5.4307, 6.6120 degrees, respectively.

A visual inspection of the compass differences showed a time-varying ~ -3 s latency between the WaMoS II and HEHDT (Figure 38). That is, the WaMoS II signal preceded the HEHDT signal. Applying the latency estimation method of Section 0 to the WaMoS NMEA log files, multiple latency functions were estimated for the WaMoS II PC. Applying these estimates to the WaMoS II time basis significantly decreased the complex cross-correlation in all cases. Thus it is concluded that the WaMoS II time basis latency could not be accurately quantified from PC clock differences alone. Dismissing the PC clock, the most probable source of time latency is the WinWaMoS software. Noting that the WaMoS II mean time between samples is 2.5 seconds, a sample-lagged cross-correlation was calculated, yielding a peak value at +1 lag for WaMoS II, in agreement with the observed difference. Applying this 1 sample latency significantly improved the statistical agreement between the two compass sources, summarized in the following table:

	Complex Correlation	90 % Probability (deg)	95 % Probability (deg)
No time correction	0.999484	5.4307	6.6120
+1 sample, ~2.5 s	0.999879	1.6069	2.6312

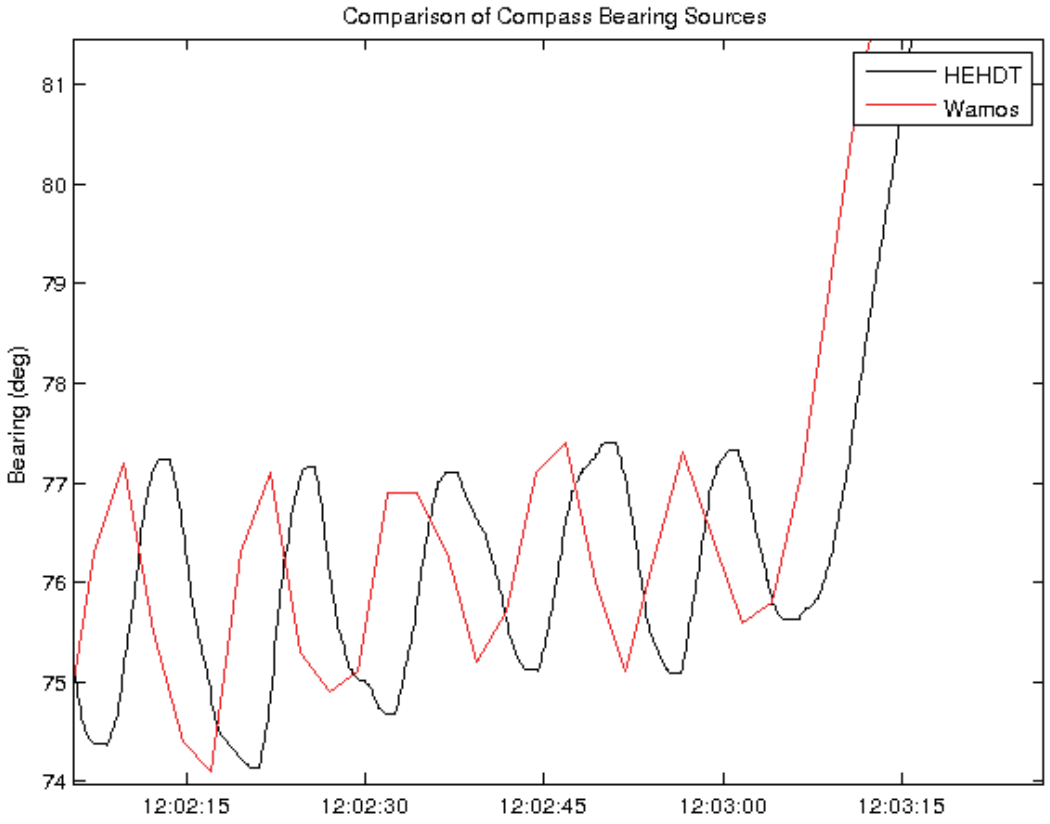

Figure 38: Difference in Compass Bearing. A consistent ~ -3 s latency between the WaMoS II and HEHDT compass values was observed throughout the trial.

Applying the 1 sample offset reduced the standard deviation, while maintaining the normal distribution of differences (Figure 39). This indicates roughly half of the angular difference can be removed with a constant offset. An inspecting of the resulting compass difference timeseries shows the same general pattern (Figure 40), with lesser magnitude. This indicates the time basis are still not aligned. Hypothetically, this could occur if the software logged the time value prior to the compass value.

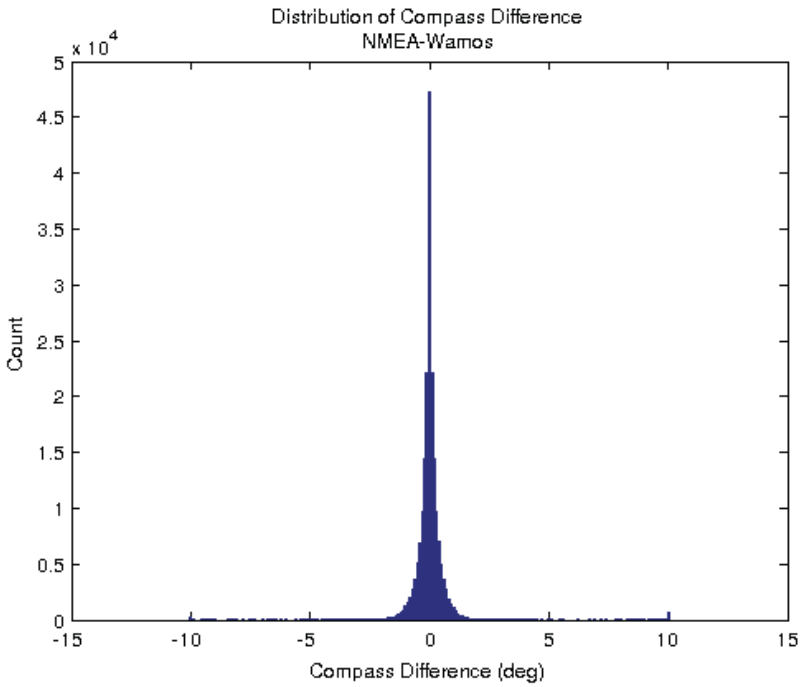

Figure 39: Distribution of Compass Differences, with +1 sample offset. The standard deviation of the differences was significantly reduced, while maintaining the normal distribution.

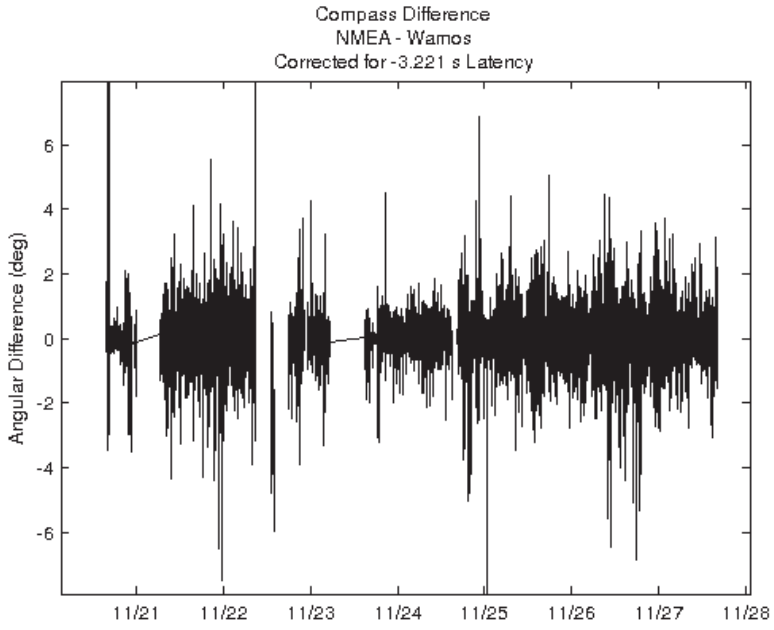

Figure 40: Difference in Compass, NMEA – WaMoS II, after applying 1 sample offset. Observed differences decreased in magnitude.

4.2.7 Summary

A summary of the known precisions and observed accuracies of the WaMoS II bases is provided in the following table. Required accuracy refers to the accuracy desired for WaMoS II to generate direct measurements. Ideally, WaMoS II should match its NMEA data sources in all fields, as they are inputs to the system. Observed accuracies of the WaMoS II bases can be estimated to the extent they are aligned with the reference bases, and the scale of the correction offsets or functions applied.

Basis	Rate (Hz)	Precision	Required Accuracy	Observed Accuracy
GPS Position	0.5	10 m	1 m	10-30 m
GPS Time	0.5	1.0 s	1.0 s	N/A
Compass	10	0.001 deg	0.1 deg	N/A
WaMoS II Position	0.4	1.8 m	1 m	< 5 m
WaMoS II Time	0.4	0.001 s	1.0 s	< 5 s
WaMoS II Compass	0.4	0.01 deg	1 deg	< 3 deg

4.3 SEA STATE PARAMETERS

4.3.1 Measurements on board

In this section, the WaMoS II measurement results are compared to the reference buoys. The main statistical sea state parameters are Significant Wave Height (Hs), Peak Wave Direction (θ_p), and Peak Wave Period (T_p). In addition, WaMoS II derives other parameters, including surface current speed and direction, and parameters for multiple wave systems. These parameters are contained in the WinWaMoS summary files, in ASCII format.

It is stressed that such a comparative analysis is purely relational between two independent instruments measuring similar aspects of the physical world. Neither instrument is measuring the phenomenon of interest directly (sea surface elevation), nor are they using similar methods. The oceanographic buoy estimates spatial displacements from integration (and other processing) of accelerometer values. The WaMoS II images the sea surface, inferring a 2-dimensional surface from electromagnetic backscatter. The true value of sea surface elevation is an unknown. Although the terminology “reference” is used to refer to the buoy data for this report, this does not imply the buoy data is of known greater accuracy. Rather, the analysis is comparative, with hopes of finding agreement between the two instruments, yielding confidence the data is approaching the true unknown value.

In contrast to all other WaMoS II measurements, the wave height must be calibrated. Fundamentally, this is because the radar measures two dimensions in space, rather than three. The significant wave height is inferred from the relative amplitudes of the wave signatures. As this is a relative measure subject to variation for each setup, a calibration is performed to yield an absolute scale. A requirement for accurate calibration is a sufficiently large range of observed sea states. Wave heights observed for this trial ranged from 1 to 6 m (Figure 41) which is clearly sufficient for calibration.

However, the calibration of the radar was not modified during the trial to keep the data set consistent. With the calibration used on board, WaMoS II clearly underestimates the true wave heights. In addition, the result correlation coefficients were 0.605, 0.612 for Buoy #1,2 respectively (Figure 38,39). For significant wave height, the agreement between WaMoS II measurements on board and the buoy is poor. Results were similar for both buoys (Figure 36, 37). The recalibration of WaMoS II in post-processing and the reasons for the low correlation values are discussed in more detail in Section 4.3.2.

In contrast, the agreement for peak wave period and direction is quite good. Results prior to 2012/11/20 12:00 should be disregarded, as Quest was in transit or in harbor at this time. As mentioned in Section 3.3.2, the initial analysis region setup performed poorly until an increase in its area. This is clearly seen in the interval from 11/20 12:00 till 11/21 00:00; as the peak wave direction varies widely.

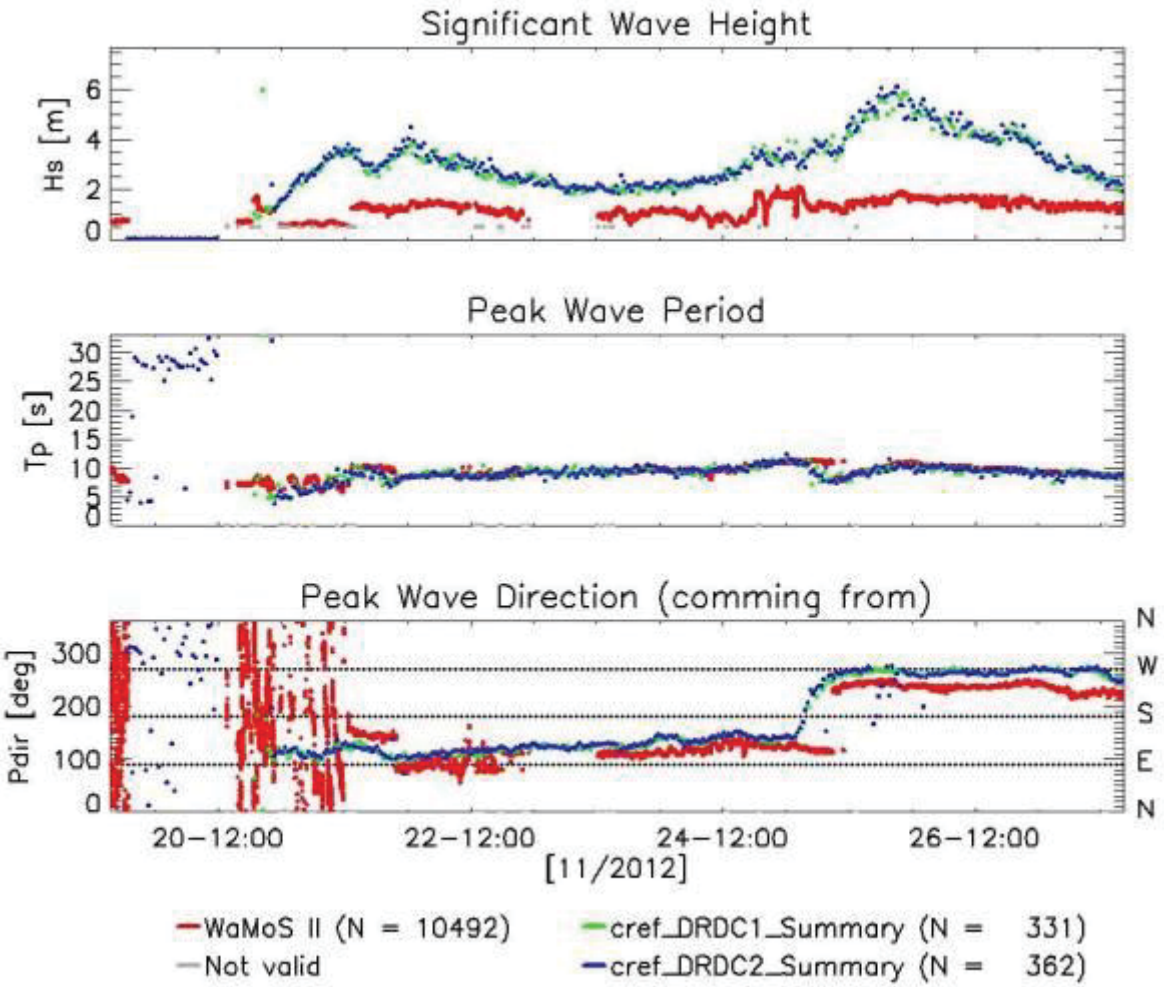

Figure 41: Oceanographic Parameter Comparison between WaMoS II and Buoy #1.

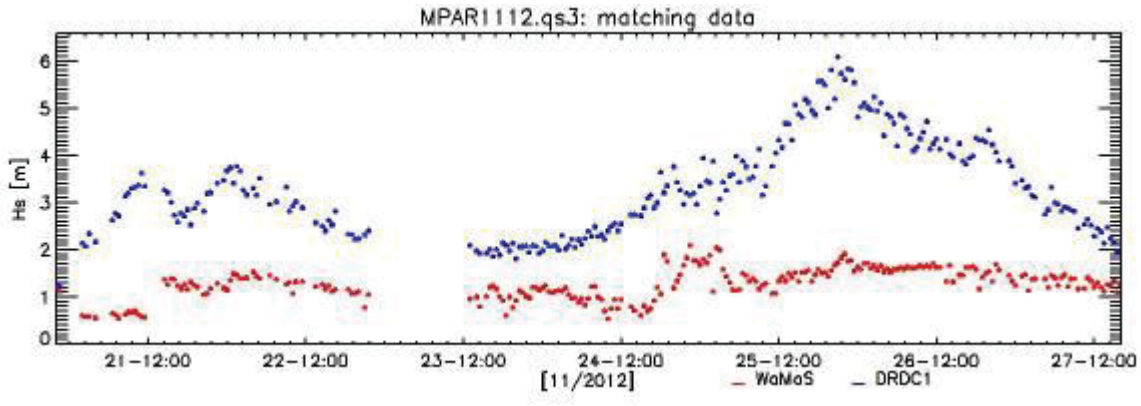

Figure 42: Significant wave height comparison between WaMoS II [red] and Buoy #1 [blue].

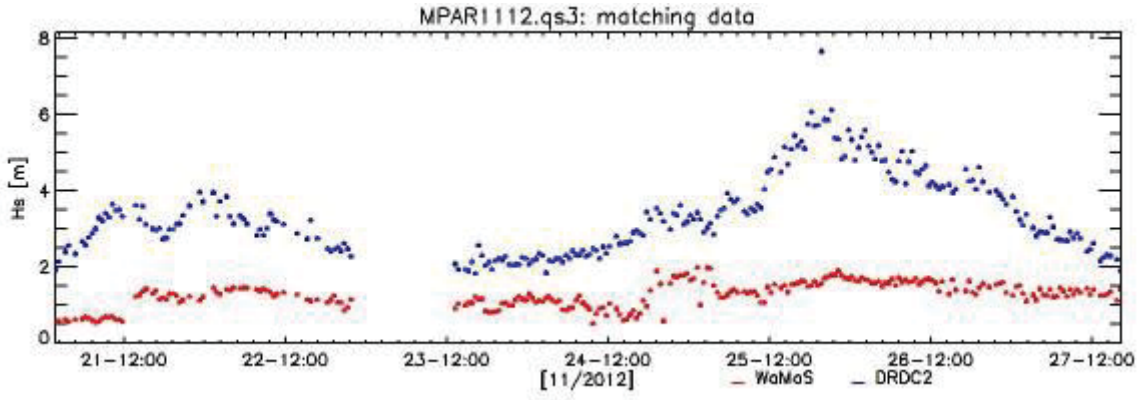

Figure 43: Significant wave height comparison between WaMoS II [red] and Buoy #2 [blue].

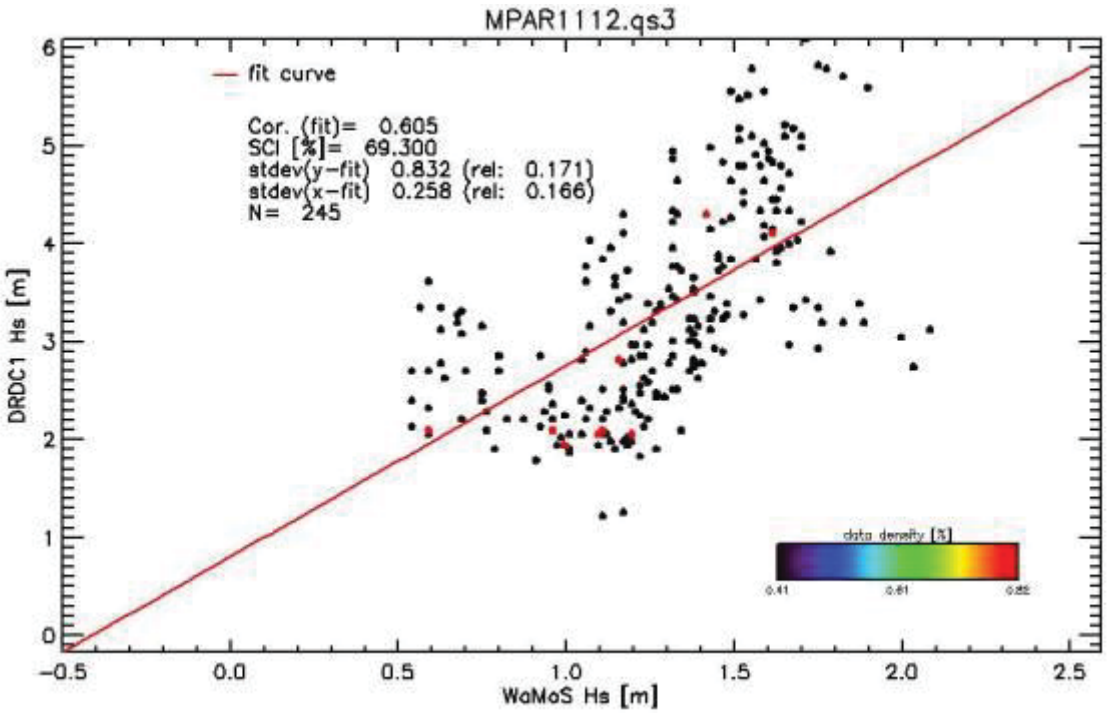

Figure 44: Significant wave height linear regression results for Buoy # 1. Correlation coefficient was 0.605.

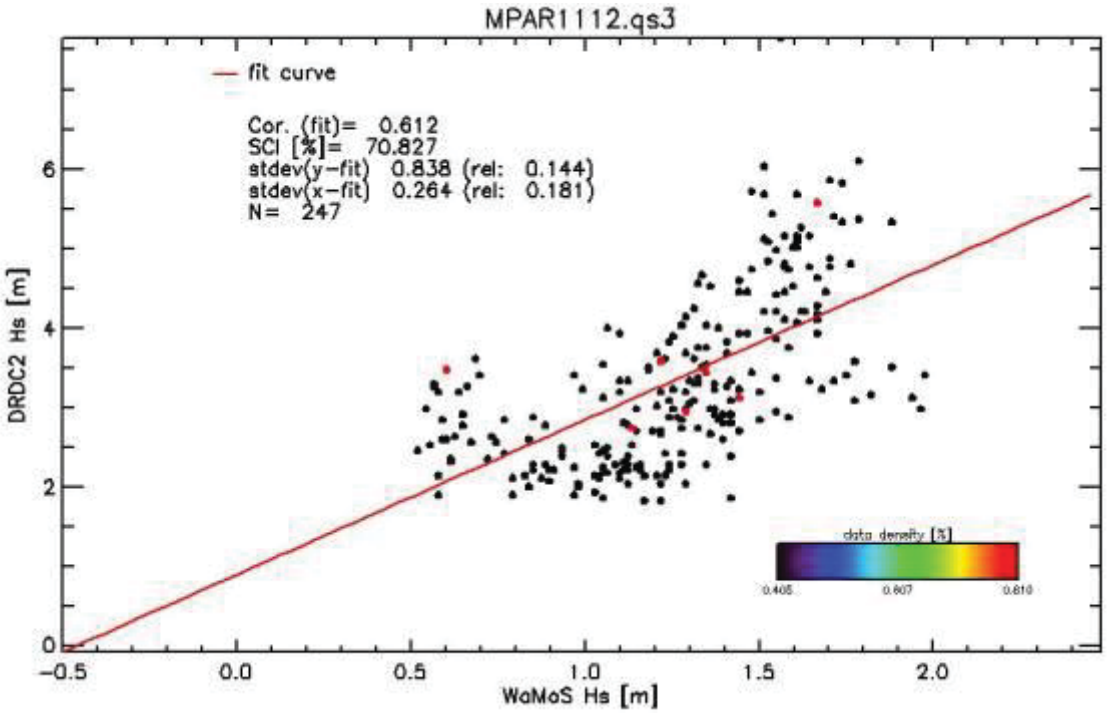

Figure 45: Significant wave height linear regression results for Buoy # 2. Correlation coefficient was 0.612.

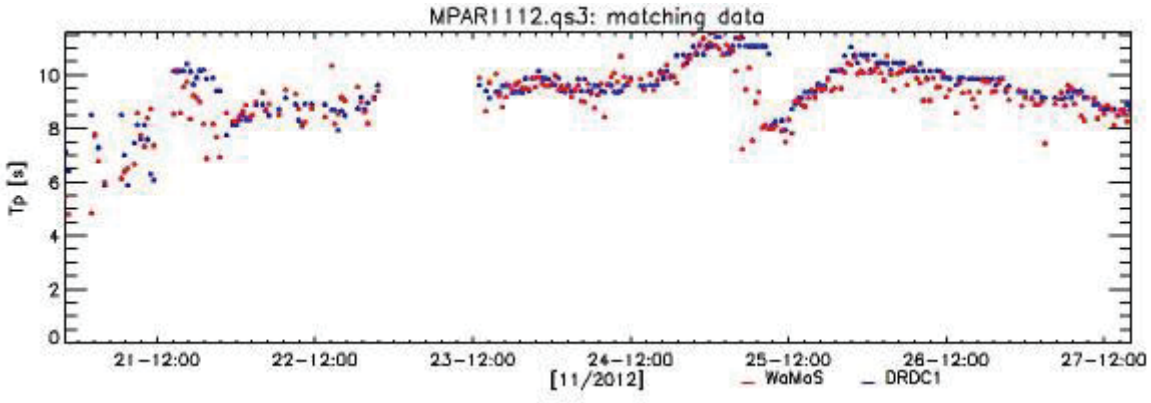

Figure 46: Peak wave period comparison between WaMoS II [red] and Buoy #1 [blue].

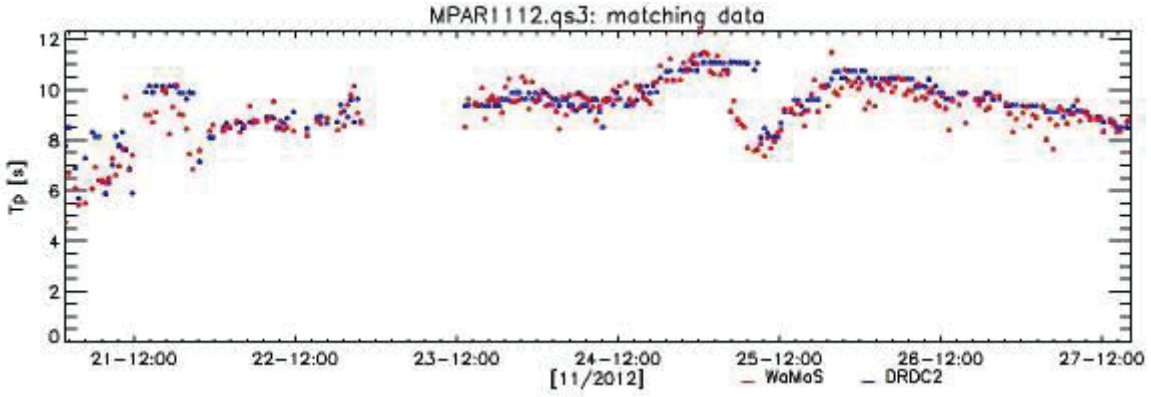

Figure 47: Peak wave period comparison between WaMoS II [red] and Buoy #2 [blue].

4.3.2 Hs Recalibration

WaMoS Hs measurements must be adapted for each specific radar and imaging geometry, as for instance the antenna height over sea level influences the backscatter strength. This is done by setting appropriate calibration coefficients in the WaMoS II set-up. As shown in Section 4.3.1, WaMoS clearly underestimated the true wave heights with the setting used aboard. In addition, the correlations to the buoy data are not satisfying. Therefore, a recalibration of the measurements was carried out after the trial. The results are described in this section.

The basis of a WaMoS II Hs calibration is a signal to noise ratio (SNR) that is a measure for the 'wave pattern strength' which is related to the wave height. Once this relation is established by comparison to external Hs data the retrieved coefficients can be applied and WaMoS get the correct wave heights. A base requirement for recalibration is a sufficiently large range of observed sea states, which is clearly given in this case (Hs ranges from 1m to 6m during the trail).

At times, part of the WaMoS II data has to be excluded from the calibration process if the SNR of the radar images do not only reflect wave properties but also other environmental parameters or image disturbances. The most commonly encountered factors are insufficient wind or rain. This decreases the SNR and lead to false, too low Hs values. Other factors might lead to overestimates, e.g. land structures seen in the images or certain sea conditions like e.g. very strong sea spray. For the recalibration of WaMoS II Hs, such parts of the data set were excluded. *Figure 48* shows the result of the recalibration procedure. Red dots show the recalibrated WaMoS II Hs values, blue dots the buoy data. Excluded WaMoS II measurements are shown in gray.

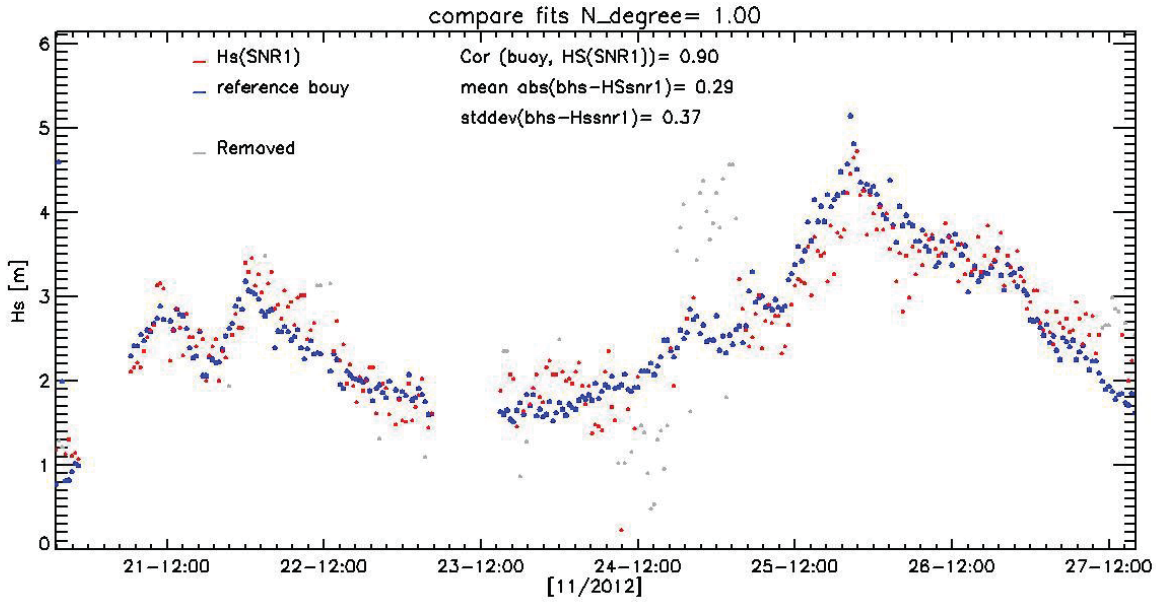

Figure 48: Recalibration result (red) in comparison to Buoy DRDC1 (blue) after excluding outliers (grey).

It can be seen that removal of obvious outliers clearly improve the overall match. When disregarding the outliers, the recalibrated WaMoS time series is well correlated to the buoy (correlation ~ 0.9) with a mean difference of 0.29m and a standard deviation of ~0.37m.

The grey outliers are mainly present on 24th, (approximately 05:30 UTC to 16:30 UTC) where WaMoS clearly underestimates the true wave height and between 24th (~18:00 UTC) and 25th (~03:00 UTC) where WaMoS II significantly overestimates the sea state. Roughly ~7% of all data sets had to be excluded due to underestimates, another 10% due to overestimates.

In most cases, underestimation was traced back to low backscatter due to heavy rain and/or low wind speeds in the Q348 data. The reason for the overestimation is not so obvious. Example radar images from this period show clear wave crests. The reason for this deviation has to be investigated in more detail. There are many possible explanations ranging from technical issues (e.g. rapid course changes or unfortunate placing of analysis areas) to environmental conditions (e.g. sea spray of wind gusts). As calibration of WaMoS is not the focus of this report, this was not investigated in more detail.

Generally it can be concluded that a recalibration of WaMoS II is possible and results into a good overall match to the reference buoy for ~80% of the investigated trial period. But in particular due to the overestimate on 24th/25th this result is not fully satisfying.

4.4 Summary of Bases analysis and Sea State Parameters

Errors and uncertainties in the bases for both the WaMoS II and reference sensors can easily exceed the characteristic time and space scales for ocean waves. Without calibration and correction for these errors, further direct comparative analyses become erroneous or impossible. Consequently, the first part of the data analysis in this report focuses on the accuracy and verification of bases data as recommended in OWS-Q341. Similarly, the predictive nature of the WDF algorithm requires direct measurements of the ocean surface.

To increase the availability of collocated data, i.e. spatial overlap, it is recommended to reduce the vessel to buoy range of the navigation grid to 2 km. A greater range, e.g. 3 km, could be used if one desired to study the effects of greater ranges. Similarly, data overlap for the correlation comparison method could be significantly (~33%) increased if burst sampling was disabled on the buoy, opting for continuous sampling.

To help constrain the WaMoS II image interval to a monotonic rate, the source of antenna rotation interval variation needs to be found. It is hypothesized this is due to wave forcing on the vessel, as the greatest variation occurred during the peak of the swell event.

The external GPS sensor added to the buoys for this trial enabled direct comparison via the shared GPS time and position bases. This was a critical improvement over Q341, and is recommended for any future trials. Whereas the GPS time basis has sufficient precision and accuracy, the position variation exceeds the required accuracy for direct comparisons. Two methods are recommended to address this. Averaging, or low-pass filtering the GPS positions from both vessel and buoy should remove the majority of variation. A minimum of 1 Hz update rate is advised for this method. An alternative method is post-processing of GPS positioning to reduce the instrumental error. Given the raw satellite stream from the GPS (supporting receivers only), the opportunity arises to post-process with differential corrections from land-based reference stations and corrected satellite tracks from internet databases. This data is typically available the next day, and can reduce positioning error to *O* (cm). In terms of an operational real-time system, post-processing is not feasible. Yet it may be an important verification step for a deterministic system.

The Quest configuration of broadcasting NMEA over Ethernet was shown to introduce latencies exceeding 30 s. For this trial, these latencies did not affect the WaMoS II required inputs. Of specific concern is the compass NMEA type HEHDT, which could be subject to such latencies in future trials, and which does not contain an internal timestamp. Alternatively, a magnetic compass equipped with an internal timestamp, could be used to correct for any potential latencies.

WaMoS II PC latency estimates could not remove all the errors in the position bases, i.e. latitude, longitude, and compass. Applying the 1 sample offset roughly halved the compass error. Since the WaMoS II bases data is a copy of the NMEA sources, any remaining differences indicate the time basis is not aligned. The hypothesized source of time latency is the WinWaMoS software.

Validation of a method via direct comparison of two instruments requires careful alignment of bases. In accordance with the characteristic time and space scales of ocean waves, the desired accuracy is 1 second, 1 meter, and 0.1 degree. This analysis has determined the WaMoS II bases to be accurate to (better than) 5 second, 5 meter, and 3 degree. Section 5 shows that this investigation is essential to validate the WaMoS II sea surface elevation maps. The common base of all involved sensors is a key factor that influences all data comparisons.

The comparison of WaMoS II statistical sea state parameters yield a good match of wave periods and direction to the respective buoy measurements while the calibration of WaMoS II on board shows a clear underestimation of Hs and a unsatisfying correlation the buoy. The recalibration described in Section 4.3.2 shows that resetting the WaMoS II calibration gives a much better match to the buoy when excluding outliers from the data set. For this, ~17% of all data sets had to be removed from analysis. The vast majority of the outliers are from two shorter periods. In the first interval, WaMoS significantly underestimated the true sea state, in the second interval WaMoS II returns too high Hs values. While the underestimation is clearly related to low radar backscatter / blurred wave signatures due to missing wind or heavy rain, there is no obvious reason for the overestimate. This needs additional research. After removing the outliers, a correlation of ~0.9 to the buoys is seen with a standard deviation of ~0.4 m which is well within WaMoS II error margins.

5 Evaluation of Sea Surface Elevation Maps

5.1 Method

5.1.1 Deriving sea surface elevation maps

For selected situations, the WaMoS inversion module is used to create sea surface elevation maps. The sample selection aims to restrict the data analysis to samples where a data comparison to the buoy can be successful. The criteria for this data selection are described in Section 5.2.2.

The inversion algorithm derives the individual waves from their radar backscatter. This procedure is based on a back transformation and rescaling of filtered 3D spectra.

The inversion is restricted to sub areas placed within the radar range, i.e. the input is a sequence of radar sub image and derives the sea surface elevation for each pixel in the selected area and for each image in the sequence. The reason for this restriction is related to the sea clutter properties and the amount of data to be processed. A full radar image usually shows areas where the sea clutter is not suitable for inversion, e.g. due to weak sea clutter pattern. As the involved transforms are global, such local features can influence the inversion result for the whole area. The simplest way to avoid this is to use smaller, homogeneous areas for inversion. This is possible as for many practical applications as often only the area of approaching waves is of interest, where the sea clutter pattern is best visible in the radar. In addition, the inversion process is time consuming, which can be significantly improved by minimizing the input data when restricting the process to an area of interest.

For this trial, a square area of 2.25 km^2, with length 1.5 km was used (512 x 512 pixels). The length of a sequence was 64 images. Such boxes are wide enough to allow a high spectral resolution while focusing on a relatively homogeneous area. The areas are placed relative to the vessel, i.e. the used parameters are distance to the vessel and look direction relative to heading. Analysis areas are placed in a way that one of the four comparison buoys is centered in the sub image frame. For the location of the buoy, the radar sequences are created in an earth fixed reference system, i.e. the geographical position of the first frame is kept and used for all images in a sequence while the vessel is moving. For each radar pixel in this area, the geographical position and the time of data acquisition at this point is stored.

The result of this procedure is a sequence of sea surface elevation maps with known coordinates and sampling times. This data can be compared to the buoy heave, i.e. vertical displacement, information.

5.1.2 Alignment of Bases for Comparison

For direct comparison between the WaMoS and buoy, the data must share bases. That is, the compared sea elevation values must exist at exactly the same point in space and time. The main differences are; the sampling rate of the buoy (~6.7 Hz), which is much higher than the antenna rotation rate (0.4 Hz); and the number of sampling points in space. WaMoS determines elevations for a large multi-point area, whereas the buoy provides a spatial point measurement at a non-constant location (see Figure 4).

Three methods were investigated for alignment of the time basis;

- Temporal linear interpolation of the buoy data down to lesser time frequency of the WaMoS, hereafter “down interpolation”
- Temporal linear interpolation of the WaMoS data up to the higher time frequency of the buoy, hereafter “up interpolation”
- Fourier Series expansion of the WaMoS data to the buoy bases, method as described below

Fourier series expansion employs the method of Fourier decomposition, using the 'partial waves' approach to describe a wave field: The sea surface elevation at a location *x* at time *t* $\eta(x,t)$ can be assumed to be composed of a series summation of *N* partial waves with amplitudes *A*, phases φ, frequencies ω, and wave numbers *k*:

$$\eta(x,t) = \sum_{i=1}^{N} A(k_i, \omega_i) \cos(\omega_i t - k_i x + \varphi_i) \qquad (1)$$

The Fourier coefficients *A* were derived from the sea surface elevation maps by means of a 3D FFT. The first and last 5 sea surface elevation maps were removed, as these contain artificial signatures caused by edge effects introduced by the Fourier transform. For the same reason, a frame of 40 pixels was removed in the space domain.

Then, the Fourier series expansion (Eq. 1) is evaluated at the known buoy positions *x* and times *t*, i.e. expanded to the buoy bases. Effectively, this means that the WaMoS sea surface elevations are temporally up-sampled to match the higher temporal resolution of the buoy. Likewise, the WaMoS spatial information is reduced to the buoy single point. In this method, the expansion bases *x* and *t*

are independent variables; they may be arbitrarily chosen, yielding an optimal interpolation given the known coefficients *A*. As discussed in Section 5.3.2, this method was also employed for a region (area) *x* centered about the buoy position.

After alignment of bases, comparison of the WaMoS and buoy was performed using the method of correlation.

5.1.3 Changes Compared to Q341

Fourier series expansion was originally implemented to compare WaMoS II data to reference data of an airborne LIDAR scanner, which yielded very good comparison results. This method was modified and applied for the analysis of the data recorded in the trial Q341 in December 2011. Comparison results from Q341 were inconclusive, which was traced back to difficulties in localizing the buoys. For this trial (Q348), the analysis method was slightly modified to enable a more efficient localization of the buoy in the radar images but the general concept was not altered. Improvements are expected due to the significantly higher resolved buoy location data available for Q348; provided by the external GPS modules. In addition, the careful corrections to the WaMoS bases (Section 4.2) should significantly improve the co-location of the sea surface elevation maps.

A second difference compared to Q341 is the radar sampling resolution. For Q348, the WaMoS radar data was sampled on a finer grid (3 m spatial resolution compared to 7.5 m used in Q341). The intention of this change was to improve the localization of the buoy. A side effect is the increased memory usage needed during data processing. To achieve sufficiently large observation areas, 512^2 pixels *(X,Y)* are needed (compared to 256^2 in Q341). Unfortunately, the larger matrix size in space limits the number of images that can be processed in one analysis cycle. In contrast to Q341 where 128 images were used, in this investigation the upper limit was 64 images per analysis. Tests showed that this limitation has minimal effect on the results.

5.2 Sample Selection and WaMoS II Setup

5.2.1 Background

This section describes both the data selection criteria and the WaMoS setup applied prior to the comparative (correlation) analysis of Section 5.3. The data selection criteria and WaMoS setup were chosen to both optimize the WaMoS performance, and to overlap the two instrument's measurement domains. The data selection criteria, described below, effectively reduced the total (original) number of WaMoS radar backscatter images to an optimal subset. The WaMoS setup refers to the parameters of the inversion process that transforms the radar backscatter into sea surface elevation maps. Both factors are important for the quality of the data comparison.

5.2.2 Sample Selection

For optimal data accuracy and comparison, several radar data properties are important. The following conditions should be met, or are favorable:

Sea clutter strength: The sea clutter signal must be clearly visible in the raw radar data, i.e. there must be ocean signal present. This condition favors situations with high Hs and high wind speeds.

Distance of vessel to the reference buoy: The reference sensor must lie within the radar observation range. This condition must hold true for the time interval of analysis, e.g. 2.7 min. for this analysis. The vessel motion and relative position must be taken into account. In addition, previous research indicates that with growing distance the correlation to the reference sensor decreases due to reduced angular resolution with range and wave shadow. Finally, the received backscatter amplitude decreases with range; far targets have a much weaker signal. This is partially compensated by the radar amplifier, but cannot correct the loss of signal to noise ratio.

Vessel speed: To allow a direct comparison to a moored buoy, the WaMoS data must be registered to an earth-fixed reference system. That is, the inherently Lagrangian (following the vessel) data of the WaMoS must be transformed to an Eulerian (earth-fixed) reference frame. The input radar images are kept at the same geographical position while the ship is moving. For high vessel speeds, this transformation may not be possible, due to the earth-fixed domain leaving the radar observation region. In addition, the imaging geometry changes with distance which may introduce errors if this change is too rapid or too large. For instance, the backscatter is stronger close to the vessel and the shadow behind a wave is longer in far range. When approaching a fixed area, these properties will change from image to image, which may have side effects on the inversion that are not studied in detail, yet.

Vessel Course: The imaging geometry and consequently the ocean signal, varies as a function of radar incidence angle relative to the wave vector. Consequently, vessel rotation introduces variations in the signal. Such situations should be avoided.

Orientation: Following the above statement on relative incidence angle, the sea clutter is best visible in the wave travel direction, both up-wave and down-wave. This geometry maximizes the reflected EM energy. In contrast, reflected EM energy is minimized for an orthogonal incidence angle, i.e. waves seen from the side. Thus, the optimal situation for both radar accuracy and comparison to buoy is when the buoy is located roughly in the wave travel direction relative to the vessel.

Blanking Sector: An additional factor is blocked look directions caused by structures in the EM propagation path. On most vessels, including Quest, this is caused by masts or structures aft of the radar. For Quest, this “blanking sector” was measured at 150 to 216 degree compass. Due to the loss of signal, no analysis is possible within the blanking sector.

To apply these criteria, all relevant parameters for all available data was compiled into a list. The criteria were applied as follows:

- **Time**: time overlap between the radar and buoy data. The burst sampling of the buoy results in approximately 1/3 reduction in comparable samples.
- **Range:** Relative ship-to-buoy range between 500 and 2036 m (at 3 m resolution, N=512 Cartesian size, and range-to-buoy = 500 m desired)
- **Angle:** The relative angle between radar incidence vector and ocean wave vector within +/- 30 degrees, allowing for both coming and going waves, i.e. also 150 to 210 degrees.
- **Blanking:** buoy not within the blanking sector of 150 to 216 degrees

- **Hs:** > 2 m
- **Nt:** Nt=64 consecutive radar images pass the above criteria. Whereas the above criteria are exclusively independent, this criterion requires all prior criteria are met for a consecutive period. That is necessary for the monotonic requirement of standard Fourier analysis.

Table 1. Sample selection criteria, all values are in percentage of total number (N=209,152) of available radar images for analysis. Criteria 1-5 (Time-Hs) are independent. Row "Union" is the set union of these exclusive criteria. Row "Nt" is the subset which pass all criteria, i.e. including "Nt".

Criterion	Buoy 1	Buoy 2	Buoy 3	Buoy 4
Time	64	62	64	65
Range	33	32	35	31
Angle	34	34	35	32
Blanking	70	29	70	29
Hs	70	71	69	72
Union	3	1	4	2
Nt	1.0	0.4	1.3	0.4

The burst sampling mode of the buoy (see 3.4.2) reduces the matches by ~33%, in accordance with the known duty cycle. The range criterion is a ~66% reduction. Although too short a range is possible, inspection of the sampling geometry (Figure 2) shows the vessel spent considerable time outside the 2036 m upper limit. The angle criterion is also a ~66% reduction. This reflects the circular nature of the vessel sampling path, whereas the angle criterion specifies a 180 degree (50%) subset (Figure 49). The two southern buoys, i.e. # 2 and 4, were in the blanking sector more often. The Hs criterion ~70% reflects relatively large (> 2 m Hs) waves for the duration of the experiment. As these criteria are pseudo random, the set union roughly corresponds to a multiplication of probabilities. Subsequent application of the Nt criterion results in a final reduction of approximately 99% for all buoys. The criteria are not hard limits, and could be relaxed for later analysis. The intent of this selection method was to choose radar data for optimal comparison.

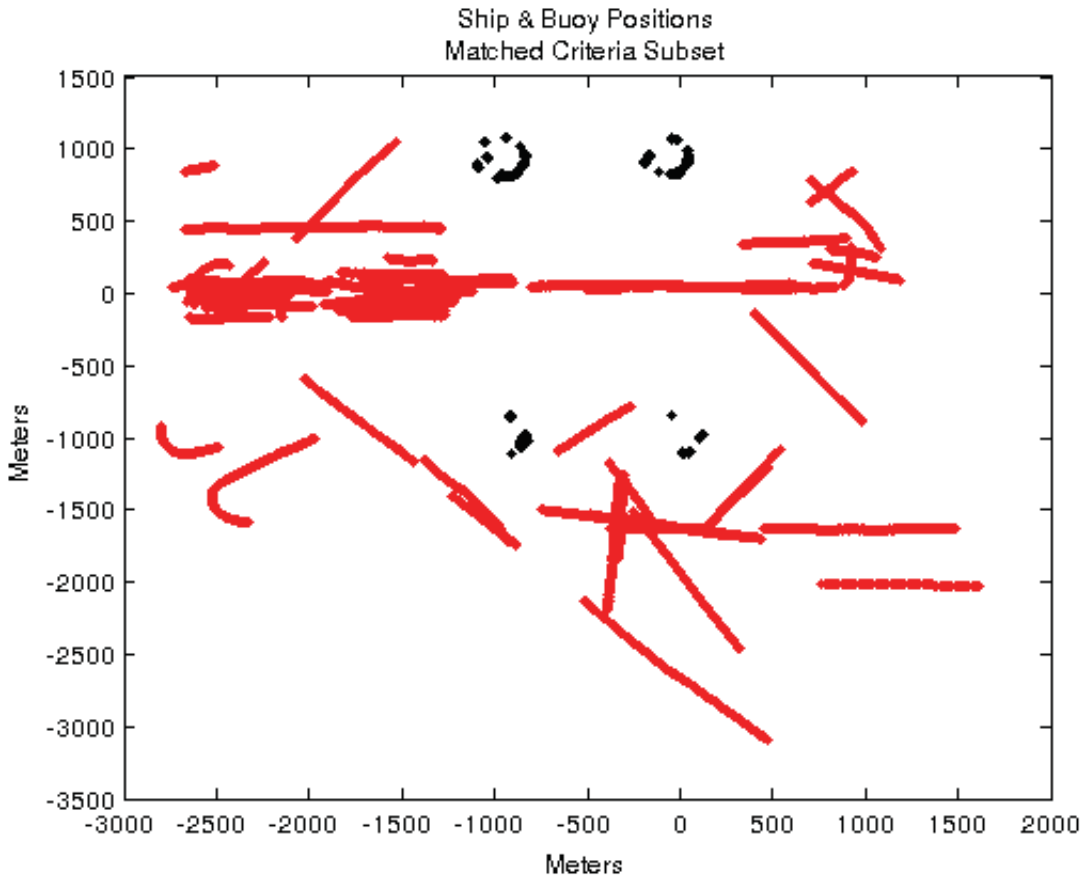

Figure 49. Sampling geometry; reduced subset passing selection criteria. The dominant wave incidence directions were 120 and 280 degrees compass.

Figure 49 shows an example radar image and the location of the reference buoy #1 “DRDC1” selected by this procedure. The retrieved optimal sampling time was 2011-11-25, 15:07:15. In this image, the radar backscatter is color coded. The white circle in the center marks an area around the radar antenna that was excluded as the backscatter is too strong for analysis. A stripe like pattern of strong radar backscatter (blue to red) is visible. These stripes are the reflections of wave crests. Behind the stripes, dark areas of low return (black) can be seen. Here, the sea surface in hidden behind the wave crest. The evaluation of such a pattern over time is the main input to WaMoS II wave analysis. Radar raw data of this quality can be analyzed with good results. In absence of wind or too low waves, radar images of the sea surface are almost uniformly black and cannot be used for wave analysis.

The image also shows clearly some of the areas that have to be avoided for inversion. A blanking sector of ~60 degrees with very low backscatter is clearly visible. Here, vessel constructions prevent the data analysis. In addition, the range decay of signal strengths can be seen. It is also obvious that the stripe pattern is better visible in the direction of upcoming waves. The sample selection algorithm takes this into account. The red frame marks the location of the analysis area found by the search algorithm. Only this part of the radar image is used for creation of sea surface elevation maps. A clear wave pattern is visible within the frame, the buoy is close to the center. These conditions are nearly ideal to compare sea surface elevations obtained from WaMoS to the buoy.

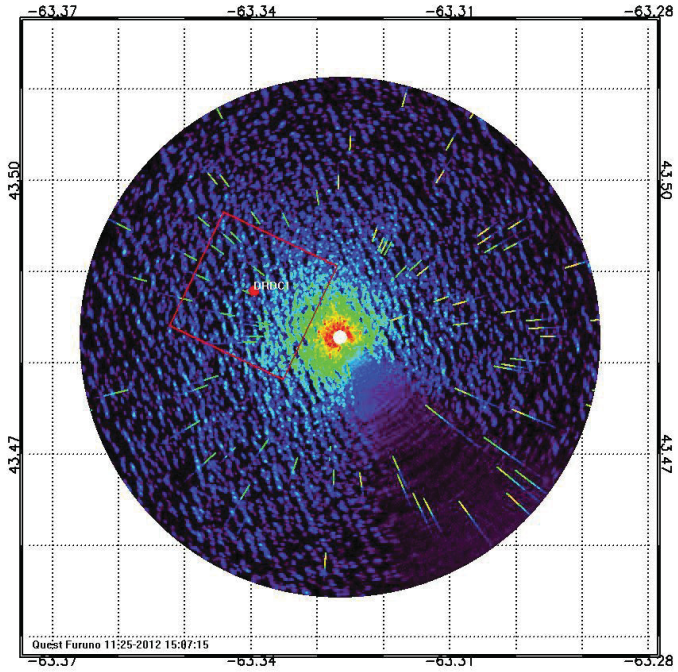

Figure 50: Example radar image for sample 2011-11-25, 15:07: 15. The buoy location and the location of the analysis area are marked

It should be noted that many these selection criteria are not principle limits of the method but chosen for optimal conditions for data comparisons. In an operational application, usually the direction of upcoming waves is the area of interest and WaMoS II is able to focus on this area automatically and uses a range in which the waves are clearly visible. For the comparison in this study, the main issue is to find times in which the buoy is within this ideal look direction and range. General restrictions of the method are related to minimum wind and wave height and the maximum vessel speed.

5.2.3 WaMoS II software and setup

For this investigation, the software modules listed in Table 3 were used.

Table 2: Software modules used in this investigation

Software Module	Revision	Purpose
mk_car	339	Create analysis areas
Wamos_inv	i551	Invert to sea surface elevations
Validate_cin	58	Interpolate sea surfaces to match the buoy grid

Range and location of the analysis areas were adjusted to center any of the four buoys matching the criteria. That is, independent output was calculated for each buoy. The areas are created in an earth

fixed reference system, i.e. they are kept at the initial position for each analyzed sequence. All areas have a side length of 512 x 512 pixels in space, each sequence containing 64 images.

5.3 Localization of the Radar to the Buoy

5.3.1 Method

Prior to data processing, bases corrections were made to the raw radar data using the corrections from Section 4.2. Despite these corrections, the bases cannot be assumed as exactly aligned, following the summary of accuracies in Section 4.2.7. Consequently, it was deemed necessary to perform a spatial-temporal search for maximum correlation. This method corresponds to an empirical estimate of the remaining bases offsets. The implementation applied the Fourier expansion method (Section 5.1.2) to a regular grid in both space and time (x,t), centered about the location of the buoy. Note that both space and relative-time offsets were evaluated. The resulting WaMoS SSE timeseries were correlated to the buoy vertical displacements, i.e. "heave". It is assumed the highest correlation resulting from this procedure is found at the time and location offset that compensates for these inaccuracies.

A systematic search was used, starting with a larger area and lower resolution, reducing to a smaller area and higher resolution. The initial pass matched the WaMoS II data resolution, i.e. grid resolution of 3 m in space and ~2.5 s in time. To further reduce processing time, fewer wave components $A(k,\omega)$ were included in the Fourier expansion (Eq. 1, Section 5.1.2). The second pass uses a finer grid and includes all wave components.

Relevant to the method of a spatial-temporal correlation search is the characteristic space and time scale of the physical process. For example, a monochromatic (single frequency) sinusoid will correlate with itself at the time scale of its frequency. Searching for such a sinusoid amongst replicas of itself, shifted in time, is redundant past the characteristic time scale. The characteristic time scale can be estimated from the autocorrelation of a signal. For this analysis, the time scale was taken as the time lag corresponding to the first peak of the absolute value of the autocorrelation function for both the buoy (Figure 51) and the WaMoS (Figure 52). Time scales were 3.8, 5.0 s for the buoy and WaMoS, respectively. These are less than the peak wave period observed during the trial (Figure 41), but the characteristic time scale is an integral property as opposed to a maximum. Another useful property of autocorrelation is the correlation coefficient R_1 of the first peak. This represents an upper threshold for lagged, i.e. offset, correlations of a periodic signal with itself. Assuming WaMoS and the buoy contain identical signals offset in space and time, and further assuming these signals are periodic, one can expect to find correlation values up to R_1 for arbitrary offsets. Thus, for the aforementioned correlation search method, correlation values greater than 0.6 are taken as possible matches to the true spatial and temporal offsets. Autocorrelation R_1 values for WaMoS and the buoy were 0.57, 0.56 respectively.

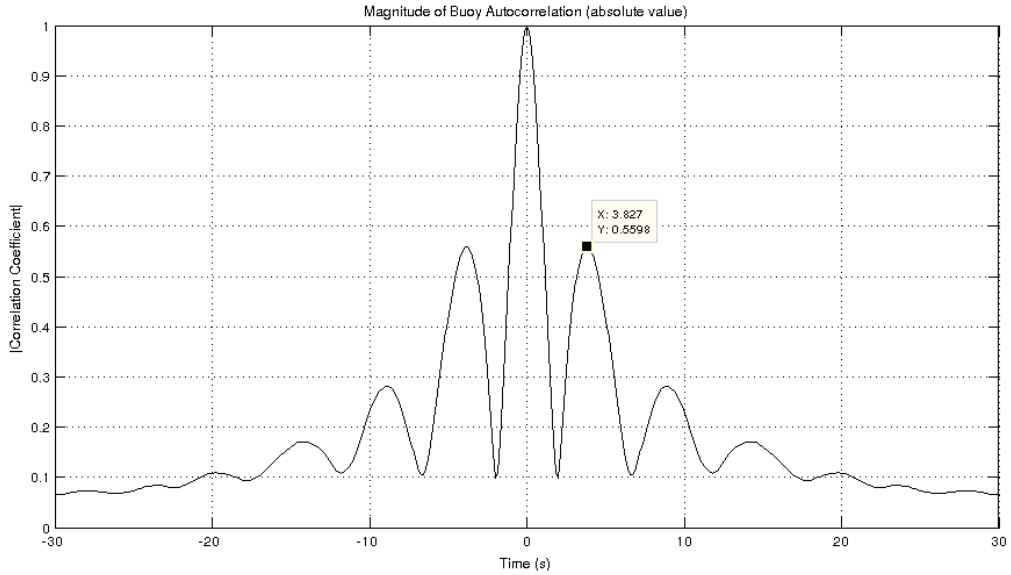

Figure 51. Autocorrelation function, magnitude, for the buoy. The first peak is at 3.8 s with R=0.56.

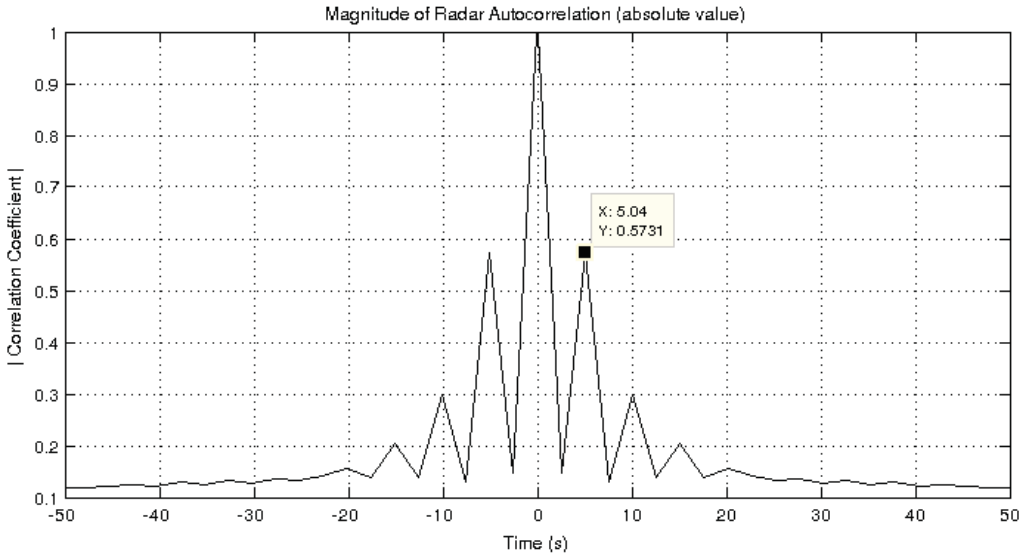

Figure 52. Autocorrelation function, magnitude, for WaMoS. The first peak is at 5.0 s and R=0.57.

5.3.2 Spatial Correlation Fields

The spatial correlation fields as a function of shift vectors in time and space give an impression of the correlation for a wide area (Figure 53). The example shown is from the analysis of radar sample '20121125150715qs3' in comparison to buoy DRDC 1. Shown are the color coded correlations for time shifts of 0,-1, and -2. Positive time shifts were tested as well but resulted in lower correlations

and are therefore not discussed here. In x and y, a step width of 4 grid cells (12m) is used to find the maximum correlation in an area of 300 m around the expected buoy position. In this step, all wave components that have at least 10% of the maximum energy found in the full 3D spectrum are used as input for Equation (1).

The maximum correlation of 0.67 was found in the map for shift ts=-1 at the location (-12m, -36m). Section 5.3.3 shows that this value increases significantly when using a finer grid and including more wave components. Here, the general pattern seen in the correlation diagram is more important than the absolute values.

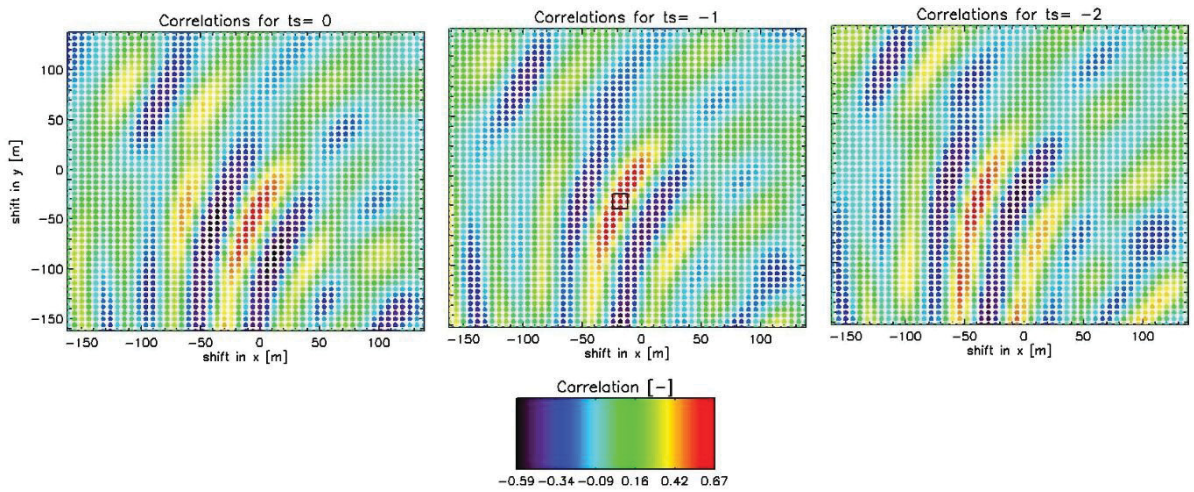

Figure 53 Correlation maps for time shifts 0 (left), -1 (center) and -2 (right). The frame marks the location of the maximum correlation.

The overall pattern seen in all maps of figure Figure 53 gives a reasonable impression. When correlating periodic signals of roughly comparable frequency it is to be expected that the result is an alternating pattern of high and low correlations. Correlations around the overall maximum are clearly higher than in all other maxima found by this procedure, indicating that the match is not accidental but reflect the true nature of the data. The resulting shift vector is well in range of the expected error margins when taking into account all factors that can influence the radar data.

For the implemented search algorithm, this complete spatial field was not calculated for all examples to reduce calculation times. As demonstrated in Section 5.3.3, a two-step approach scanning a smaller area on a coarser initial grid is sufficient to find the location of the best match.

5.3.3 Example Result of Correlation Search

The implemented search algorithm uses two grids and two energy cuts for the wave components included in reconstruction of the time trace when applying Equation (1). In the first step, 3 time layers (ts=-1, 0, +1) are scanned for the best correlation using a resolution of 15 m in X and Y for an area of 120 m around the expected buoy position. In this step, all wave components that have at least 10% of the maximum energy found in the full 3D spectrum are used as input for Equation (1).

The area of the highest correlation is scanned again on a finer grid of 3 m and a reduced search area of 30 m, again the energy cut for wave components is now lowered to 1 % of the maximum. Finally, for the best match a reconstruction of the surface with all wave components is calculated. This correlation is the final result of the search algorithm.

Figure 54 shows the resulting correlation map for the example case '20121125150715qs3' in comparison to buoy DRDC1. Only the time shift plane 'ts=-1' is discussed here. The figure shows both search grids, the correlation is color coded as indicated in the color bar. The maximum correlation is found for the shift vector (-15m, -36m) with a value of 0.81. The distribution of correlations give a realistic impression and matches the wide area scan shown in Figure 53.

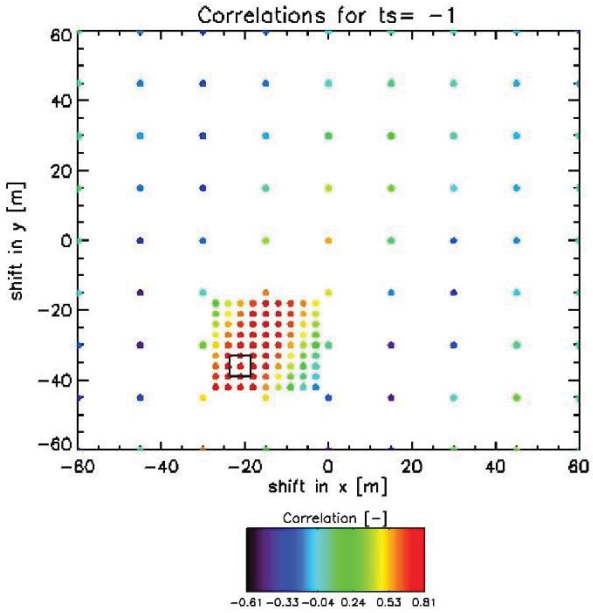

Figure 54: Correlation map for time shift -1 on two resolution scales in x and y. The black frame marks the maximum correlation found, R=0.81

This example shows that a reasonable match of WaMoS II and buoy can be achieved by applying shifts in time and space that are well in the range of inaccuracies to be expected. This example is further discussed in Section 0

Dropping the requirement for the temporal offset in the search, i.e. assuming no time offset, allows for a significantly shorter computation time. Consequently, the spatial correlation field can be calculated at the resolution of the WaMoS directly. This approach was used for the aforementioned

temporal “up” and “down” interpolation methods. The resulting fields were in good agreement with the Fourier expansion method (Figure 55). The observed spatial periodicities in correlation did not exceed the expected R_1=0.6 from autocorrelation.

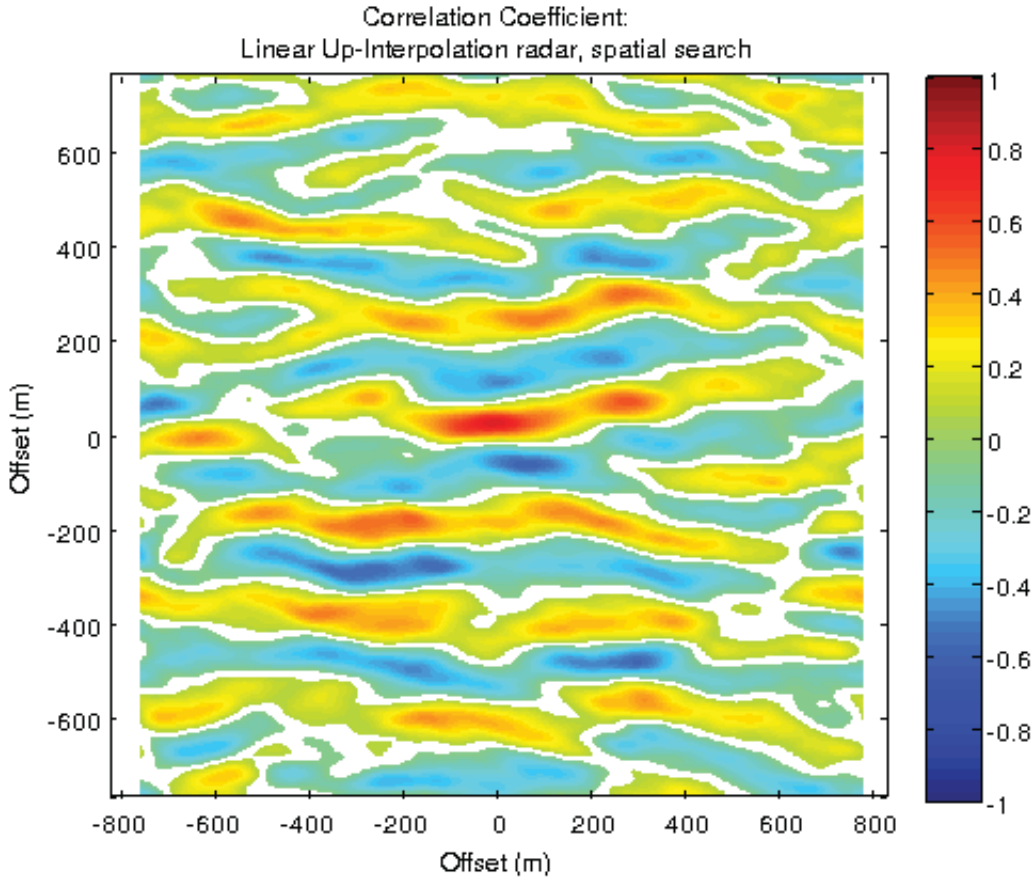

Figure 55. Spatial correlation field for the temporal up-interpolation method, i.e. WaMoS up-interpolation to buoy rate. The peak correlation R=0.82 was found near the center of the image (dx, dy = 12.9, 25.0 m), which closely corresponds to the expected location of the buoy (dx, dy = 0 m). Initial time for this sample was 2012.11.25 23:12:04. The spatial periodicity of the correlation illustrates the difficulty in obtaining a definite match. Note the periodic structures do not exceed the expected R_1=0.6 from autocorrelation.

Student’s p-values for the associated spatial correlation fields were accumulated for all evaluated fields. Most correlation values passed the significance test with a p-value of 0.05. Inspecting the cumulative distribution of p-values, the up-interpolation method exhibited a greater probability for significance relative to the down-interpolation method. For a p-value of 0.05, the probability of a spatial point being significantly correlated with the buoy is approximately 68, 52% for the up, and down- interpolation methods respectively.

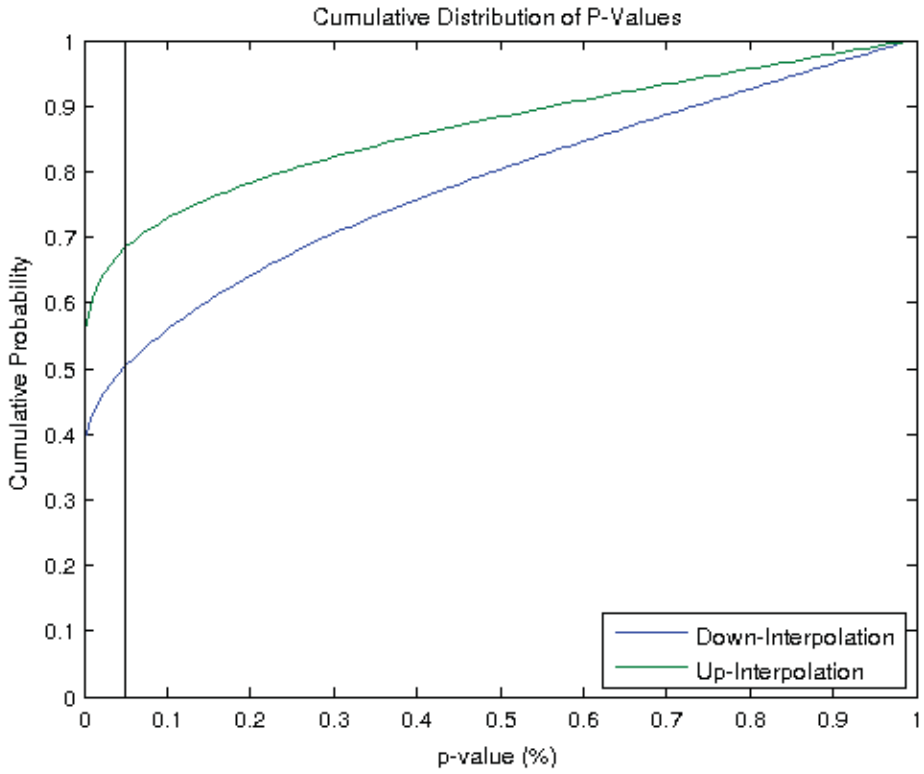

Figure 56. Cumulative distribution of P-values for all spatial correlation fields. The up-interpolation method has a significantly greater probability of significance than the down-interpolation method. For a p-value of 0.05, the probability of a spatial point being significantly correlated with the buoy is approximately 68, 52% for the up, and down-interpolation methods respectively.

5.4 Comparison of Sea Surface Elevation Timeseries

5.4.1 General

For all examples discussed in this section, the best comparison location and time was estimated as described in Section 5.3. This means, that estimated shift vectors in time and space are applied to the WaMoS II data before using equation 1 to get time traces of WaMoS II sea surface elevations that are compared herein to the buoy data in more detail. In this section, example cases are described in more detail. All results are presented by summary data diagrams in terms of correlations in Section 5.5.

5.4.2 Example 2012-11-25, 15:07:15, compared to DRDC1

This example was previously presented in Section 5.3 to show the method of localizing the buoy in the radar data. Here it is discussed in more detail to show the processing steps and evaluation criteria that are applied for all other data sets.

Figure 57 shows that the sea surface elevation map derived from the radar data presented in Figure 54 gives a realistic impression. The figure shows a color coded sea surface elevation map taken from

the set of 64 maps derived from sample 2012-11-25, 15:07:15. The expected buoy location is marked in black. This figure shows that the data selection procedure successfully placed the analysis area in distance and direction that centers on the buoy. Such a set-up minimizes the impact of FFT side effects on the comparison.

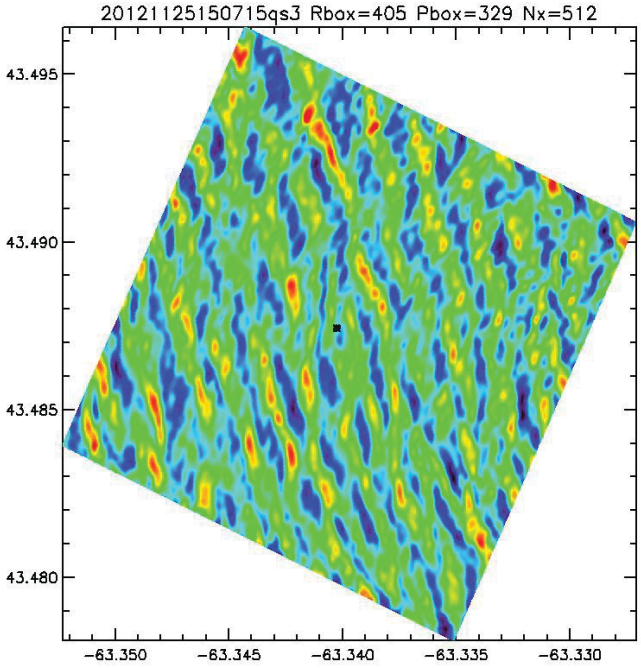

Figure 57 Sea surface for Example 2012-11-25, 15:07:15. The buoy location is marked in black

Figure 58 shows the buoy positions during the comparison interval. The displacement is shown in meters relative to the estimated mean buoy location. The buoy drift does not exceed the resolution area of one WaMoS cell (3 m).

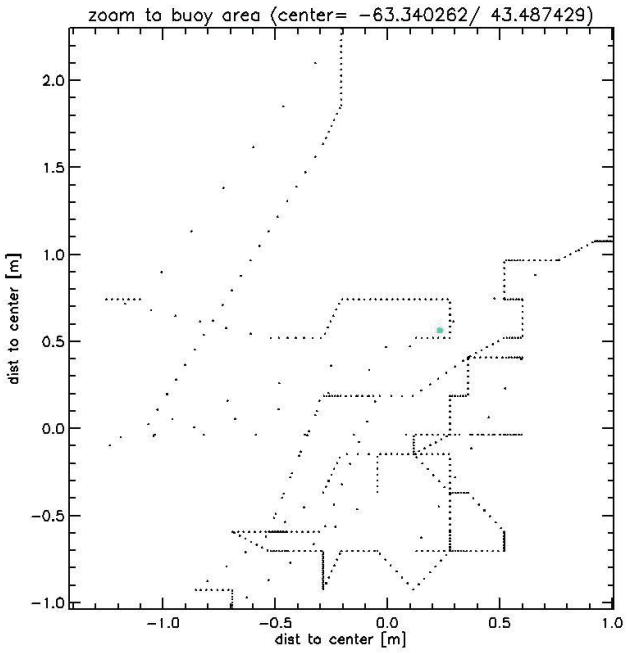

Figure 58: Buoy location during the comparison interval surface for example 2012-11-25, 15:07:15

In Figure 59, the buoy heave data (green) is compared to the time trace derived from the WaMoS II sea surface elevation maps (red) using the method described in Section 5.1.2. The blue line shows the buoy data after applying a low pass filter to match it to the spectral resolution of the WaMoS II sea surface elevations. This new comparison needs a bit more explanation:

As described in section 5.1.2, the sampling grid of the buoy is used for the comparison. Effectively, this means that the WaMoS II data is up sampled to match the buoy time stamps. But this method cannot really increase the WaMoS II data information content, it simply increases the number of samples for comparison. The real WaMoS II data resolution in time is limited by the radar rotation time, which is about 2.5 s. This means, that WaMoS II cannot detect wave components with periods lower than approximately 5 s, the spectrum of the data is limited to ~0.2 Hz. In contrast to that, the buoy has an update rate of ~0.15 s and thus is capable of measuring waves with much lower periods (up to ~0.3 s). A comparison of buoy to WaMoS II 1D spectra derived from the traces in the measurement interval shows that the buoy measures a significant amount of energy for a frequency range of up to 0.3 Hz while the respective WaMoS II data does not show any energy beyond 0.2 Hz (Figure 60). By application of a low pass filter with a limit of 0.2 Hz to the buoy data, the resolution is reduced to the WaMoS II data resolution. Whereas loss of information content is usually undesirable, it is necessary in the context of comparing the same signal.

In Figure 59, the comparison is quantified by correlation and standard deviation. It can be seen that the WaMoS II time trace shows a high correlation of 0.81 to the not filtered and 0.87 to the filtered buoy record. The standard deviation is ~0.62 m compared to the not filtered and 0.49 m compared to the filtered buoy data.

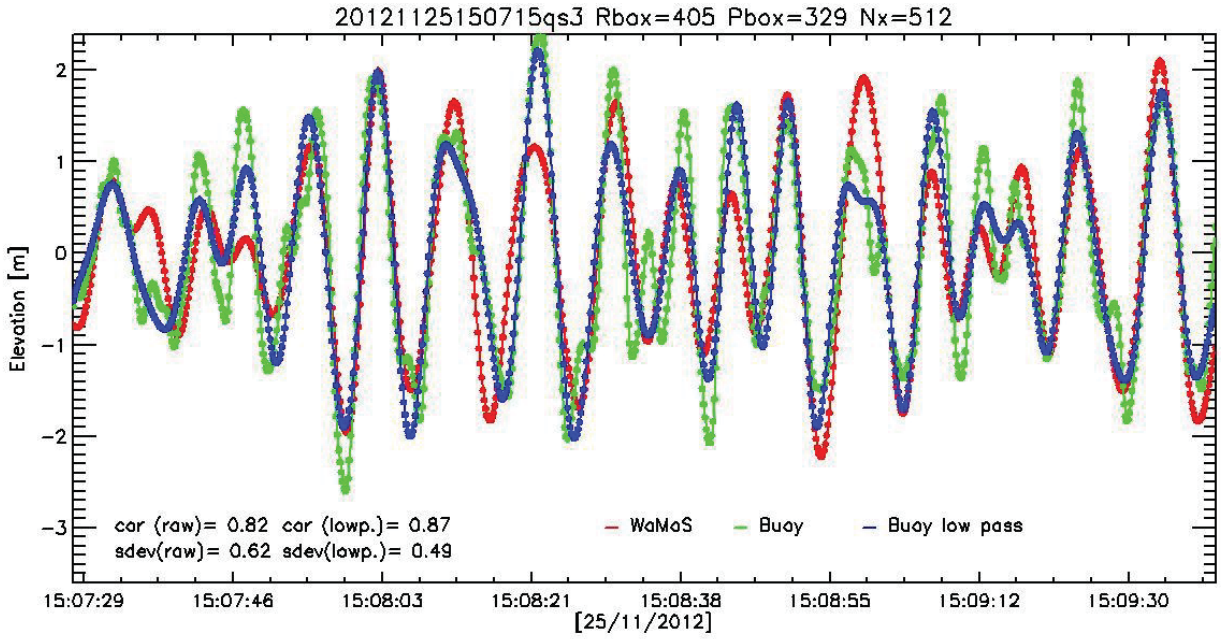

Figure 59: Time trace comparison surface for example 2012-11-25, 15:07:15

Judging from the impression of the time traces and the correlation it can be stated that this comparison shows a good match of buoy and WaMoS II elevation data. The match is statistically significant and can be considered as a proof that WaMoS is able to measure the waves in this case. However, there are still noticeable differences of the amplitudes.

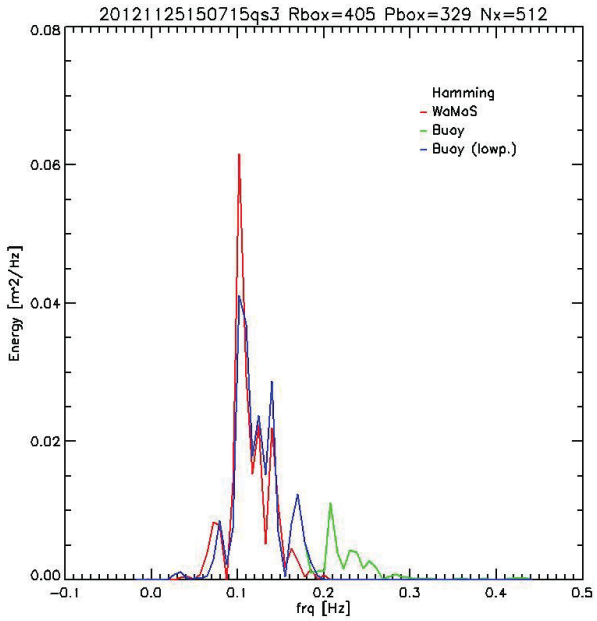

Figure 60: Spectra of buoy data and WaMoS II sea surface for the comparison interval surface for example 2012-11-25, 15:07:15. For frequencies below 0.2 Hz, the green and the blue line are identical.

5.4.3 Example 2012-11-24 16:42:18, compared to DRDC1

This example shows the best match to one of the buoys found in the data set. The comparison buoy is DRDC1.

The sea surface diagram in Figure 61 shows that the orientation of the sea surface elevation map is nearly perfect in this case. The wave crests are parallel to the x-axis of the analysis area, showing that the area is very well placed into the wave travel direction. It can be seen that the buoy is in the center of the frame.

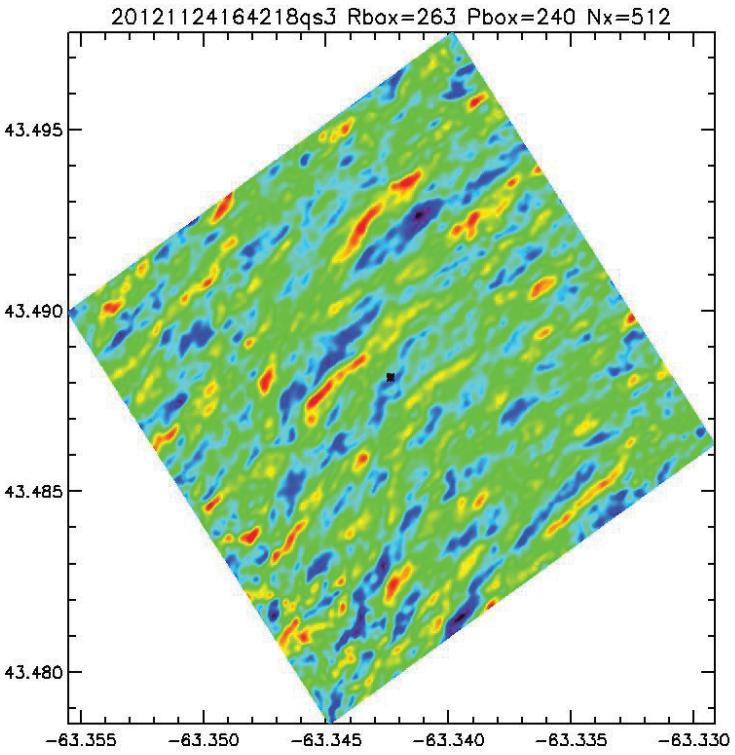

Figure 61: Example sea surface for sample 2012-11-24 16:42:18

Figure 62 shows that the buoy is only slightly moving during the comparison interval in a radius of 4 m. This means that the reference is roughly stationary within one pixel of the sea surface elevation map.

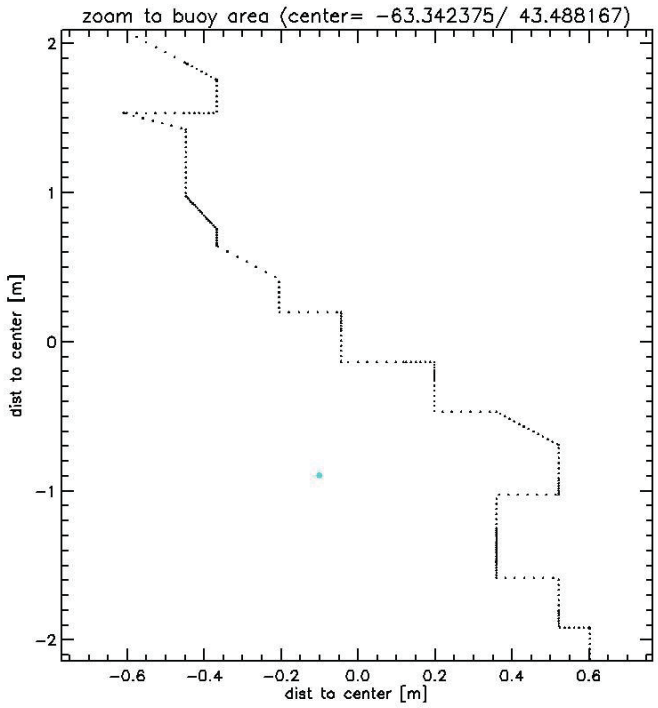

Figure 62: Buoy location during the comparison interval for sample 2012-11-24 16:42:18

The direct comparison of buoy to WaMoS sea surface in Figure 63 shows a high degree of correlation to both the raw buoy data (0.85) and the low pass filtered buoy data (0.87) with a low standard deviation of ~0.37 m. In this sample, wave groups can be seen that were measured by both WaMoS and the buoy. The comparison of the 1D spectra in Figure 64 shows that in this example the buoy has little energy beyond the 0.2 Hz limit of WaMoS, which clearly contributes to the excellent match.

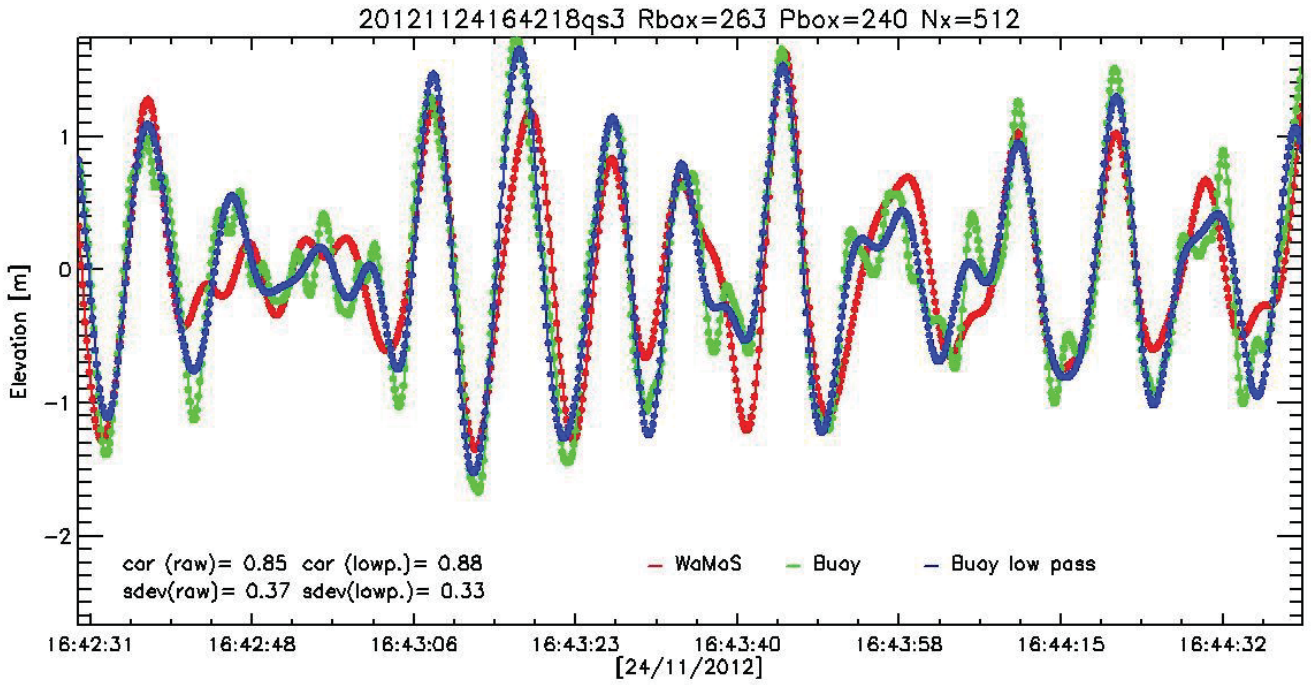

Figure 63: time series comparison for sample 2012-11-24 16:42:18

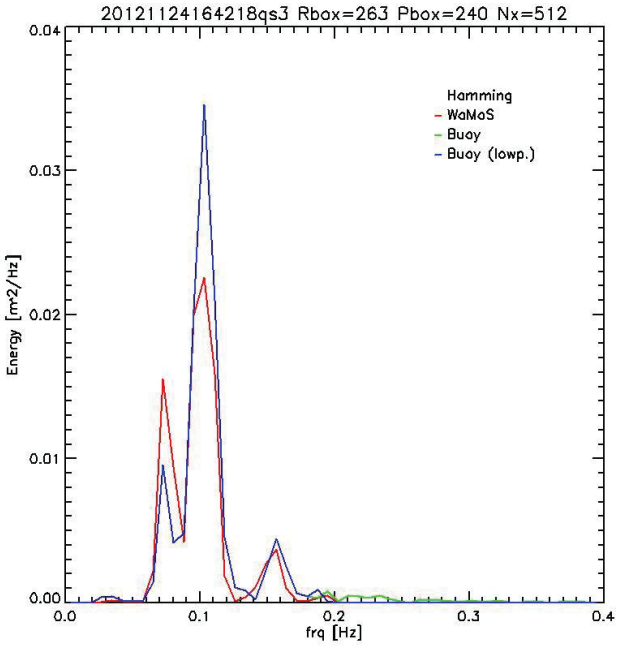

Figure 64: Spectra of buoy data and WaMoS II sea surface for the comparison interval surface for example 2012-11-24, 16:42:21. For frequencies below 0.2 Hz, the green and the blue line are identical.

5.4.4 Example 2012-11-25 04:02:50, compared to DRDC3

This example shows the impact on WaMoS II frequency limitation on the comparison. The example surface in Figure 65 shows that WaMoS sea surface elevations give a reasonable impression of a true sea state, the buoy is well localized in the center of the frame. As shown in Figure 66, the buoy is only slightly moving during the comparison interval in a radius of 3 m, so the conditions for a valid comparison are maybe not ideal, but are clearly met. However, the comparison of the time traces is not satisfying on the first look, as shown in Figure 67. The correlation of the raw buoy signal to the WaMoS II time trace is only 0.48, which means that no significant match was found. However, the correlation to the low pass filtered buoy data is significantly higher, about 0.58 which still is not a good match but at least indicates some similarities. This is backed by the visual impression of the time traces.

The reason for the low correlation can be explained by the spectra shown in Figure 68. Two peaks in lower frequencies are seen by both WaMoS and the buoy. In contrast to the two other examples (Sections 5.4.2 and 5.4.3), the buoy data has also significant percentage of energy in the frequency range above 0.2 Hz, with a clear peak at ~0.22 Hz. This peak is not observed in the WaMoS II data. As the high frequency variation is not seen by WaMoS II, the correlations of time traces results in low correlations despite the fact that longer waves in both records generally match. It should be noted, that the shift compensation (Section 5.3) is based on comparison to the not filtered buoy data. It is possible that new search using low pass filtered buoy data might result in better matches.

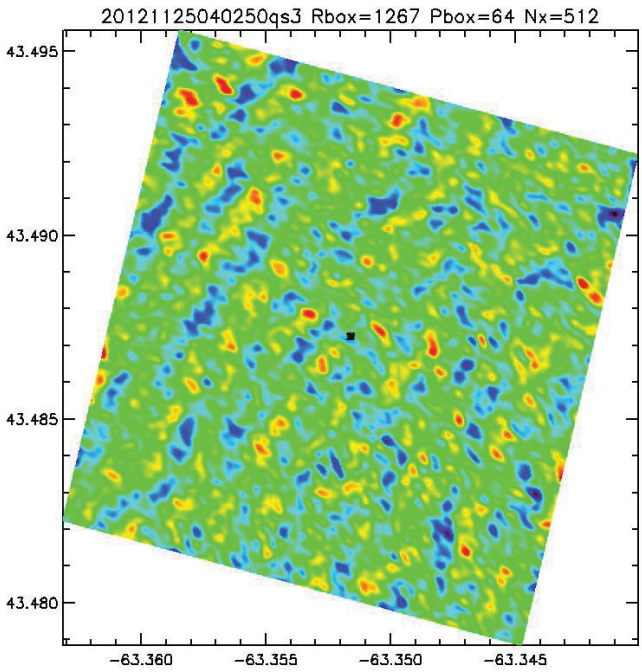

Figure 65: Sea surface elevation map and buoy location for sample 2012-11-25 04:02:50

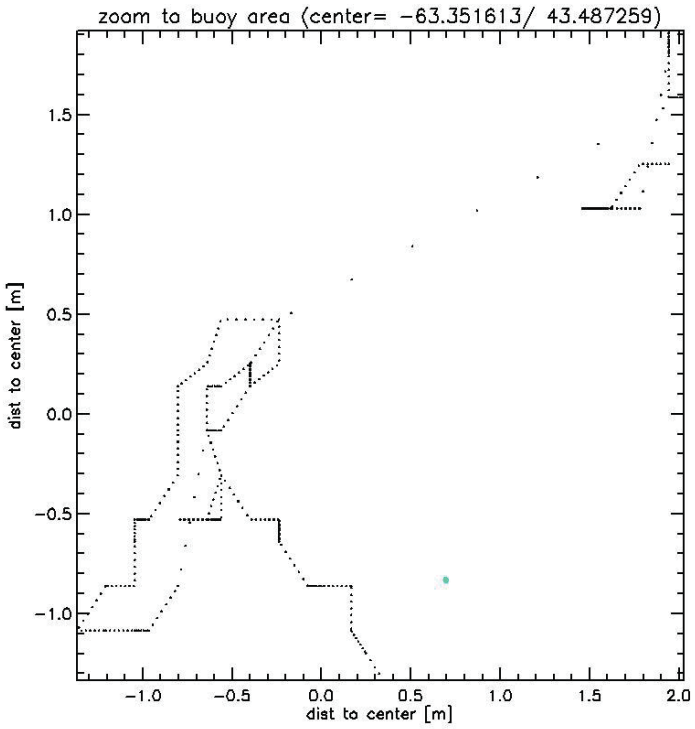

Figure 66: Buoy location during the comparison interval for sample 2012-11-25 04:02:50

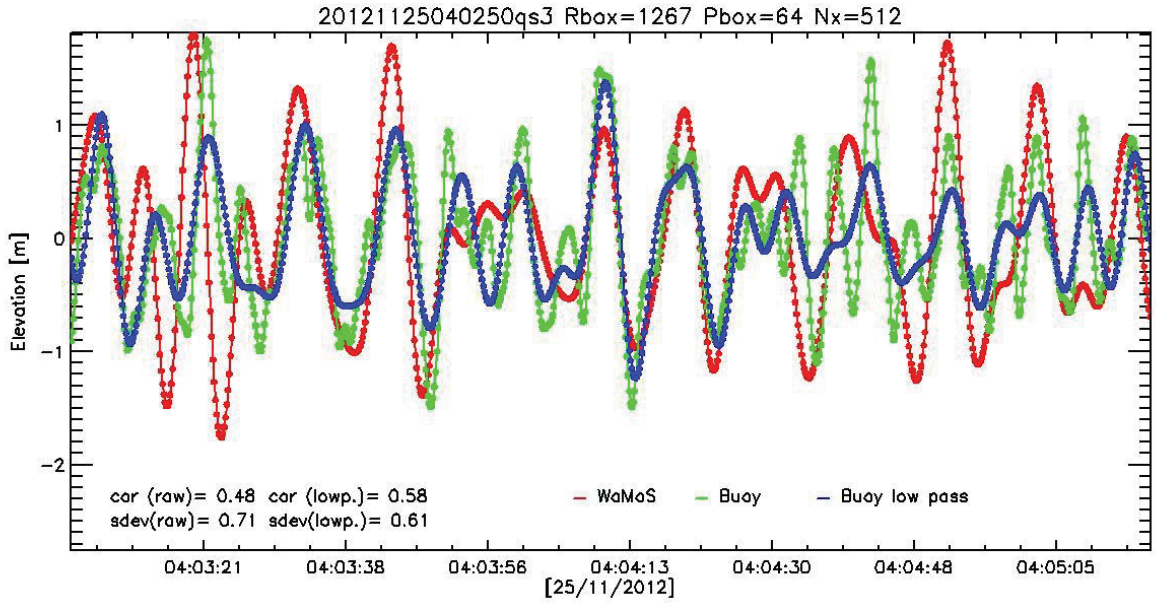

Figure 67: time series comparison for sample 2012-11-25 04:02:50

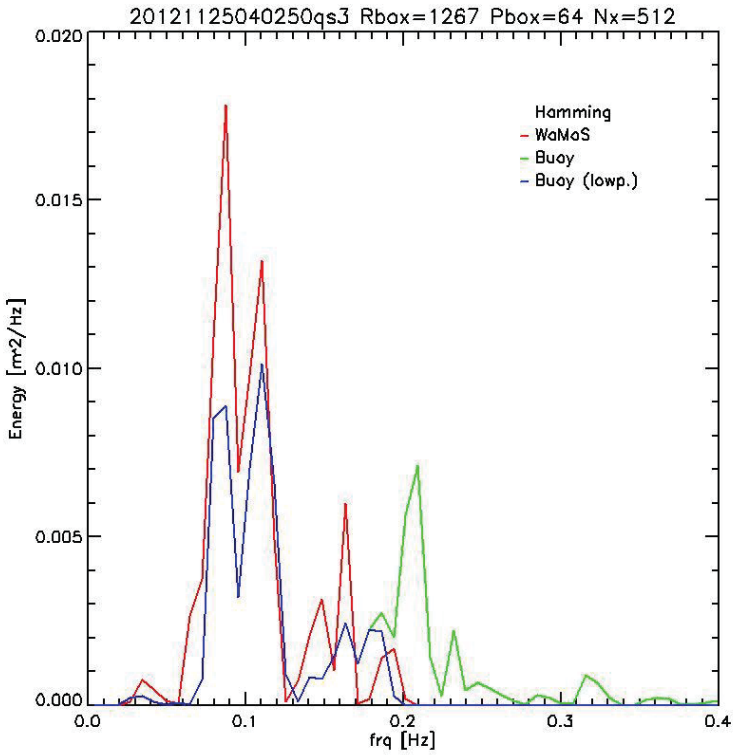

Figure 68: Spectra of buoy data and WaMoS II sea surface for the comparison interval surface for example 2012-11-25 04:02:50. For frequencies below 0.2 Hz, the green and the blue line are identical.

5.5 SUMMARY OF ALL DATA COMPARISONS

5.5.1 Background

To all samples found by the data scan algorithm (Section 5.2.2) the localization procedure (Section 5.3) was applied to compensate shifts in time and space. Time traces at the buoy location were created using the procedure described in Section 5.1.2. They were correlated to the buoy measurements. In this Section, the result of all comparisons are summarized in terms of correlations to the buoy. In addition, the shifts applied to the WaMoS II data are shown for all samples.

For all samples, several possible influences on the correlation to the buoy were checked:

- Significant wave height
- Peak wave period
- Distance of buoy to the radar
- Difference of look direction towards the buoy to main wave travel direction

None of these tests revealed a significant impact on the correlation to the buoy. Therefore, the results are not discussed in more detail in this report. It should be noted that the data selection of

samples prior to this comparison already excluded cases where such issues would definitely influence the match, e.g. by defining a minimum wave height for the comparison (compare Section 5.2). Thus, it seems that once some base requirements are met, the WaMoS II data is not severely influenced by such factors.

For buoys DRDC1 and DRDC3 more situations were found that are suitable for comparison. This seems to be caused by the vessel movement relative to the main wave travel direction. There are more occasions in which the buoy was seen roughly in wave travel direction for DRDC1 and DRDC3 than for the buoys DRDC2 and DRDC4.

5.5.2 Buoy DRDC1

5.5.2.1 Correlations

For the buoy DRDC1 a total of 27 suitable comparison data sets were found by the data selection method described in Section 5.2.2. The comparisons to this buoy gave the best matches. As shown in the overview diagram in Figure 69, the majority of comparisons resulted into correlations of 0.7 and higher for both the raw buoy data (red) and the low passed buoy data (blue). Only in one case, on 2012-11-25 14:42:45 a drop out to a very low correlation of 0.42 was observed. Here, it seems that the buoy GPS did not work as expected, in contrast to all other buoy data samples only two positions were recorded for this sample while all other buoy data show clear traces on a very fine grid as demonstrated e.g. in Figure 58. However, there might be other reasons for this deviation.

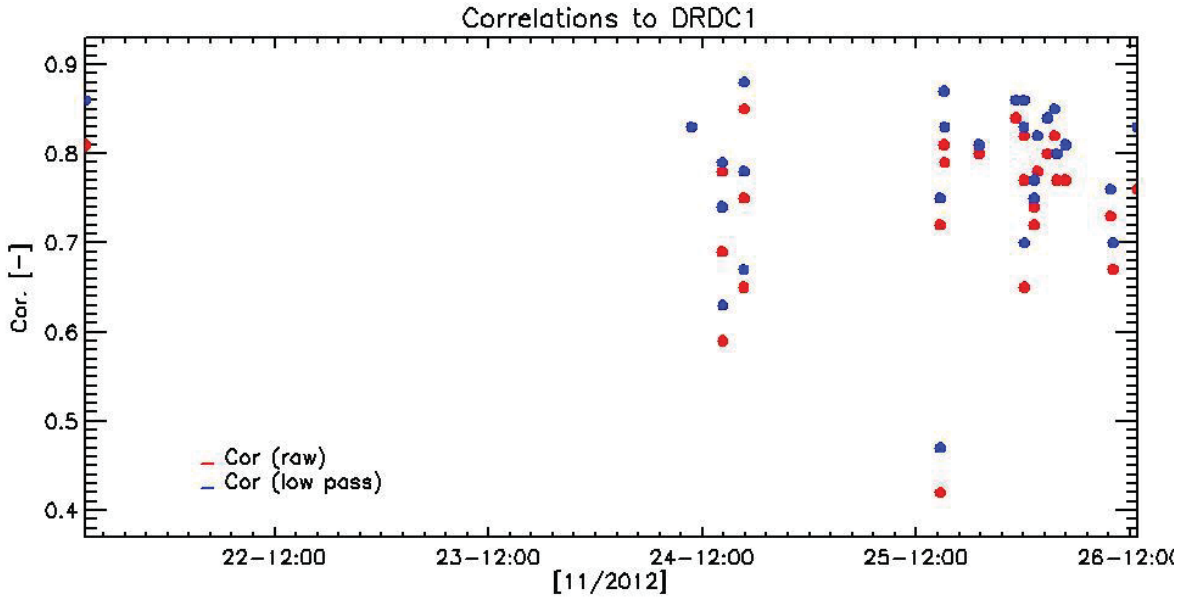

Figure 69: Summary of all comparisons to buoy DRDC1

The diagram also shows that application of a low pass filter to the buoy data significantly improves the match in many cases. This indicates that the frequency limitations of WaMoS II have a considerable impact on the results. Using radar antennas with a higher rotation speed might be needed for some applications of the inversion method.

5.5.2.2 Shift vectors

When localizing the buoy in the sea surface elevation maps, shifts in space and time are added to the WaMoS data to get the best match (see Section 5.3). Figure 70 to 69 show the applied shifts in time, x and y added to the sea surface elevation map for each comparison. The shifts are denoted in 'Pixel' relative to the assumed start time of the buoy record/location. The grid units used for the shifts. In time, the step width is one antenna rotation time (RPT), in x and y it is the spatial WaMoS data resolution (3 m).

The majority of shifts in time was -1, in some cases a shift of 0 gave the best match. In x and y, a constant offset was not observed. All shifts in space are in a range of up to 20 pixel (60 m) around the expected buoy position in both dimensions.

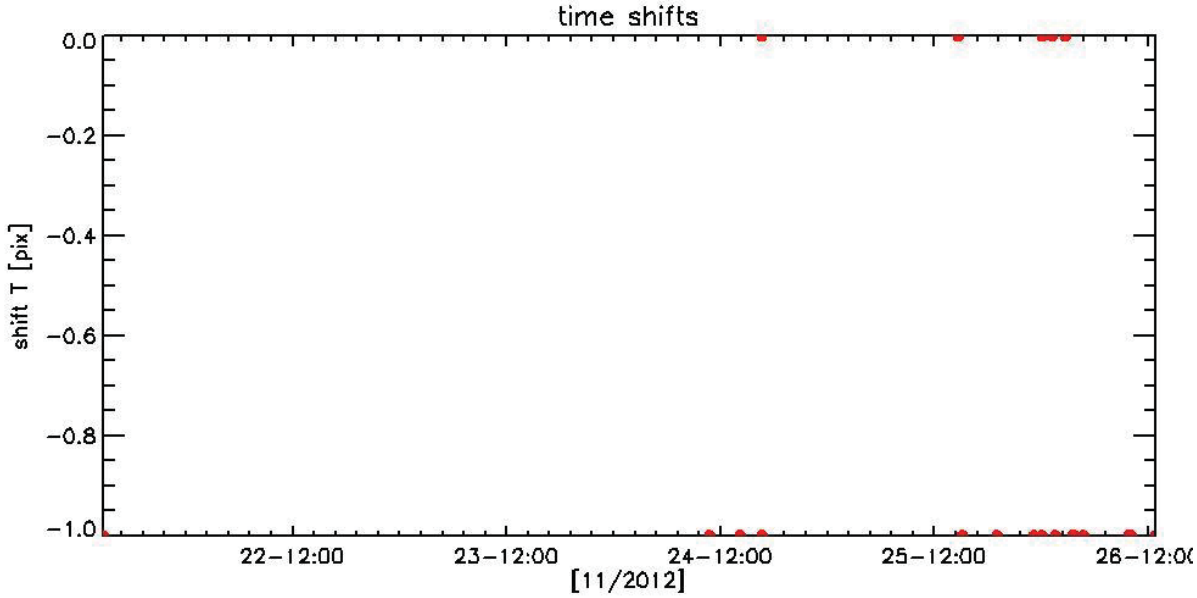

Figure 70: Shifts in time added to WaMoS data for comparisons to buoy DRDC1

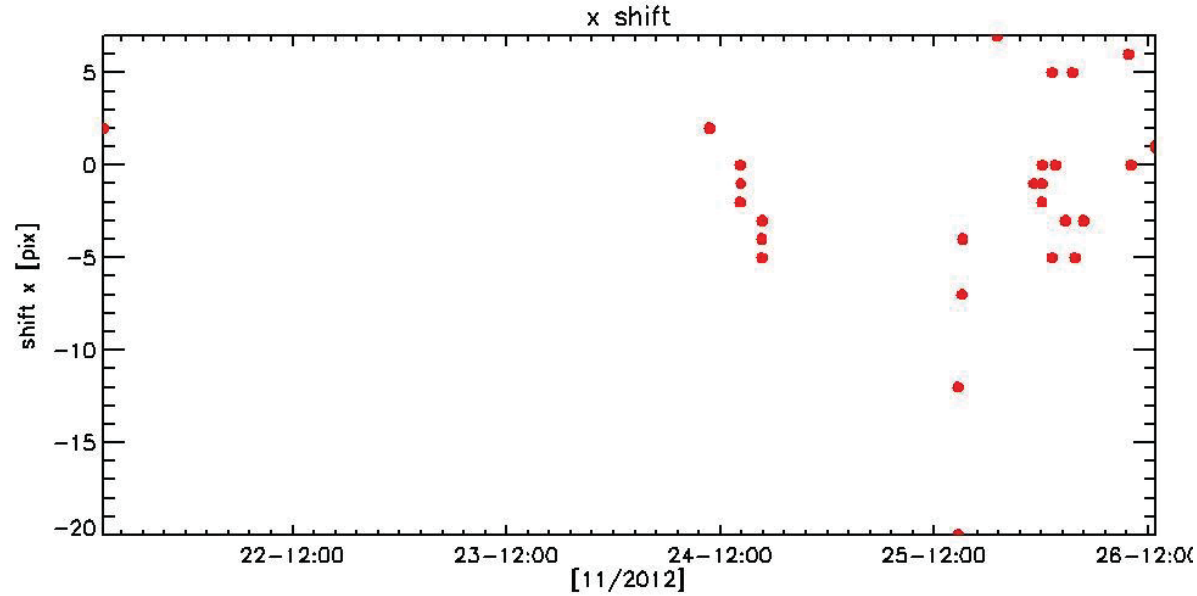

Figure 71: shift in x added to WaMoS data for comparisons to buoy DRDC1

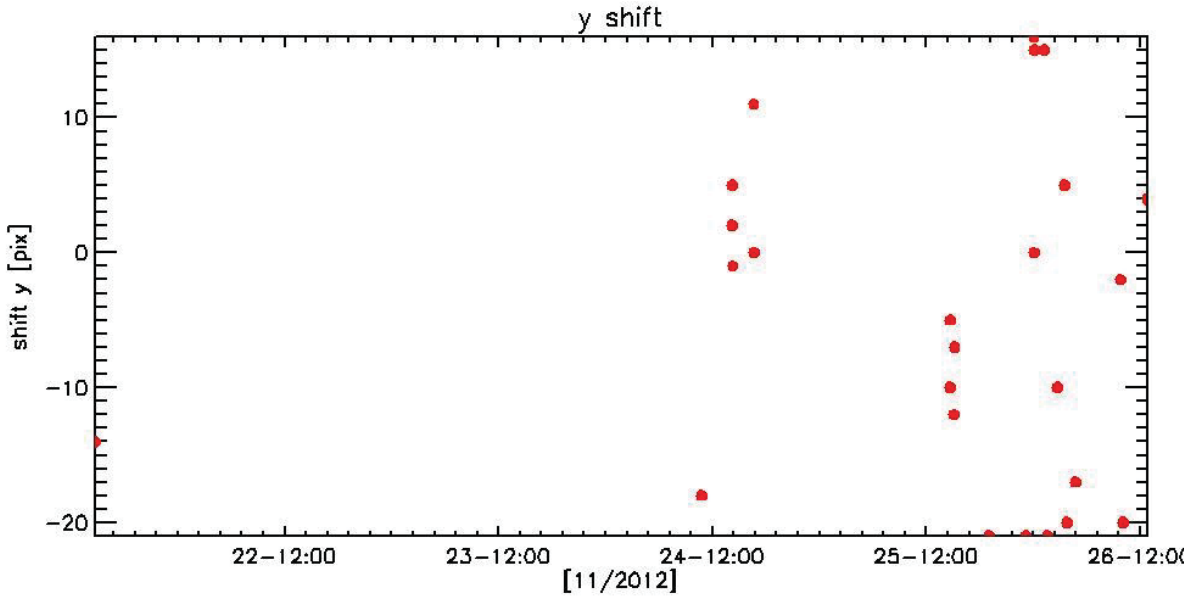

Figure 72: Shift in y added to WaMoS data for comparison to buoy DRDC1

5.5.2.3 Effect of Bases Corrections

To show the impact of the bases corrections described in Section 4, the comparison to buoy DRDC1 was in addition carried out for uncorrected data. All settings of the inversion and validation procedure are identical to the conditions used for the results shown in Section 5.5.2.1.

Figure 73 shows the result of the rerun for WaMoS II radar with uncorrected NMEA data. The correlations in this diagram should be identical to Figure 69, all differences are caused by the different NMEA input.

It can be seen, that the level of correlation is much lower. The majority of cases show correlations below 0.6 here, whereas in Figure 69 most samples are above 0.7. This shows that correct NMEA input is crucial for comparisons to wave rider buoys. This important result should be considered for any application of the method.

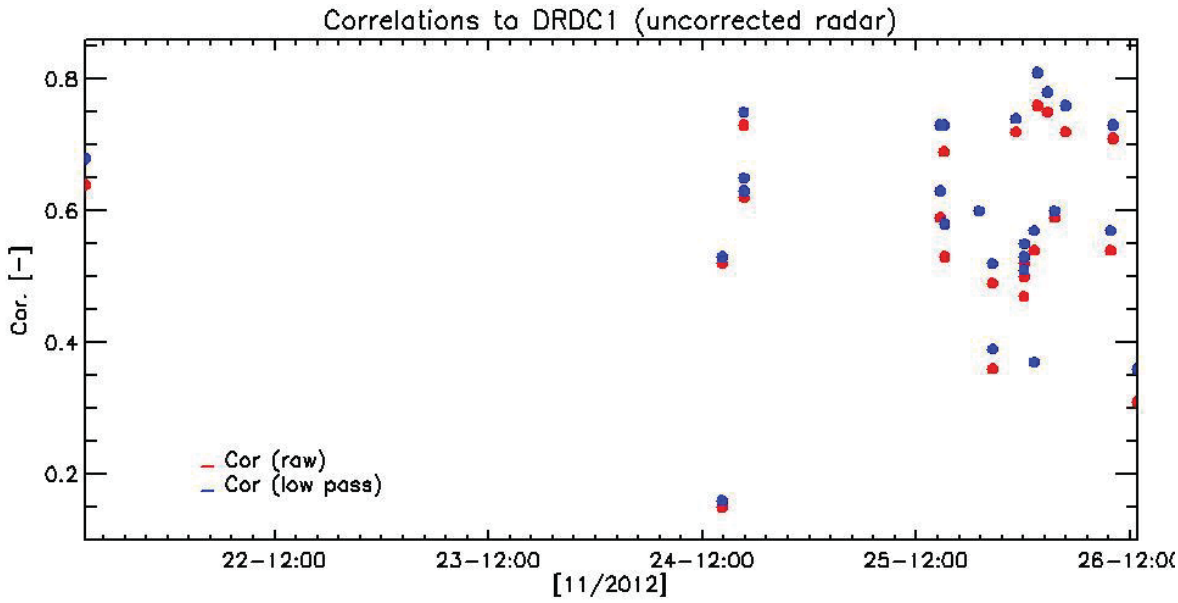

Figure 73: Results for WaMoS using uncorrected NMEA data in comparison to DRDC1. Compare to Figure 69.

5.5.3 Buoy DRDC2

For buoy DRDC2 the data scan algorithm found 8 matching WaMoS samples.

5.5.3.1 Correlations

The resulting correlations to Buoy DRDC2 are shown in Figure 74. Two comparisons yield correlations below 0.6. It seems that these cases of low correlations can be explained by the different sampling rates of the instruments as discussed in Section 5.4.4. In both samples, the buoy spectra have significant energy above 0.2 Hz that is not recorded be WaMoS II. The correlations for the other cases are in the same order of magnitude as for DRDC1.

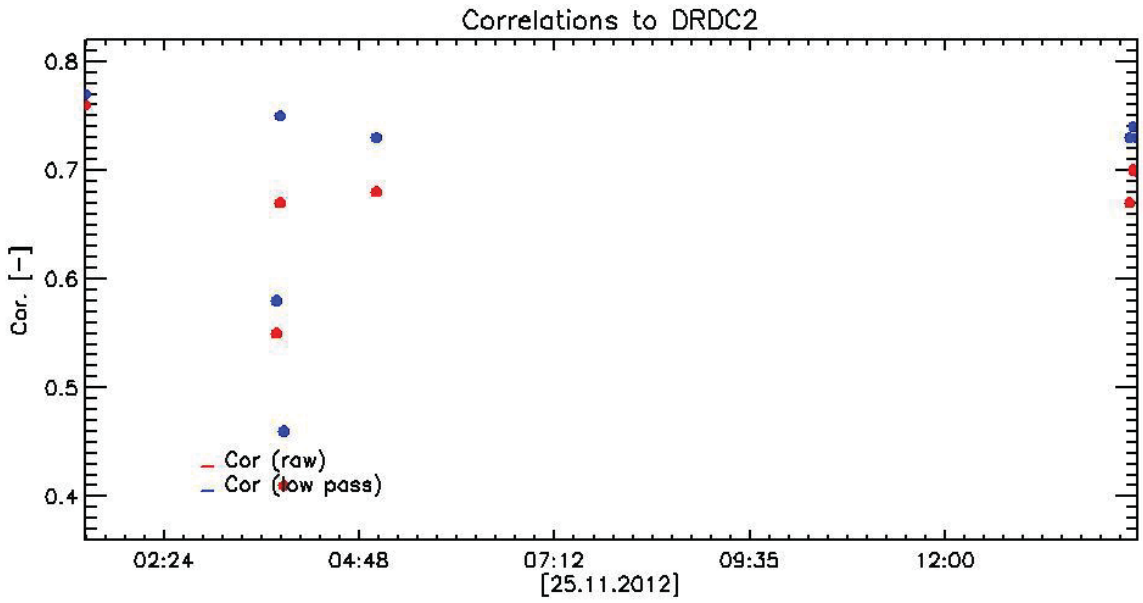

Figure 74: Summary of all comparisons to buoy DRDC2

5.5.3.2 Shift vectors

Figure 75 to Figure 77 show the applied shift vectors in time and space. They are generally in the same range as for the DRDC1 comparisons.

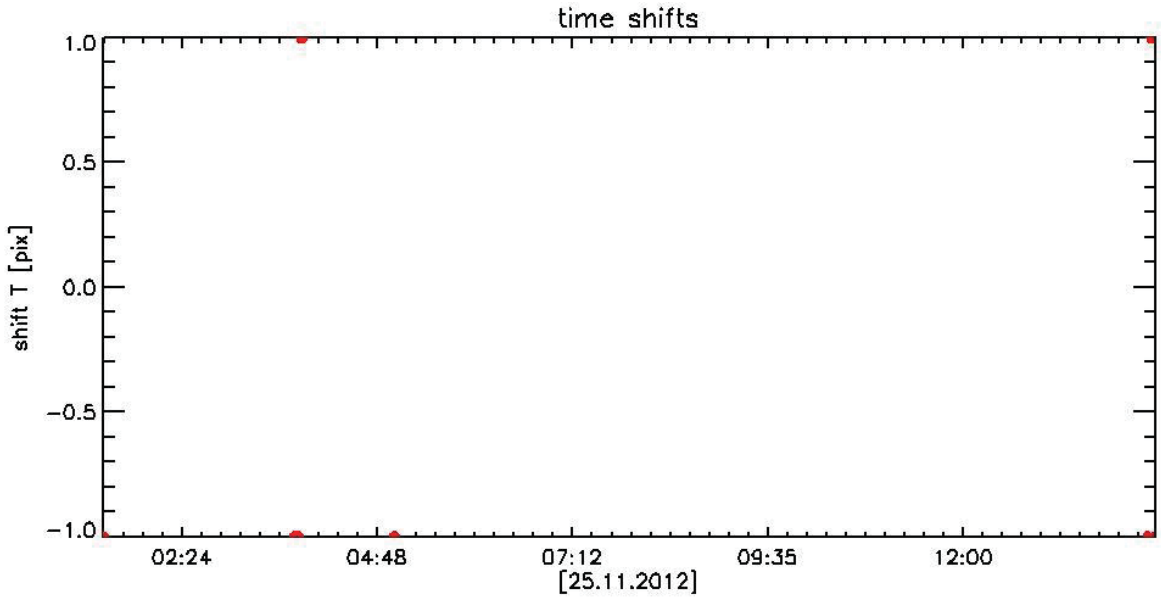

Figure 75: Time shifts added to WaMoS data for comparisons to buoy DRDC2

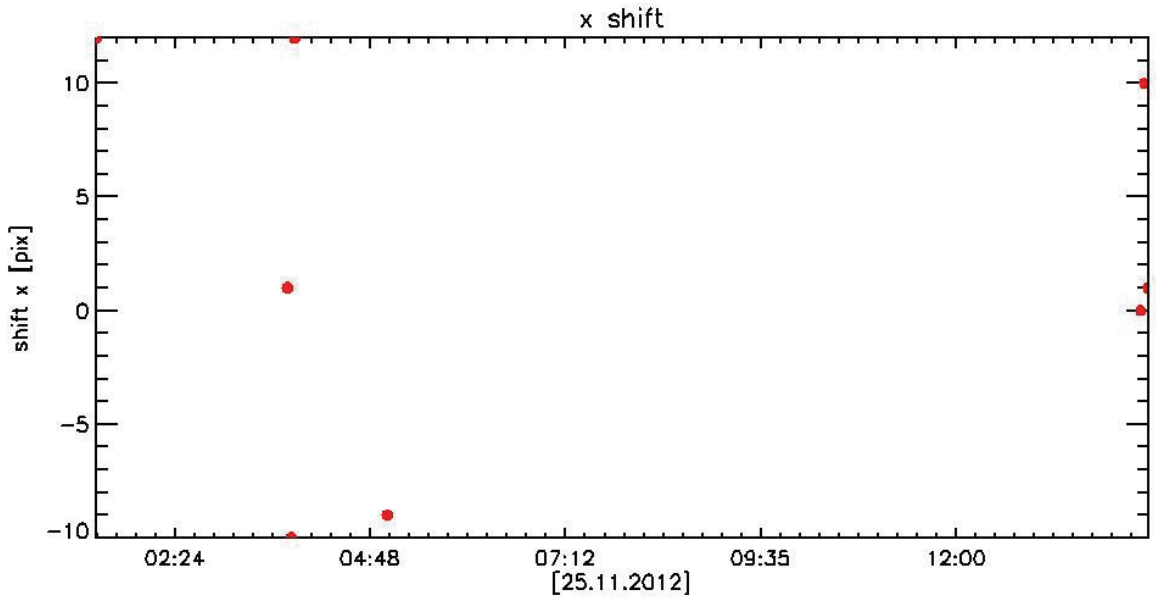

Figure 76: x shift added to WaMoS data for comparisons to buoy DRDC2

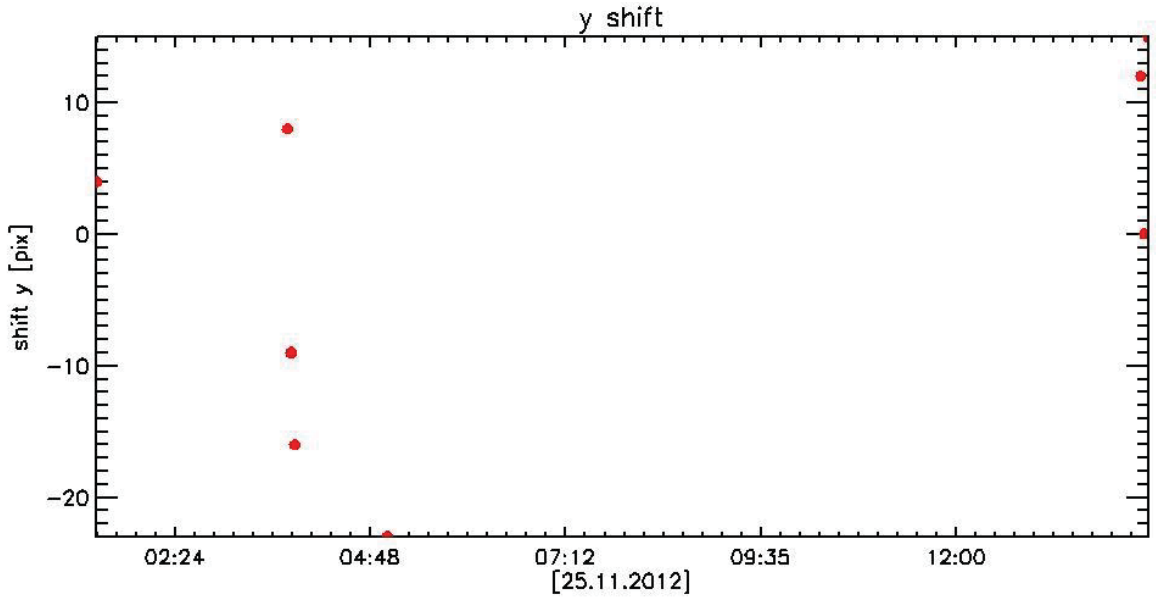

Figure 77: y shifts added to WaMoS data for comparisons to buoy DRDC2

5.5.4 Buoy DRDC3

For buoy DRDC2 the data scan algorithm found 29 matching WaMoS samples.

5.5.4.1 Correlations

Figure 78 shows the correlation for all samples to the buoy, for both the raw buoy data (red) and the low pass filtered buoy data. As in all other comparisons, the low pass filter improves the correlation.

Compared to the DRDC1 data, the overall match is less obvious. More cases of correlations below 0.7 were found than for the buoy DRDC1. As discussed in Section 5.4.4, one reason for low correlations can be the different sampling rates. WaMoS II cannot detect waves with frequencies above 0.2 Hz with the given radar rotation time. However, the reason for the lower correlations compared to DRDC1 is not obvious. The general conditions for all comparisons were the same as for DRDC1, most found matches are dating form 25th and 26th for both buoys. The only systematic difference between the two comparisons seems to be the choice of the reference sensor. For the example discussed in Section 5.4.4, spectra of DRDC1 to DRDC3 were compared, hinting to a tendency of DRDC3 to measure higher frequencies. Still, this comparison was not examined in depth or for a longer sample and is thus not conclusive. It merely points out that further investigation is needed.

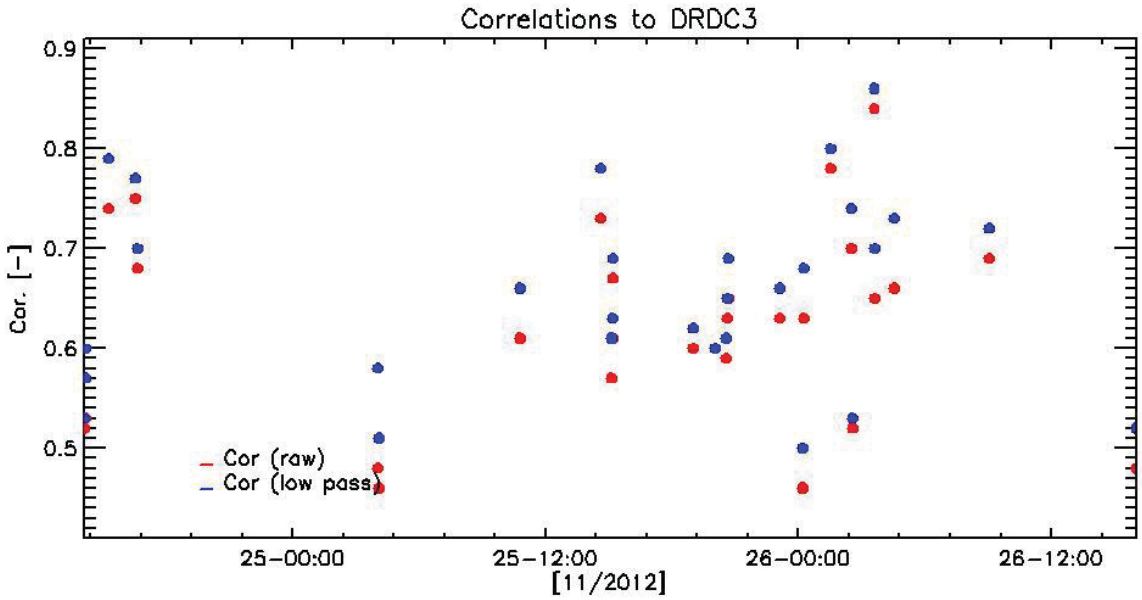

Figure 78: Summary of all comparisons to buoy DRDC3

5.5.4.2 Shift vectors

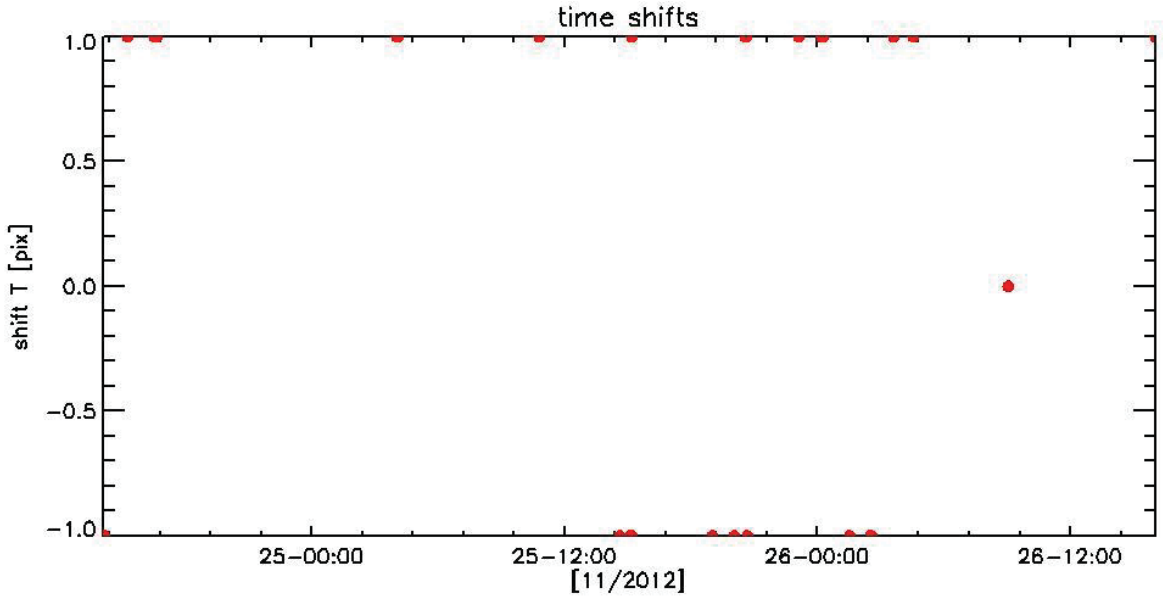

Figure 79: time shifts added to WaMoS data for comparisons to buoy DRDC3

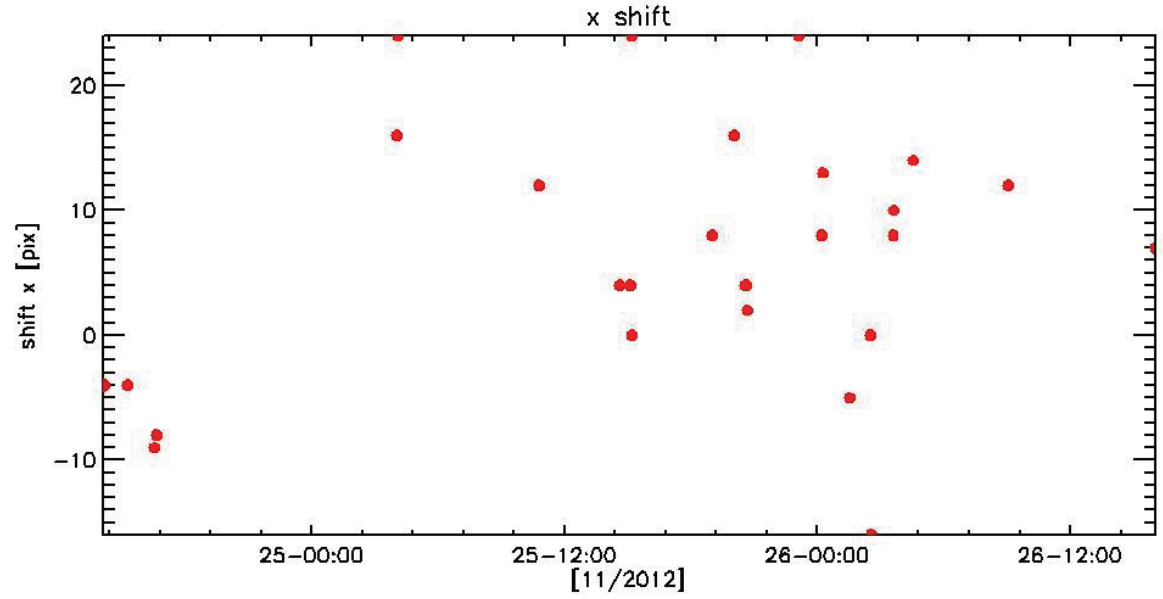

Figure 80: shift in x added to WaMoS data for comparisons to buoy DRDC3

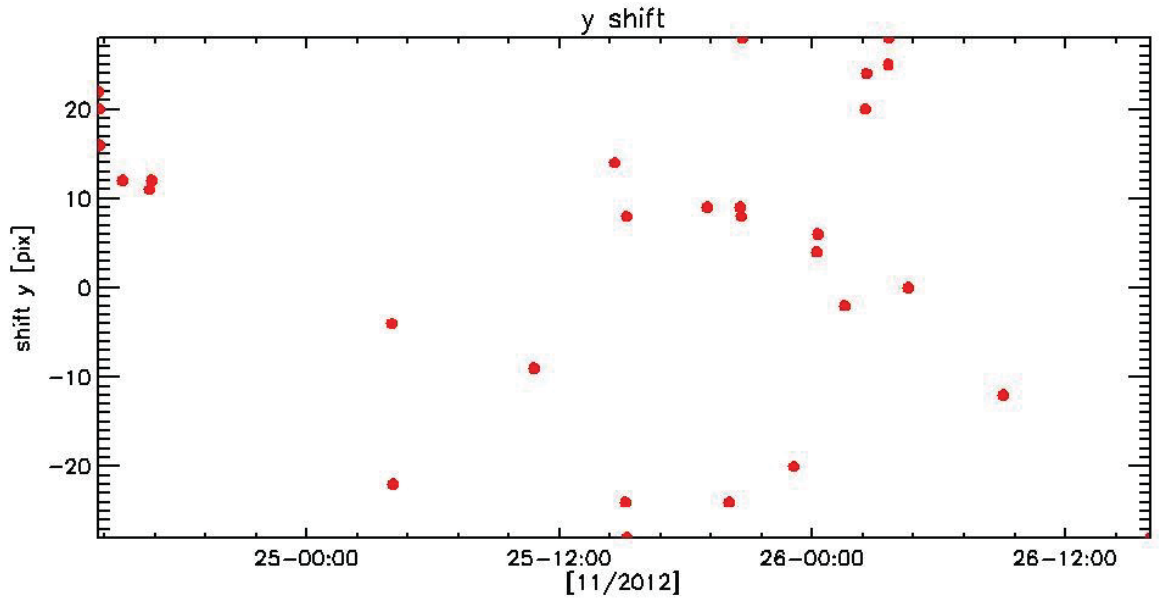

Figure 81: shift in y added to WaMoS data for comparisons to buoy DRDC3

5.5.5 Buoy DRDC4

For buoy DRDC4, a total of 7 samples was found.

5.5.5.1 Correlations

Compared to the results for DRDC1 and DRDC2, the correlations are generally lower as shown in Figure 82. It seems that many cases of low correlations can be explained by the different sampling rates of the instruments as discussed in Section 5.4.4. Only one example with a correlation above 0.75 was found for this buoy.

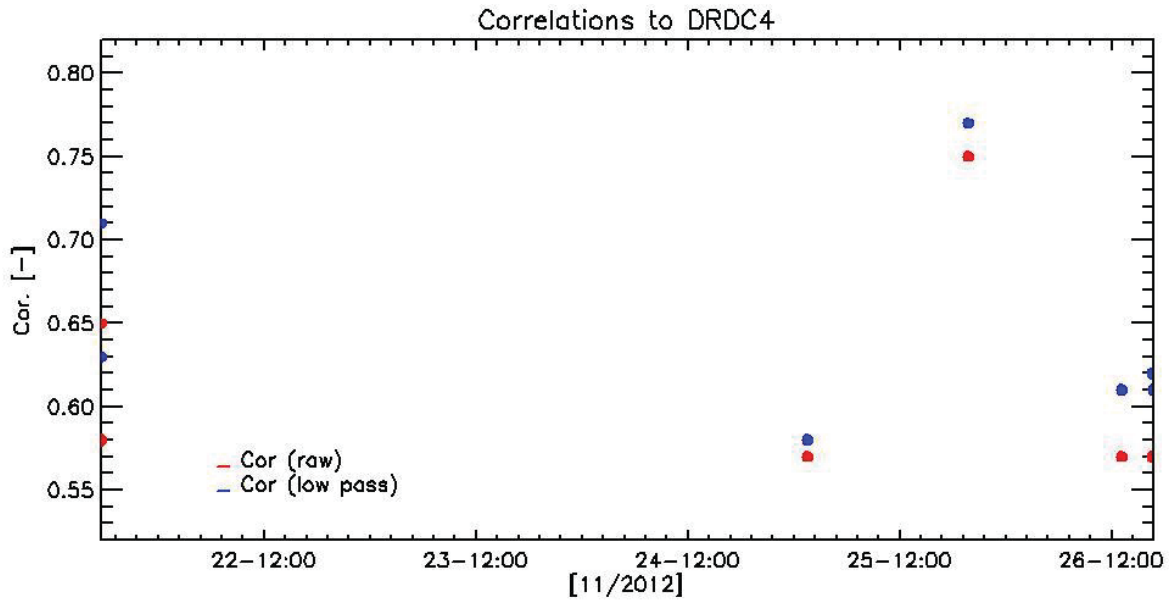

Figure 82: Summary of all comparisons to DRDC4

5.5.5.2 Shift vectors

The shift vectors in time and space added to the WaMoS data are shown in Figure 83 to Figure 85. They are generally in the same order of magnitude as for the other buoys.

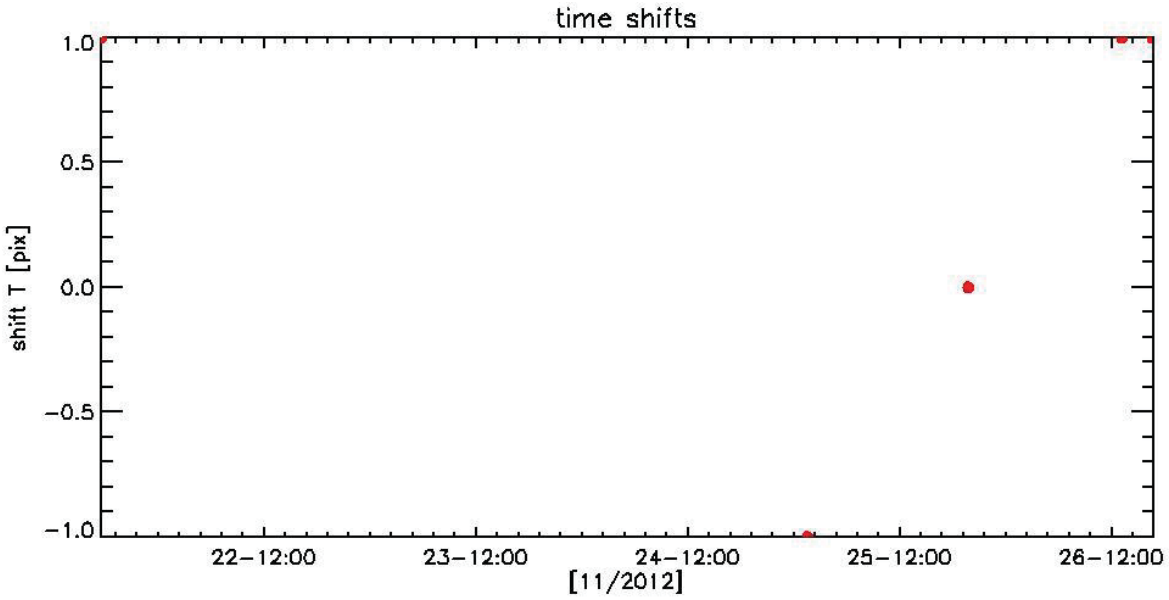

Figure 83: Time shifts added to WaMoS data for comparisons to buoy DRDC4

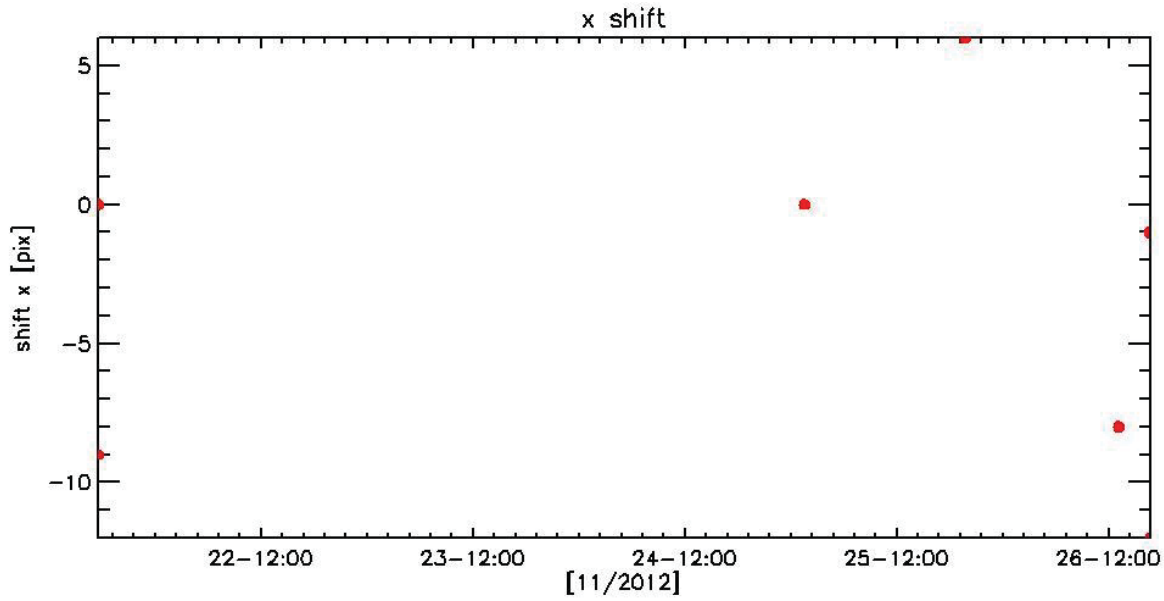

Figure 84: shifts in x added to WaMoS data for comparisons to buoy DRDC4

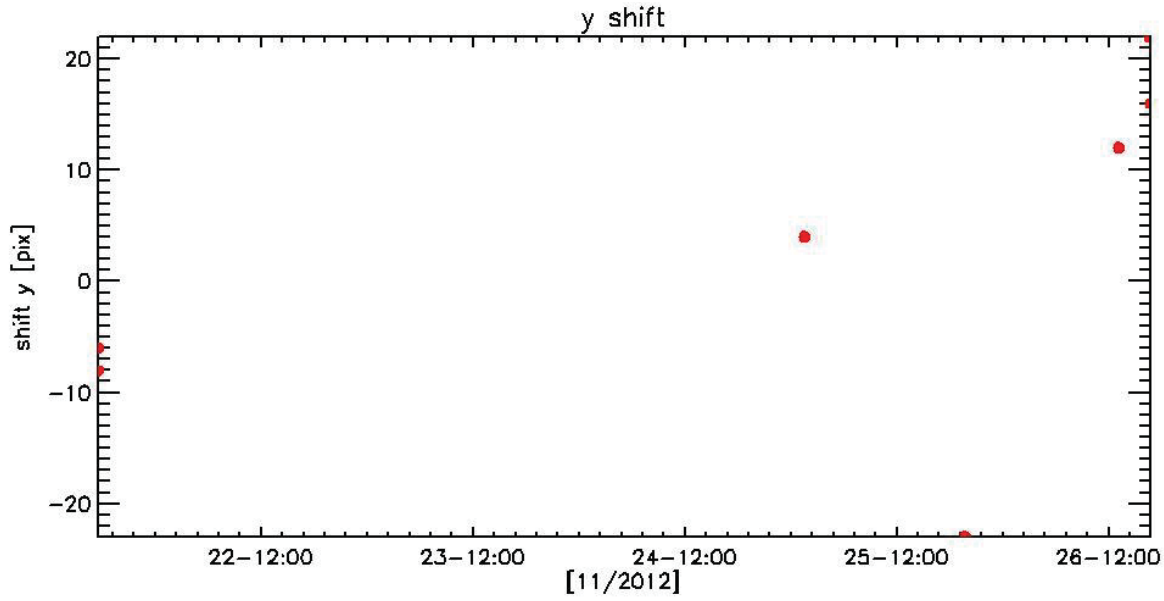

Figure 85: shifts in y added to WaMoS data for comparisons to buoy DRDC4

5.5.6 Temporal Up- and Down- Interpolation Methods

Although not investigate to the same extent as the Fourier expansion method, the temporal up- and down- interpolation methods were evaluated for the DRDC buoy 1. Spatial offsets corresponding to the peak correlation values were often exceedingly large for the down-interpolation method, suggesting erroneous results (Figure 86). Excluding these outliers, similar results were observed for

both methods. Approximately 30 m of offset are observed, and randomly distributed (Figure 87). The four combinations of up- and down- interpolation, combined with spatial search or none (assume zero spatial offset), yielded trends in correlation. Higher correlation values were observed for the up-interpolation methods, with the best result for combined up-interpolation and spatial search (Figure 88).

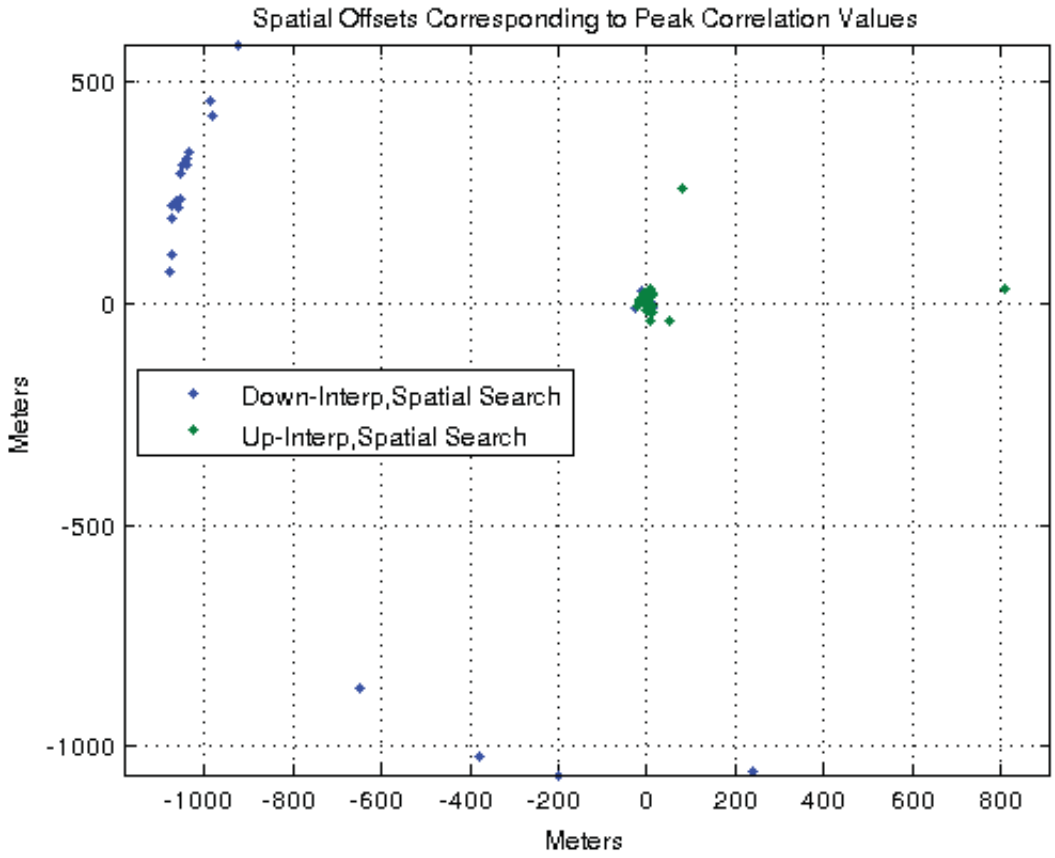

Figure 86. Spatial offsets corresponding to peak correlation values from the up- and down-interpolation methods. The down-interpolation method exhibited exceedingly large offsets, suggesting erroneous results.

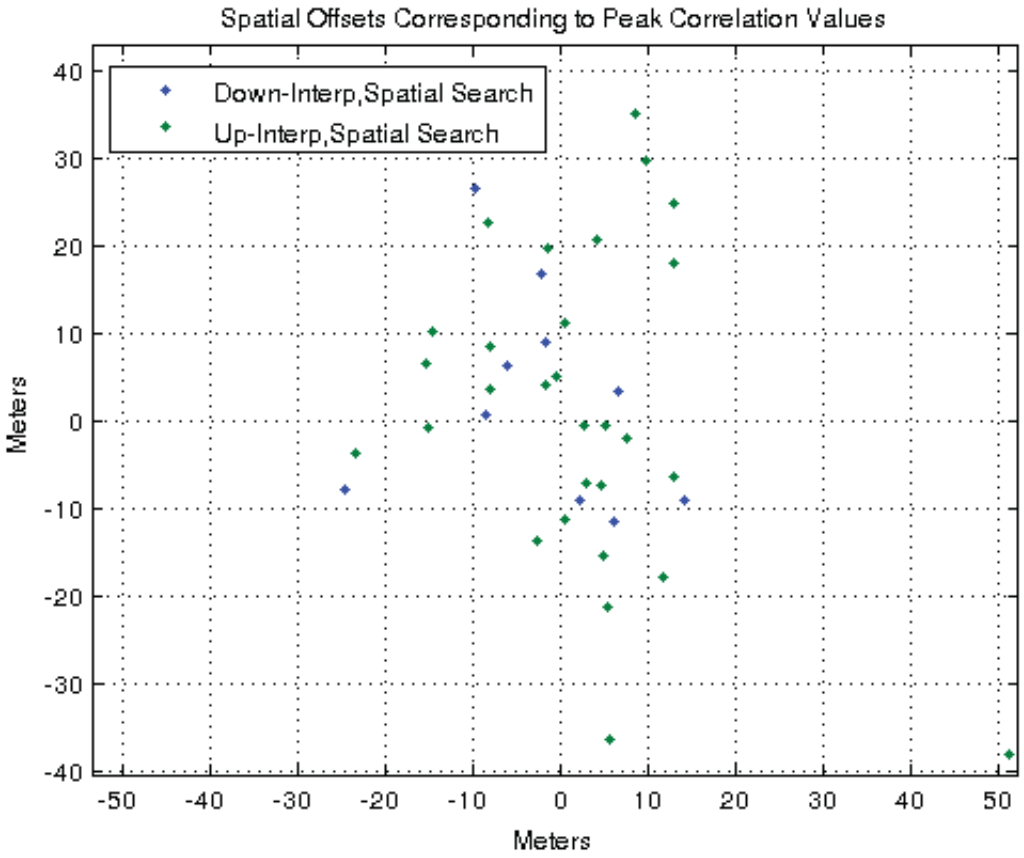

Figure 87. Zoomed-subset of spatial offsets from correlation search. Similar results are observed for both methods, excluding the outliers from the down-interpolation method. Approximately 30 m of offset are observed, and randomly distributed.

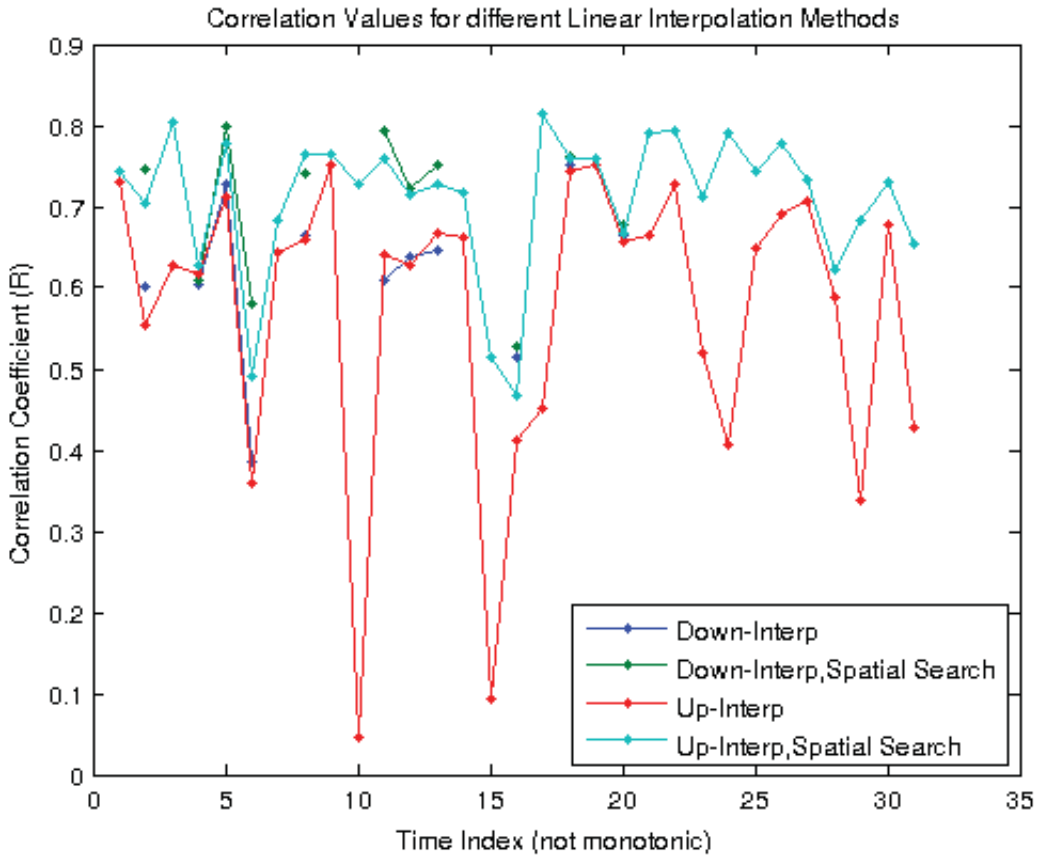

Figure 88. Timeseries of correlation values for the temporal interpolation methods. The time axis is not monotonic. Higher correlation values are observed for the up-interpolation methods, with the best result for combined up-interpolation and spatial search.

5.6 Summary of Sea Surface Validation

In this section, the results for comparisons of WaMoS II sea surface elevations to the buoy vertical displacements are summarized. A primary issue for the success of this comparison is to correctly localize the buoy in the WaMoS II data and to focus on situations where the WaMoS II can retrieve a clear wave pattern. The crucial factors here are the sample selection criteria and the correction of bases required for accurate localization of the buoy. The criteria for data selection focused on situations where the buoy is seen in wave travel direction and in a distance to the vessel where the inversion process can be successfully applied. This data pre selection step leads to a significant reduction of comparison data. Overall, approximately 80 situations were identified for which a comparison to one of the four buoys was possible. It should be noted that this reduction is mainly caused by the strict criteria, which could be relaxed for subsequent analysis. General factors that limit the application of WaMoS II are the wind conditions, situations of low wave heights and the presence of blocked look directions. The other factors that reduce the number of evaluable cases will not be an issue for an operational system as the area of observation can be automatically adjusted to focus on the main wave travel direction.

As discussed in Section 5.3, it was necessary to allow shifts in time and space in the WaMoS data to achieve good correlations to the buoy. The shift vectors found by this method are presented for all comparison results to check if they are in an acceptable order of magnitude. It seems, that for all comparisons the applied threshold can be explained by known inaccuracies in the bases (Section 4.2.7). Generally, peak correlations were found for time offsets up to 2.5 s, and spatial offsets of ~60 m in x and y dimensions.

Detailed comparison results are presented for three example cases in Section 0, all other comparison are summarized in terms of correlations to the buoys in Section 5.5.

Overall the results of the comparison are very promising. In particular for Buoy DRCD1 many examples of high correlations were found, for the other three buoys the resulting correlations are generally lower but still prove the general good match of WaMoS to the buoys.

Theoretical considerations imply that correlations of more than 0.6 are needed to prove that the match is statistically significant. The majority of cases shown in Section 5.5 are well above this limit, the best matches show correlations of up to 0.85. This can be considered as clear evidence that WaMoS II is able to retrieve the sea surface elevations. However, there are still many cases where the correlation is low.

One key factor that seems to influence the correlation is the time resolution of the measurements. Due to the relatively low antenna rotation time (~2.5 s), WaMoS II cannot resolve waves with a frequency of above 0.2 Hz, whereas the buoys have a much higher resolution (~0.15 s) and can thus resolve waves with much higher frequencies. In many cases of lower correlations, it was found that the buoy recoded significant energy for short waves. A general increase of correlation coefficients when comparing WaMoS II data to filtered buoy elevation data shows that this effect is seen for many examples. After application of a low pass filter to the buoy record, the correlations factor is often significantly increased. In all situation with excellent matches (correlations of 0.8 and higher) the buoy spectra shows no significant amount of energy beyond 0.2 Hz and applying the low pass filter only slightly improves the correlation (for the best match, it is increased from 0.85 to 0.88). In contrast to this, low correlation factors are significantly increased when filtering the buoy data (e.g. from 0.48 to 0.58 in the example shown in Section 5.4.4). For an operational system, a radar with a fast rotating antenna would help to negate this issue.

An interesting property of this data set is the fact that comparisons to buoy DRDC1 shows a significantly better match than to the three other buoys. For Buoys DRDC2 and 4 this might be explained by the lower number of found comparison samples. Here, the vessel motion pattern leads to fewer matching cases as theses buoys usually were not seen in wave travel direction. In contrast, buoy DRDC3 provides roughly the same number of samples as DRDC1. Still, the correlations found for this sample are in general lower than for buoy DRDC1. As discussed in Section 5.5.4, this is not easy to understand as the general conditions for this comparison are basically identical to the comparisons for DRDC1. There are indications that the buoy DRDC3 has a tendency to measure waves with higher frequencies than DRDC1 and therefore has more examples where the comparison is influenced by the time resolutions of the instruments. However, this was not examined in detail, yet. A detailed investigation of the buoy data is needed to verify this assumption.

A second important result of this investigation is the need for accurate NMEA data. As shown in Section **Error! Reference source not found.** for the example of DRDC1, the correction of NMEA data significantly improves the correlations of WaMoS II to the buoy. This shows that for an operational application, the accuracy and update rate of NMEA data is a critical issue.

In general, it can be concluded that the validation of WaMoS II sea surfaces was successful in this trial. The good results show the significance of accurate NMEA data and a high update rate of reference buoy positions.

6 CONCLUSIONS

The DRDC trial Q348 yielded valuable new insights in the capabilities of WaMoS II to measure individual wave heights in a remote area by means of radar. The set-up of this trial allowed to validate the WaMoS II sea surface elevation maps by direct comparison to wave rider buoys. The very promising results of this validation were only possible due to a significant improvement of the buoy reference data. For the first time, the location of each buoy was known exactly for each individual buoy measurement. This allowed to prove the general match of WaMoS II sea surface to the buoy and important new insights in instrumental requirements to obtain correct sea surface elevations.

Of particular interest are issues related to the accuracy and update rates of NMEA data and the impact of the radar resolution in time and space. The trial proves how essential the bases of WaMoS and the reference data are for a successful validation. Only after establishing common bases as summarized in Section 4.4, is it possible to compare the WaMoS II sea surface data to the heave elevation of a buoy. It was clearly shown that the accuracy, update rate and time stamps of external NMEA data stored by WaMoS II can be considerably improved. The investigation of the sea surface elevation maps in Section 5 shows that this is needed to obtain significant results when comparing WaMoS elevation data to the corresponding buoy elevations. For these comparisons, it is still required to correct offsets of the WaMoS II data grid in time and space, but these are equivalent in magnitude to the offsets expected due to sensor inaccuracies.

In addition, the main WaMoS II sea state parameters were compared to the reference buoy. It was shown that peak wave directions and periods are in good agreement to the buoy data whereas WaMoS II Hs calibration had to be reset to obtaina good match to the buoy data. In this process, data outliers had to be removed as discussed in Section 4.3.2. It was concluded, that WaMoS Hs measures reasonable Hs values for approximately 80% of the full trial data set with high correlation (0.9) to the buoys. Mismatches are limited mainly to two shorter time intervals. These times should be examined in more detail.

Finally, the time traces obtained from WaMoS sea surface elevation maps were compared to buoy heave data. As summarized in Section 5.6 of this report, the comparisons of WaMoS II to the buoys showed a very promising, at times excellent match. The validation method developed for this investigation accounted for specific situations in which the buoy is well located within the observation area under conditions which would be used in operational applications. Basically, this means that the area of interest is aligned to the main wave travel direction placed in a distance where clear wave

pattern can be seen in the radar. While such a setup can be automatically established for most sea conditions in a practical application, for the validation purpose this leads to a significant reduction of comparison data as the buoys are not always placed ideally relative to the moving vessel. However, enough samples were found that allow to state that WaMoS II measures the wave profiles correctly. Correlations of up to 0.85 were found, the majority of samples show correlations of more than 0.6. This threshold for valid comparisons was estimated by a study of WaMoS II data autocorrelation. A new, interesting insight here was the impact of WaMoS II temporal update rates on the results. Applying a low pass filter to the raw buoy elevation records aiming to match the high time resolution to the lower WaMoS II update rates considerably improves the correlation for almost all samples.

From these result the following issues for improvement were identified to optimize the method:

- WaMoS II inversion requires very precise NMEA data with a high update rate and accurate time stamps to correctly localize an area both in time and space
- Radar offsets in space must be carefully evaluated and corrected. It seems that control points with known coordinates (e.g. in port) can be used to determine such offsets.
- The data spatial resolution of the radar should be as high as technically possible to fully exploit the precise NMEA data input. Particularly in angle, this is possible by using long antennas with small aperture and by storing all beams of a radar sweep.
- The radar should use a fast rotating antenna to improve the time resolution of the data. In this trial, a radar sweep required ~2.5 s, WaMoS II was successfully used withradars with ~1.2 s scan time.
- Time stamps of the radar can be improved by inclusion of a PPS signal. This was planned for Q348 but the data storage failed due to a missing WaMoS II hardware modification.

Accounting for all these factors should improve the WaMoS II sea surface elevation maps and should be considered for new trials.